CHAPTER FOUR

Spin-Torque Oscillators

Joo-Von Kim[*,†,1]
[*]Institut d'Electronique Fondamentale, Université Paris-Sud, Orsay, France
[†]UMR 8622, CNRS, Orsay, France
[1]Corresponding author: e-mail address: joo-von.kim@u-psud.fr

Contents

Solid State Physics, Volume 63
ISSN 0081-1947
http://dx.doi.org/10.1016/B978-0-12-397028-2.00004-7

1. INTRODUCTION

The advent of magnetic nanostructures has led to the appearance of physical phenomena not present in bulk materials. One prominent example is spin-transfer torques, which arise from spin-dependent transport processes in transition metal ferromagnets. Because electron transport is inherently spin-polarized in these materials, resulting from an exchange interaction between the conduction electron spins and local moments, torques appear when the spin current polarization and magnetization become noncollinear. Torques are observed in single thin films in regions in which large spatial gradients in the magnetization occur, such as in domain walls [1,2] and vortices, and in magnetic multilayers where layer magnetizations are tilted from one another [3,4]. Spin-transfer torques can initiate a number of physical processes without the need for applied magnetic fields, such as magnetization reversal in nanopillar structures [5], domain wall propagation along magnetic wires [6,7], and vortex displacement [8] and gyration [9] in magnetic dots. The magnitude of spin-transfer torques scales with the applied current density, which is why appreciable effects on magnetization dynamics are seen only for structures in the submicron limit.

Spin-transfer torques represent dissipative processes that cannot be described by or derived from a magnetic potential. The essential feature involves the transfer of spin angular momentum from the spin-polarized current to the local magnetization. Depending on the physical geometry and micromagnetic state, spin torques can either contribute to magnetic relaxation processes that are inherent in magnetization dynamics, leading to stronger damping, or compensate for these processes in such a way that the overall damping is reduced. Indeed, one of the first experimental demonstrations of spin-transfer torques involved the amplification of thermal spin waves in multilayer structures under dc currents [10–12]. Under sufficiently high currents, magnetic damping can become entirely compensated by spin torques, leading to either instabilities in the magnetic state or self-sustained oscillations of the magnetization [13,14]. The latter occurs for spin waves, large-angle (quasi-)uniform magnetization precession, and magnetic vortices (whose motion is intrinsically gyrotropic).

For self-sustained oscillations involving magnetoresistive structures such as spin valves and magnetic tunnel junctions, the time-varying magnetization (of the free magnetic layer, for example) translates into a high-frequency electrical signal by virtue of the giant- or tunnel-magnetoresistance effects

(Fig. 4.1) [13,14]. As the underlying dynamics is driven by dc currents only, the experimental realization of such current-driven magnetization oscillations has inspired many proposals for electrical oscillators in the gigahertz range. These systems are referred to as *spin-torque oscillators*. From a fundamental perspective, these systems are of interest because the oscillatory behavior is a result of the interplay between strongly nonlinear magnetization processes and spin-dependent transport through magnetic heterostructures where the strong nonlinearity can lead to large variations in the oscillation frequency with applied currents. From a technological perspective, such systems are enticing because of the prospect of constructing frequency-tunable oscillators on the nanoscale, with potential applications in mobile telecommunications, for example, where several frequency bands could be handled by a single oscillator.

The aim of this chapter is to provide an introduction to the theoretical basis of spin-torque oscillators, with important points being supplemented by key experimental results. Emphasis is given to describing current-driven magnetization processes relevant to transition metal ferromagnets, such as iron, cobalt, nickel, and their alloys, as these material systems are the subject of the vast majority of experimental studies to date and show the greatest promise for future applications in spintronics. The chapter is intended to be more of a tutorial for readers unfamiliar with the physical aspects of the topic rather than an exhaustive review of published experimental and theoretical results. The chapter is organized as follows. In Section 2, a brief introduction to key concepts is given, which includes basic oscillator theory, magnetization dynamics in the presence of spin torques, and the different formulations used to construct theories for spin-torque oscillators. In Section 3, a description of oscillators based on linear and nonlinear spin-wave modes is given. In Section 4, the oscillator model is extended to include thermal noise, which leads to a stochastic theory that is relevant to describing room temperature experimental spectra. The focus shifts to oscillating magnetic vortices in Section 5, where a description of dynamics in confined and extended geometries is presented. A summary of other nonlinear phenomena is given in Section 6 and some final remarks are given in Section 7.

2. SELF-SUSTAINED OSCILLATIONS AND SPIN TORQUES

2.1. Basic notions of self-sustained oscillations

Self-sustained oscillations occur in a system in which a periodic signal is generated without the stimulus of an external periodic force. Such systems are ubiquitous in nature. Examples include the laser, the flashing of fireflies,

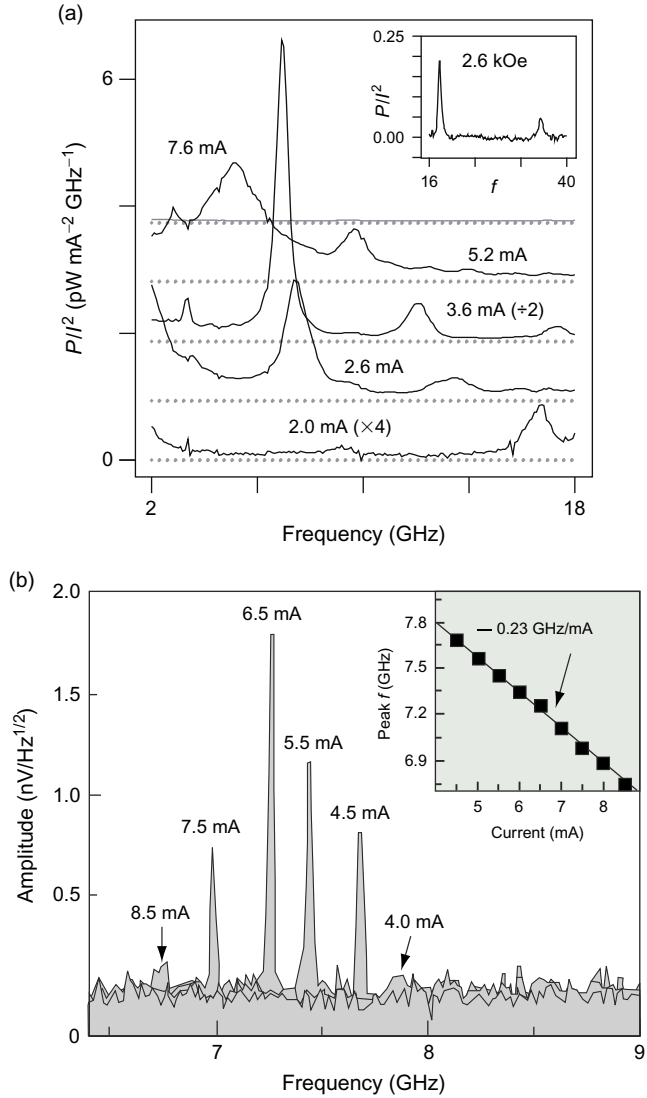

Figure 4.1 Experimental power spectra of voltage oscillations in spin-torque oscillators. (a) Current-driven dynamics in a pseudo spin-valve nanopillar under an applied field $\mu_0 H = 0.2$ T at several applied currents. The inset shows the power spectrum $\mu_0 H = 0.26$ T and $I = 2.2$ mA, for which both the first and second harmonics are visible. (b) Current-driven dynamics in a magnetic nanocontact under an applied field of $\mu_0 H = 0.1$ T at several applied currents. The inset shows the current dependence of the mode frequency. *(a) After Fig. lc of Ref. [13] (© Nature Publishing Group). (b) After Fig. 1b of Ref. [14] (© American Physical Society).*

the beating of a heart, and the firing of neurons. Three essential components underpin all self-oscillatory systems. The first is a resonant component, which determines the frequency of oscillation. The second is a dissipative component, which relates to the energy lost from the system toward its environment. This is a feature of any real physical system. The third is an "active" component, which represents a source of energy that compensates for losses due to the dissipative part.

The central feature of all self-oscillatory systems is the existence of a stable limit cycle in their phase space. A limit cycle represents an isolated closed trajectory, where motion along the cycle is periodic and neighboring trajectories spiral toward (and are attracted by) this cycle. Limit cycles are inherently nonlinear; while closed (periodic) orbits can occur in a linear conservative system, these orbits are not isolated as the amplitude of oscillation is determined purely by the initial conditions (Fig. 4.2a). For example, a slight perturbation to a linear system will result in a change in the oscillation amplitude that persists, while for a nonlinear system, such perturbations eventually die out as the system relaxes back toward the stable limit cycle (Fig. 4.2b). As such, the limit cycle is related to the inherent nonlinear properties of the dynamical system.

To see how a limit cycle appears, let us consider the following dynamical system,

$$\frac{\mathrm{d}r}{\mathrm{d}t} = \left(\mu - r^2\right)r, \frac{\mathrm{d}\theta}{\mathrm{d}t} = \omega, \qquad [4.1]$$

where r and θ represent polar variables in the xy plane, and μ and ω are parameters of the system. The phase space of this system is spanned by the

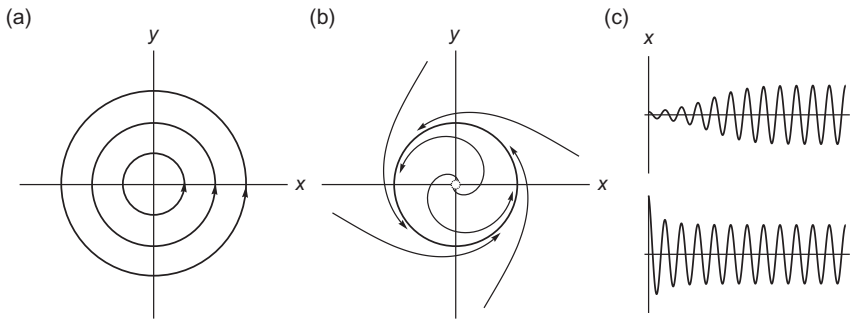

Figure 4.2 Illustration of periodic orbits; (a) Linear oscillatory system with an infinite family of periodic orbits. (b) Nonlinear self-oscillatory system with a stable limit cycle (unit circle). Initial states inside or outside the unit circle are attracted toward the limit cycle, as indicated by the flows in the *xy* phase space. The origin is an unstable fixed point. (c) Transient behavior for initial conditions inside (top) and outside (bottom) the limit cycle. The system settles into steady-state oscillations after the transient phase.

variables (r,θ) (or, equivalently (x,y) in Cartesian coordinates). In this example, the radial and angular variables are uncoupled, which allows the dynamics in each of these variables to be considered separately. In physical terms, the radial equation describes a nonlinear damping in the amplitude r, where the sign of μ controls whether the damping is positive or negative at small r, while the nonlinear term always contributes to negative damping (losses). The quantity $(\mu - r^2)$ corresponds to the balance between intrinsic relaxation and energy flow into a system via an active element. In this example, the resonant part is described simply by the constant angular frequency ω.

For $\mu < 0$, the system possesses only one stable fixed point at the origin, $r^* = 0$. The trajectories in this case comprise spiraling flows toward the origin, as shown in Fig. 4.3a, with the sense of rotation depending on the sign of ω. As the parameter is varied through $\mu = 0$ and becomes positive, $\mu > 0$, the origin loses its stability and a stable limit cycle appears at $r^* = \sqrt{\mu}$ (Fig. 4.3b). The process by which this limit cycle appears is referred to as a supercritical Hopf bifurcation [15]. For $\mu > 0$, all trajectories in the phase space of the system, with the exception of the point $r^* = 0$, converge toward the circle $r^* = \sqrt{\mu}$ at a constant angular velocity of ω. This gives rise to the spiraling trajectories shown in Figs. 4.2b and 4.3b. Any perturbation away from the limit cycle is always restored back toward this cycle as a result of the nonlinear term $(\mu - r^2)$, which is essential for the existence of a limit cycle, in contrast to the free oscillations depicted in Fig. 4.2a. It is straightforward to see that the time evolution of either the x or y variables on the limit cycle is described by a sinusoidal oscillation, as shown in Fig. 4.2c.

It is useful and important to make the distinction between self-oscillatory and resonant systems, both of which exhibit oscillations in the steady state. In

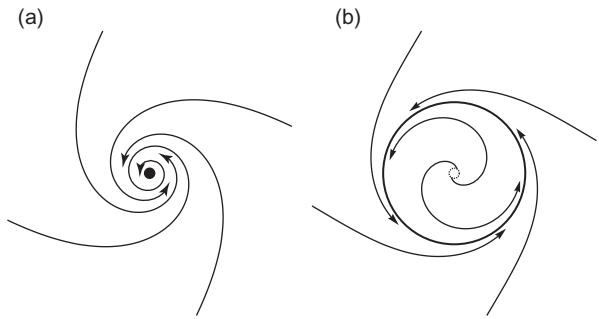

Figure 4.3 Illustration of a supercritical Hopf bifurcation. (a) $\mu < 0$, showing damped oscillations where all trajectories in phase space spiral toward the origin. (b) $\mu > 0$, where all trajectories are attracted to the limit cycle.

a resonant system, the order parameter is driven into a steady-state oscillation in response to a periodic external force. The amplitude of this response is frequency-dependent and is largest when some resonance condition is met. More importantly, the phase of the oscillation is exactly defined by how the system responds to the external force, in particular, on the frequency of this periodic force, that is, it is governed by a (complex) susceptibility. In contrast, the oscillation amplitude in a self-oscillatory system is stable but its phase is arbitrary. This is an important distinction and allows for rich nonlinear phenomena such as phase-locking and synchronization to occur in self-sustained oscillators. These topics are briefly discussed toward the end of the chapter.

2.2. Magnetization precession and the torque equation

The main focus of this chapter is on how self-sustained oscillations appear in the magnetization dynamics of transition metal ferromagnets. These materials can be classified as strong ferromagnets as the Curie temperatures of the bulk state are well above room temperature (i.e., 1043 K for Fe, 1388 K for Co, and 627 K for Ni). As a result of the strong exchange interaction, the micromagnetic approach represents a good approximation for describing magnetization processes in these materials at room temperature. This approach involves the assumption that the magnetic order can be described by a continuous field $\mathbf{M} = M_s\hat{\mathbf{m}}(\mathbf{r})$, whose norm is always conserved ($\|\hat{\mathbf{m}}\| = 1$) and has the magnitude of the saturation magnetization M_s of the material [16].

The time evolution of the magnetization vector in the micromagnetic approximation is described by the torque equation

$$\frac{\mathrm{d}\hat{\mathbf{m}}}{\mathrm{d}t} = -\gamma_0\hat{\mathbf{m}} \times \mathbf{H}_{\mathrm{eff}} + \sum_i \mathbf{T}_{i,\mathrm{NC}}, \qquad [4.2]$$

where $\gamma_0 = |\gamma|\mu_0$ is the gyromagnetic constant and $\gamma = g\mu_B/\hbar$. The first term on the right-hand side describes magnetization precession about its local effective field $\mathbf{H}_{\mathrm{eff}}$,

$$\mathbf{H}_{\mathrm{eff}}(\mathbf{r}) = -\frac{1}{\mu_0}\frac{\partial \mathcal{E}(\mathbf{r})}{\partial \mathbf{M}(\mathbf{r})}, \qquad [4.3]$$

where $\mathcal{E}$ is the magnetic energy per unit volume and represents the sum over all magnetic interactions present. The precession term represents the resonant part of the spin-torque oscillator, where the frequency of precession is governed by the relevant energy terms in the effective field. The second

term on the right-hand side describes a summation over nonconservative torques $\mathbf{T}_{i,\mathrm{nc}}$ that cannot be derived from a potential. The relevant nonconservative torques for spin-torque oscillators are described in detail further on in this section.

For materials of technological interest, the important contributions to the magnetic energy are the Zeeman, exchange, and dipole–dipole interactions. The Zeeman term describes the interaction of magnetization with an external applied magnetic field $\mathbf{H_0}$,

$$\mathcal{E}_Z(\mathbf{r}) = -\mu_0 M_\mathrm{s}\hat{\mathbf{m}}(\mathbf{r})\cdot\mathbf{H}_0(\mathbf{r}), \qquad [4.4]$$

which originates in the lifting of the degeneracy between spin-up and spin-down electrons as a result of the magnetic field. The exchange interaction represents the coupling between neighboring local moments that leads to a spontaneous magnetic order. In the continuum limit, the isotropic form of the interaction can be written as

$$\mathcal{E}_\mathrm{ex}(\mathbf{r}) = A\frac{\partial m_i(\mathbf{r})}{\partial x_j}\frac{\partial m_i(\mathbf{r})}{\partial x_j}, \qquad [4.5]$$

where $m_i = \{m_x, m_y, m_z\}$, $x_i = \{x, y, z\}$, and summation of repeated indices is assumed. The dipole–dipole interaction is a long-ranged interaction that couples together all the local moments in the system. It is useful to cast this energy in terms of an effective dipolar field $\mathbf{H}_\mathrm{d}$,

$$\mathcal{E}_\mathrm{d}(\mathbf{r}) = -\frac{1}{2}\mu_0 M_\mathrm{s}\hat{\mathbf{m}}(\mathbf{r})\cdot\mathbf{H}_\mathrm{d}(\mathbf{r}). \qquad [4.6]$$

The dipolar field is derived from a magnetostatic potential Φ_m,

$$\mathbf{H}_\mathrm{d}(\mathbf{r}) = -\nabla\Phi_\mathrm{m}(\mathbf{r}), \qquad [4.7]$$

which comprises contributions from surface (ρ_s) and volume (ρ_v) magnetic charges,

$$\Phi_\mathrm{m}(\mathbf{r}) = \frac{M_\mathrm{s}}{4\pi}\left[\int \mathrm{d}V' \frac{\rho_\mathrm{v}(\mathbf{r}')}{\|\mathbf{r}-\mathbf{r}'\|} + \int \mathrm{d}S' \frac{\rho_\mathrm{s}(\mathbf{r}')}{\|\mathbf{r}-\mathbf{r}'\|}\right], \qquad [4.8]$$

where the integrals are taken over the volume and the surface of the material, respectively, and the magnetic charge densities are defined as

$$\rho_\mathrm{v}(\mathbf{r}) = -\nabla\cdot\hat{\mathbf{m}}(\mathbf{r}); \quad \rho_\mathrm{s}(\mathbf{r}) = -\hat{\mathbf{m}}(\mathbf{r})\cdot\hat{\mathbf{n}}(\mathbf{r}), \qquad [4.9]$$

with $\hat{\mathbf{n}}(\mathbf{r})$ being a unit vector representing the outward normal to the surface. The nonlocal character of the magnetostatic potential reflects the long-ranged character of the dipole–dipole interaction. While a direct evaluation

of this interaction is not tractable analytically and is computationally intensive, useful approximations can be obtained for special cases. A convenient approach involves the use of demagnetizing factors $\mathcal{N}_{ij}$,

$$\mathcal{E}_{\mathrm{d}}(\mathbf{r}) = \frac{1}{2}\mu_0 M_{\mathrm{s}}^2 m_i(\mathbf{r})\mathcal{N}_{ij}(\mathbf{r})m_j(\mathbf{r}), \qquad [4.10]$$

which reduces the dipole–dipole energy to a local interaction [16]. $\mathcal{N}_{ij}$ represents a dimensionless 3×3 matrix whose elements are determined by the geometry of the magnetic material. For an infinite thin film, for example, the only nonvanishing component is $\mathcal{N}_{zz} = 1$ (where z represents the direction normal to the film plane), which reduces the dipolar interaction to a hard-axis anisotropy of the form

$$\mathcal{E}_{\mathrm{d}}(\mathbf{r}) = \frac{1}{2}\mu_0 M_{\mathrm{s}}^2 \mathcal{N}_{zz} m_z^2(\mathbf{r}). \qquad [4.11]$$

In general, the finite size of a nanoelement gives rise to a shape anisotropy of this form.

2.3. Magnetic relaxation

A significant contribution to the nonconservative torques in Eq. (4.2) arises from energy losses due to magnetic relaxation or damping. This represents the ensemble of dissipative processes that transfers energy out of the magnetic system toward other heat baths with which it is in contact. For example, the interaction between magnetization with phonons and conduction electrons contributes to such relaxation processes.

Damping allows a micromagnetic configuration to reach an equilibrium state in which the magnetization vector is oriented along its local effective fields. In micromagnetics, such relaxation processes can be described with a phenomenological damping term in the torque equation (Eq. 4.2). Gilbert proposed a term of the form [17,18]

$$\mathbf{T}_{\mathrm{G}} = \alpha\hat{\mathbf{m}} \times \frac{\mathrm{d}\hat{\mathbf{m}}}{\mathrm{d}t}, \qquad [4.12]$$

where α is a dimensionless damping constant. This term represents viscous damping and is analogous to friction in mechanical systems in which the magnitude of the frictional force acting on a body is proportional to its velocity. A geometrical interpretation of this damping term is more easily seen by rewriting it in terms of a vector product with the effective field. Consider the full equation of motion for the damped magnetization dynamics,

$$\frac{d\hat{\mathbf{m}}}{dt} = -\gamma_0 \hat{\mathbf{m}} \times \mathbf{H}_{\text{eff}} + \alpha \hat{\mathbf{m}} \times \frac{d\hat{\mathbf{m}}}{dt}. \quad [4.13]$$

By applying $\hat{\mathbf{m}}\times$ to both sides of Eq. (4.13),

$$\hat{\mathbf{m}} \times \frac{d\hat{\mathbf{m}}}{dt} = -\gamma_0 \hat{\mathbf{m}} \times (\hat{\mathbf{m}} \times \mathbf{H}_{\text{eff}}) - \alpha \frac{d\hat{\mathbf{m}}}{dt}, \quad [4.14]$$

and substituting the right-hand side of this equation for the damping term in Eq. (4.13), the equation of motion becomes

$$\frac{d\hat{\mathbf{m}}}{dt} = -\frac{\gamma_0}{1+\alpha^2} \hat{\mathbf{m}} \times \mathbf{H}_{\text{eff}} - \frac{\alpha\gamma_0}{1+\alpha^2} \hat{\mathbf{m}} \times (\hat{\mathbf{m}} \times \mathbf{H}_{\text{eff}}). \quad [4.15]$$

As the illustration in Fig. 4.4 shows, the damping torque acts in a direction perpendicular to the precessional motion, leading the magnetization to spiral toward the direction of the effective field until it becomes aligned with this field. When this occurs, all torques acting on the magnetization vector vanish.

It should be noted that the damping term in Eq. (4.15) is mathematically equivalent to the phenomenological form originally proposed by Landau and Lifshitz [19]:

$$\mathbf{T}_{\text{LL}} = -\gamma_0 \lambda \hat{\mathbf{m}} \times (\hat{\mathbf{m}} \times \mathbf{H}_{\text{eff}}), \quad [4.16]$$

where λ is another dimensionless damping constant. While the Gilbert and Landau–Lifshitz formulations share the same mathematical structure, the physical consequences are different in the limit of large damping. In the Landau–Lifshitz formulation, the damping constant acts only on the torque perpendicular to the precessional motion, with no theoretical upper limit on

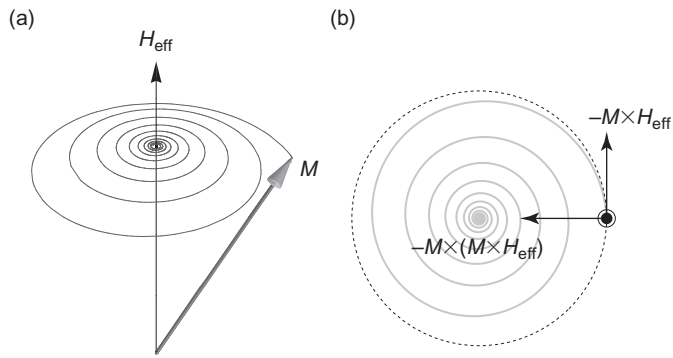

Figure 4.4 Illustration of damped precessional magnetization dynamics. (a) Damped spiraling trajectory of the magnetization M about its effective field $\mathbf{H}_{\text{eff}}$. (b) Top view of the dynamics, with the directions of the precessional and damping torques drawn.

the magnitude of this torque. The Gilbert form of damping, on the other hand, acts on the entire magnetization dynamics, which can be seen from the presence of α in both the precessional and damping terms in the equations of motion. In practice, the distinction between the two is academic, as the Gilbert damping constant of technologically relevant materials, such as YIG or permalloy, is on the order of 10^{-3}–10^{-2}. As such, the term $\alpha^2 \ll 1$ in the denominator of Eq. (4.15) can be neglected, which makes both the Landau–Lifshitz and Gilbert formulations physically equivalent. However, it has been suggested that the Landau–Lifshitz formulation may be more relevant for specific cases [20], but there is a general preference toward using the Gilbert form because of its connection to viscous damping. For example, nonlinear corrections to the Gilbert damping can be made naturally by using a power-series expansion to the damping constant [21],

$$\alpha = \alpha_0 + c_1 \left\| \frac{d\hat{\mathbf{m}}}{dt} \right\|^2 + \ldots \qquad [4.17]$$

which is motivated by the identification of $\|d\hat{\mathbf{m}}/dt\|^2$ as the square of a generalized velocity for the magnetic system.

2.4. Spin-transfer torques

Electron currents in transition metal ferromagnets are naturally spin-polarized. The magnetization defines a natural quantization axis for the conduction electron spins and the asymmetry between spin-up and spin-down transport channels results from a difference in mobility between the two. The origin of this asymmetry is in the exchange interaction that leads to the spontaneous ferromagnetic state. This exchange interaction leads to a splitting of the conduction electron bands, which results in different parts of the band structure being present at the Fermi energy. The segments of the spin-up and spin-down band structures that intersect the Fermi level generally have different densities of states, which results in different scattering probabilities, and therefore different resistivities, for the two spin channels.

A useful picture for understanding the effects of spin-polarized transport on magnetization dynamics in transition metals is the *sd* model. The electronic states at the Fermi level are divided into two distinct groups: delocalized 4*s* electrons that are responsible for electrical conduction, and localized 3*d* electrons that are responsible for the magnetic order. These two species of electrons interact via an exchange interaction,

$$\mathcal{E}_{sd} = -\mathcal{J}_{sd}\hat{\mathbf{m}}(\mathbf{r})\cdot\mathbf{s}(\mathbf{r}), \qquad [4.18]$$

where $\mathcal{J}_{sd}$ is an exchange integral, $\hat{\mathbf{m}}$ represents the local moments of the $3d$ electrons, and $\mathbf{s}$ represents the expectation value of the conduction electron spin,

$$\mathbf{s}(\mathbf{r}) = \sum_i \psi_i^*(\mathbf{r})\hat{\sigma}\psi_i(\mathbf{r}), \qquad [4.19]$$

with ψ_i being an occupied single-particle wave function in state i and $\hat{\sigma} = (\sigma_x, \sigma_y, \sigma_z)$ being the vector of Pauli matrices. While detailed electronic structure calculations have established that the electronic states at the Fermi energy are more likely to be hybridized s and d states, this simplified picture is useful for understanding the qualitative features of spin-transfer torques.

From the torque equation (Eq. 4.2) and the form of the sd exchange interaction (Eq. 4.18), it would appear that no torques should be exerted on the local moments by the conduction electron spins if these spins are collinear with the local magnetization. How do torques get transferred from a spin-polarized current to the magnetic order parameter? For any torques to appear, it is necessary for the spin polarization of the current to be noncollinear with the background magnetization. This noncollinearity can arise in patterned multilayered films, such as spin valves or magnetic tunnel junctions. Consider the multilayer stack in Fig. 4.5 in which there are two ferromagnetic layers, a "reference" layer and a "free" layer. Suppose a current is applied perpendicularly to the film plane (CPP) in which the electrons flow from the reference layer to the free layer. The incident current arriving from a normal metal is unpolarized, but it becomes polarized upon passage through the reference layer and the outgoing electron flux is collinear with the

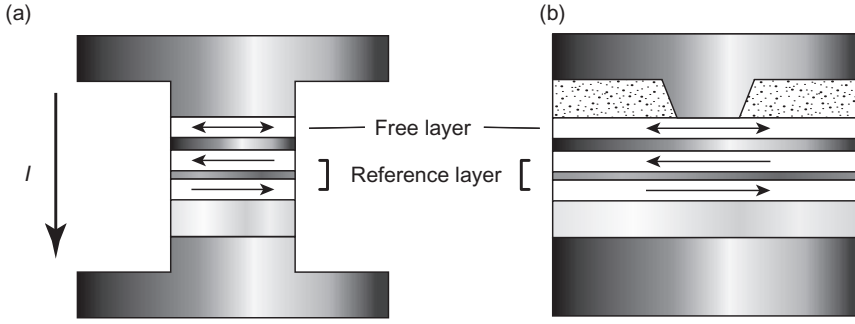

Figure 4.5 Typical examples of physical geometries in which CPP torques appear, where I indicates the current flow perpendicular to the film plane. (a) Nanopillars. (b) Nanocontacts.

reference layer magnetization. The reference layer, therefore, acts as a "polarizer" for the incident electron current. If the reference and free-layer magnetizations are noncollinear, then the spin-polarized current incident on the free layer will lead to a torque on the free-layer magnetization, by virtue of the *sd* exchange interaction described earlier. If the free layer is sufficiently thin, this torque will be exerted on the magnetization across the entire thickness of the free layer.

A description of these spin-transfer torques was first given independently by Berger [3] and Slonczewski [4] in 1996. Consider the multilayer structure in Fig. 4.5a, where the magnetization orientation of the reference layer is labeled by $\hat{\mathbf{p}}$ and the free-layer magnetization by $\hat{\mathbf{m}}$. It was shown that the spin-transfer torque acting on $\hat{\mathbf{m}}$ can be expressed as

$$\mathbf{T}_{\mathrm{CPP}} = \eta(\theta)\frac{\hbar}{\mathrm{e}}\frac{\gamma}{M_{\mathrm{s}}\mathrm{d}}J\hat{\mathbf{m}}\times(\hat{\mathbf{m}}\times\hat{\mathbf{p}}), \qquad [4.20]$$

where J is the CPP current density. Under this convention, $J>0$ represents conventional current flow from the reference layer to the free layer (i.e., electron flow from the free layer to the reference layer). Note that the prefactor to the double vector product has units of angular frequency, which can be interpreted as the rate of spin-momentum transfer to the free-layer magnetization. The dimensionless function η depends on the details of the transport through the multilayer (materials, film thicknesses) and is a function of the angle between the free- and reference-layer magnetizations, $\cos\theta = \hat{\mathbf{m}}\cdot\hat{\mathbf{p}}$. In the simplest case, the constant form $\eta(\theta)=\eta_0$ yields the sine approximation (as the cross product gives a sine dependence on the torque). The angular dependence of the spin torque, as originally obtained by Slonczewski, can be written in the form [22]

$$\eta(\theta) = \frac{q}{A+B\cos\theta}, \qquad [4.21]$$

where q, A, and B are material- and transport-dependent parameters. This form is referred to as the symmetric Slonczewski approximation and was obtained for a pseudo spin-valve system in which the free and polarizer layers have equal thickness. In general, due to the asymmetry of the spin-valve layer thicknesses and composition, the more general asymmetric form is expected,

$$\eta(\theta) = \frac{q+}{A+B\cos\theta} + \frac{q-}{A-B\cos\theta}, \qquad [4.22]$$

which is referred to as the asymmetric Slonczewski form. There is a general consensus that the angular dependence of the spin torque depends strongly on the details of the multilayer structure [22–34]. More complicated forms for $\eta(\theta)$ have been reported in the literature. An interesting case involves a "wavy" angular dependence, in which the transport properties of a spin valve are tailored such that $\eta(\theta_0) = 0$ for $\theta_0 \neq 0, \pi$, with θ_0 being a stable magnetization configuration for the free layer [32,34]. Some experimental evidence has been put forward for the realization of such wavy torques [35,36].

Spin-transfer torques also appear with currents flowing through continuous systems in which there are spatial gradients in the magnetization. We denote these torques as current-in-plane (CIP) torques to distinguish them from the CPP torques discussed earlier. Such torques were first proposed by Berger and coworkers from studies of magnetic domain wall dynamics in permalloy under applied currents [1,2]. Some relevant experimental geometries for CIP torques are shown in Fig. 4.6.

The magnitude of these torques depends largely on how closely the conduction electron spins track the local magnetization as the current flows through the region of nonuniform magnetization [37–40]. In the limit of adiabatic transport, the spin-up and spin-down electrons remain in their energy eigenstates (with respect to the exchange splitting induced by the *sd* interaction) as they traverse the magnetization gradients. This occurs through a gradual precession of the conduction electron spin about the local *sd* effective field associated with the local moments, which in turn results in the mutual precession of the local moments about the *sd* effective field associated with the conduction electron spins. In the nonadiabatic limit, processes involving spin-flip scattering for the conduction electrons become important.

A quantitative description of CIP torques comprising adiabatic and nonadiabatic contributions has been given by Zhang and Li [39]. They

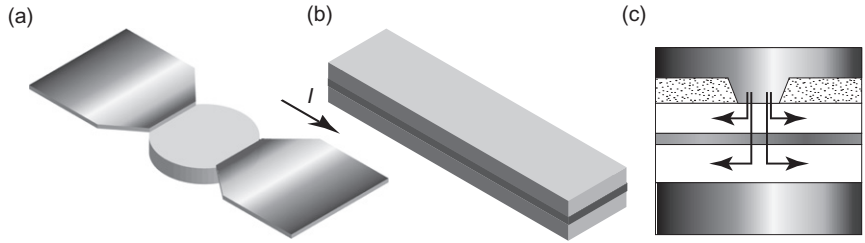

Figure 4.6 Examples of physical geometries in which CIP torques appear. (a) Submicron disks. (b) Wires. (c) Nanocontacts. The arrows indicate the current flow.

considered the *sd* model in the diffusive limit for spin transport and derived the effective torques acting on the local magnetization in this limit. It was found that the spin torques can be included into the torque equation (Eq. 4.2) as

$$\mathbf{T}_{\mathrm{CIP}} = -(\mathbf{u}\cdot\nabla)\hat{\mathbf{m}} + \beta\hat{\mathbf{m}} \times [(\mathbf{u}\cdot\nabla)\hat{\mathbf{m}}], \qquad [4.23]$$

where $\mathbf{u}$ has the units of velocity and represents an effective spin drift velocity of the spin current [41],

$$\mathbf{u} = P\frac{\hbar}{2e}\frac{\gamma}{M_s}\mathbf{J}(\mathbf{r}), \qquad [4.24]$$

and $\mathbf{J}(\mathbf{r})$ is the current density flowing in the film plane, with P representing the spin polarization of this current. The first term on the right-hand side of Eq. (4.23) represents the adiabatic torque and the second term the nonadiabatic torque, which is characterized by the dimensionless parameter β.

Like the Gilbert damping constant α, the nonadiabatic parameter β represents a phenomenological constant that is related to the dissipative part of CIP spin torques. While there remains much debate in the community concerning the precise value of β, it is generally accepted that β is on the same order of magnitude as α, with estimates for the ratio $\kappa = \beta/\alpha$ ranging from 1 to 10 [42–47]. Recent theoretical work has shown that nonlocal transport processes can strongly influence the magnitude of β for regions of sharp magnetization gradients, such as in micromagnetic configurations containing vortex structures [48,49]. In such cases, it has been shown that terms involving higher-order spatial derivatives are required to supplement the torque equation (Eq. 4.23).

2.5. Lagrangian formulation of magnetization dynamics

Up to this point, the three key elements of current-driven magnetization dynamics—precession, damping, and spin-transfer torques—have been presented in terms of torque equations. This approach is the most commonly followed for historical reasons, as it provides a simple and direct way of visualizing the influence of various torques on the time evolution of the magnetization vector, as Fig. 4.4 illustrates. However, for dynamics involving nontrivial micromagnetic states, such as fluctuations about nonuniform ground-state configurations or the dynamics of topological solitons such as domain walls and vortices, it is more convenient to cast the dynamics in terms of variables that characterize the amplitude of these dynamical modes.

The Lagrangian formulation of magnetization dynamics is one such approach that allows the dynamics of specific micromagnetic states to be described while taking into account the constraints that define such states. The conservative part of the magnetization dynamics can be described by the Lagrangian density

$$\mathcal{L} = \frac{M_s}{\gamma}\dot{\Phi}(1 - \cos\Theta) - \mathcal{E}[\Theta, \Phi], \qquad [4.25]$$

where $\dot{\Phi} = \partial_t \Phi$, and $\Theta = \Theta(\mathbf{r})$ and $\Phi = \Phi(\mathbf{r})$ represent the orientation of the local magnetization vector in spherical coordinates, that is, $\hat{\mathbf{m}} = (\cos\Phi\sin\Theta, \sin\Phi\sin\Theta, \cos\Theta)$. The first term on the right-hand side is often referred to as the "Berry-phase" term and plays the role of a "kinetic" energy. The second term is the magnetic free energy functional, $\mathcal{E}$, which comprises the usual contributions that lead to the effective field defined earlier for the Landau–Lifshitz equation (Eq. 4.2). If the micromagnetic state can be parameterized in terms of a set of reduced variables representing generalized coordinates q_i, for example, the position of the core in the film plane (X_0, Y_0) of a magnetic vortex, then the dynamics can be obtained from the total Lagrangian L,

$$L = \int \mathrm{d}V \mathcal{L}([\Theta(\mathbf{r}), \Phi(\mathbf{r})]), \qquad [4.26]$$

with the usual Euler–Lagrange equations,

$$\frac{\mathrm{d}}{\mathrm{d}t}\frac{\partial L}{\partial \dot{q}_i} - \frac{\partial L}{\partial q_i} = 0, \qquad [4.27]$$

describing the conservative dynamics.

Nonconservative forces can be included into this description using a Rayleigh dissipation function W, which is obtained from the density, $\mathcal{W}$, as $W = \int \mathrm{d}V \mathcal{W}$. This leads to the additional term in the Euler–Lagrange equations

$$\frac{\mathrm{d}}{\mathrm{d}t}\frac{\partial L}{\partial \dot{q}_i} - \frac{\partial L}{\partial q_i} + \frac{\partial W}{\partial \dot{q}_i} = 0. \qquad [4.28]$$

For Gilbert damping, the dissipation function density is

$$\mathcal{W}_G = \frac{\alpha M_s}{2\gamma}\left\|\frac{\mathrm{d}\hat{\mathbf{m}}}{\mathrm{d}t}\right\|^2, \qquad [4.29]$$

which in spherical coordinates for the magnetization vector becomes

$$\mathcal{W}_{\mathrm{G}} = \frac{\alpha M_{\mathrm{s}}}{2\gamma}\left(\dot{\Theta}^2 + \sin^2\Theta\dot{\Phi}^2\right). \qquad [4.30]$$

This form makes explicit the analogy between Gilbert damping and general viscous damping where the frictional force is proportional to the square of the generalized velocities.

Consolo *et al.* showed that the CPP spin torques can be derived from the dissipation function density [50]

$$\mathcal{W}_{\mathrm{CPP}} = -\eta(\theta)\frac{\hbar J}{\mathrm{e}\, d}\hat{\mathbf{p}}\cdot\left(\hat{\mathbf{m}}\times\frac{\mathrm{d}\hat{\mathbf{m}}}{\mathrm{d}t}\right). \qquad [4.31]$$

In contrast to the dissipation function for Gilbert damping, which is positive-definite, the sign of the dissipation function for the CPP spin torques depends on the polarity of the applied current J. As such, spin torques can either increase or decrease the energy dissipation in the system, and it is the latter that is important for allowing self-sustained magnetization oscillations.

For the CIP spin torques, it is interesting to note that the full equations of motion with these torques,

$$\left(\frac{\mathrm{d}}{\mathrm{d}t} + \mathbf{u}\cdot\nabla\right)\hat{\mathbf{m}} = -\gamma_0\hat{\mathbf{m}}\times\mathbf{H}_{\mathrm{eff}} + \alpha\hat{\mathbf{m}}\times\left[\left(\frac{\mathrm{d}}{\mathrm{d}t} + \kappa\mathbf{u}\cdot\nabla\right)\hat{\mathbf{m}}\right], \qquad [4.32]$$

where $\kappa \equiv \beta/\alpha$, can *almost* be obtained directly from the Landau–Lifshitz equation with Gilbert damping,

$$\frac{\mathrm{d}\hat{\mathbf{m}}}{\mathrm{d}t} = -\gamma_0\hat{\mathbf{m}}\times\mathbf{H}_{\mathrm{eff}} + \alpha\hat{\mathbf{m}}\times\frac{\mathrm{d}\hat{\mathbf{m}}}{\mathrm{d}t}, \qquad [4.33]$$

by substituting the time derivative with a "convective" derivative, $\mathrm{d}/\mathrm{d}t \to \mathrm{d}/\mathrm{d}t + \mathbf{u}\cdot\nabla$. The simple substitution fails to account for the κ term in the dissipative part of the dynamics. For $\kappa = 1$, the system becomes Galilean invariant with respect to the translations afforded by the vector $\mathbf{u}$, and the substitution of the time derivative with the convective derivative leads to the exact equations of motion. However, almost all experiments on current-driven domain wall motion to date have shown that generally $\kappa > 1$, which suggests that Galilean invariance is broken due to the fact that dissipation processes in the laboratory frame are not equivalent to the processes in the stationary reference frame given by $\mathbf{u}$. This suggests that dissipation

channels that do not drift with the effective spin drift current **u**, such as local magnetic impurities or defects, are at the origin of this broken Galilean invariance. The dynamics can be obtained by substituting the appropriate convective derivatives into the Berry phase and Gilbert dissipation functions,

$$\mathcal{L}_{\mathrm{CIP}} = \frac{M_s}{\gamma}\left[\left(\frac{\mathrm{d}}{\mathrm{d}t} + \mathbf{u}\cdot\boldsymbol{\nabla}\right)\Phi\right](1-\cos\Theta) - \mathcal{E}[\Theta,\Phi], \qquad [4.34]$$

$$\mathcal{W}_{\mathrm{CIP}} = \frac{\alpha M_s}{2\gamma}\left\{\left[\left(\frac{\mathrm{d}}{\mathrm{d}t} + \mathbf{u}\cdot\boldsymbol{\nabla}\right)\Theta\right]^2 + \sin^2\Theta\left[\left(\frac{\mathrm{d}}{\mathrm{d}t} + \mathbf{u}\cdot\boldsymbol{\nabla}\right)\Phi\right]^2\right\}. \qquad [4.35]$$

3. LINEAR AND NONLINEAR SPIN-WAVE MODES

3.1. Transformation to spin-wave variables

The magnetization dynamics described by Eq. (4.2) represents a complicated micromagnetics problem, which has strong space and time dependence of the magnetization variables. For the class of current-driven excitations involving spin-wave modes, the problem can be simplified by integrating out the spatial profiles of these modes. This simplification allows the entire dynamics to be described in terms of the respective spin-wave mode amplitudes, which represent the normal modes of the system. These modes can represent oscillations about a uniform or nonuniform ground state, with the latter being more likely in confined geometries such as nanopillars.

A standard prescription for obtaining the normal modes or spin-wave coordinates is through the Holstein–Primakoff transformation [51]. It involves transforming the spin operators describing the magnetic state into creation and annihilation operators for a harmonic oscillator. This allows for the magnetic Hamiltonian to be diagonalized in terms of harmonic oscillator states at lowest order, with a controlled prescription for including higher-order interactions between the different normal modes of oscillation.

In the following example, a brief overview of the transformation to spin-wave variables is given. Consider a uniformly magnetized ground state in which the magnetization is oriented along the z direction, which defines the quantization axis for the spin-wave modes. It is convenient to define

the (normalized) circular magnetization $m_{\pm} = m_x \pm \mathrm{i} m_y$. These variables are then transformed into the dimensionless fields $a(\mathbf{r})$ and $a^{\dagger}(\mathbf{r})$,

$$\begin{aligned} m_{+}(\mathbf{r}) &= \left(\frac{2g\mu_{\mathrm{B}}}{M_{\mathrm{s}}V}\right)^{1/2}\left[1-\left(\frac{g\mu_{\mathrm{B}}}{2M_{\mathrm{s}}V}\right)a^{\dagger}(\mathbf{r})a(\mathbf{r})\right]^{1/2}a(\mathbf{r}), \\ m_{-}(\mathbf{r}) &= \left(\frac{2g\mu_{\mathrm{B}}}{M_{\mathrm{s}}V}\right)^{1/2}a^{\dagger}(\mathbf{r})\left[1-\left(\frac{g\mu_{\mathrm{B}}}{2M_{\mathrm{s}}V}\right)a^{\dagger}(\mathbf{r})a(\mathbf{r})\right]^{1/2}, \\ m_{z}(\mathbf{r}) &= 1-\left(\frac{g\mu_{\mathrm{B}}}{M_{\mathrm{s}}V}\right)a^{\dagger}(\mathbf{r})a(\mathbf{r}), \end{aligned} \qquad [4.36]$$

which satisfy the commutation relation,

$$\left[a(\mathbf{r}), a^{\dagger}(\mathbf{r}')\right] = \delta(\mathbf{r}-\mathbf{r}'). \qquad [4.37]$$

For a uniform magnetic ground state, it is useful to expand the fields $a(\mathbf{r})$ and $a^{\dagger}(\mathbf{r})$ in terms of plane wave states,

$$a(\mathbf{r}) = \sum_{k} \mathrm{e}^{-\mathrm{i}\mathbf{k}\cdot\mathbf{r}} a_k; a^{\dagger}(\mathbf{r}) = \sum_{k} \mathrm{e}^{\mathrm{i}\mathbf{k}\cdot\mathbf{r}} a_k^{\dagger}, \qquad [4.38]$$

where the a_k variables are boson operators that satisfy the commutation relations

$$\left[a_k, a_{k'}^{\dagger}\right] = \delta_{k,k'}. \qquad [4.39]$$

In the macroscopic limit such as the micromagnetics approximation considered here, it suffices to take the spin-wave variables $(a_k, a_k^{\dagger})$ as dimensionless complex numbers (a_k, a_k^{*}). By substituting these variables for the spin deviation operators, the magnetization components can be expressed as

$$\begin{aligned} m_{+}(\mathbf{r}) &= \left(\frac{2g\mu_{\mathrm{B}}}{M_{\mathrm{s}}V}\right)^{1/2}\left[\sum_{k}\mathrm{e}^{-\mathrm{i}\mathbf{k}\cdot\mathbf{r}}a_k - \left(\frac{g\mu_{\mathrm{B}}}{2M_{\mathrm{s}}V}\right)\sum_{k,q,q'}\mathrm{e}^{\mathrm{i}(\mathbf{k}-\mathbf{q}-\mathbf{q}')\cdot\mathbf{r}}a_k^{*}a_q a_{q'} + \ldots\right], \\ m_{-}(\mathbf{r}) &= \left(\frac{2g\mu_{\mathrm{B}}}{M_{\mathrm{s}}V}\right)^{1/2}\left[\sum_{k}\mathrm{e}^{\mathrm{i}\mathbf{k}\cdot\mathbf{r}}a_k^{*} - \left(\frac{g\mu_{\mathrm{B}}}{2M_{\mathrm{s}}V}\right)\sum_{k,q,q'}\mathrm{e}^{\mathrm{i}(-\mathbf{k}+\mathbf{q}+\mathbf{q}')\cdot\mathbf{r}}a_k a_q^{*}a_{q'}^{*} + \ldots\right], \\ m_{z}(\mathbf{r}) &= 1-\frac{g\mu_{\mathrm{B}}}{M_{\mathrm{s}}V}\sum_{kq}\mathrm{e}^{\mathrm{i}(\mathbf{k}-\mathbf{q})\cdot\mathbf{r}}a_k^{*}a_q. \end{aligned} \qquad [4.40]$$

Note that the expression for m_z is exact, while the expressions for the transverse magnetization components represent a power series expansion of the square root function in Eq. (4.36).

A number of magnetic interactions are diagonalized directly by this transformation. One example concerns the Zeeman energy associated with an applied magnetic field along the z-axis, $\mathbf{H} = H_0\hat{\mathbf{z}}$. Because this term couples only to the z component of the magnetization, the total energy expressed in terms of spin-wave variables can be obtained by integrating over the m_z component,

$$E_Z = -\mu_0 H_0 M_s \int \mathrm{d}V m_z(\mathbf{r}) = E_0 + \sum_k \hbar\omega_0 a_k^* a_k, \qquad [4.41]$$

where $E_0 = -\mu_0 H_0 M_s V$ is a constant background term and $\omega_0 = \gamma_0 H_0$. As $n_k = a_k^* a_k$ represents the occupation number of the spin-wave mode k, the Zeeman energy can be interpreted as a sum over all occupied magnon states, where each state costs $\hbar\omega_0$ in energy. In other words, each spin flip created by a magnon increases the total system energy by $\hbar\omega_0$. Another example is the isotropic exchange interaction, which involves terms such as $(\nabla m_+)(\nabla m_-)$ and $(\nabla m_z)^2$. By applying Eq. (4.40) to this interaction, it can be shown that

$$E_{\mathrm{ex}} = \int \mathrm{d}V \mathcal{E}_{\mathrm{ex}}(\mathbf{r}) = \sum_k \hbar\omega_k a_k^* a_k + \sum_{klmn} V_{klmn} a_k^* a_l^* a_m a_n + \cdots \qquad [4.42]$$

where $\omega_k = (2A\gamma/M_s)k^2$ is the linear contribution to the spin-wave frequency in the long wavelength limit. This interaction also leads to higher-order nonlinear terms in the Hamiltonian, such as V_{klmn}, which represents the scattering potential for the four-magnon process.

On the other hand, dipolar interactions are not diagonalized by the spin-wave variables in Eq. (4.40). A pertinent example involves the induced shape anisotropies in nanoscale magnetic elements. For an in-plane magnetized thin film, the dipolar interactions lead to a hard-axis anisotropy of the form

$$E_{\mathrm{d}} = \frac{1}{2}\mu_0 M_s^2 \mathcal{N}_{xx} \int \mathrm{d}V m_x(\mathbf{r})^2, \qquad [4.43]$$

with $\mathcal{N}_{xx}$ being a transverse component of the demagnetizing tensor. As m_x^2 contains terms such as $m^+ m^+$ and $m^- m^-$, in addition to the $m^+ m^-$ terms, the lowest-order spin-wave expansion of the hard-axis anisotropy leads to

$$E_{\mathrm{d}}^{(2)} = \sum_k \left(A_k a_k^* a_k + B_k a_k a_{-k} + B_k^* a_k^* a_{-k}^* \right), \qquad [4.44]$$

where A_k and B_k are complex scattering amplitudes that depend on the details of the geometry [52,53]. The dipolar interaction leads to a scattering between $+\mathbf{k}$ and $-\mathbf{k}$ spin waves, which indicates that the plane wave states chosen in the transformation (Eq. 4.40) are not the true eigenmodes of the system. The correct eigenmodes can be found by applying a Bogoliubov transformation to a set of spin-wave variables b_k,

$$\begin{bmatrix} a_k \\ a_{-k}^* \end{bmatrix} = \begin{bmatrix} u_k & v_k^* \\ v_k & u_k \end{bmatrix} \begin{bmatrix} b_k \\ b_{-k}^* \end{bmatrix} \quad [4.45]$$

where the transformation coefficients are

$$u_k = \sqrt{\frac{A_k + \omega_k}{2\omega_k}}, \quad [4.46]$$

$$v_k = \sqrt{\frac{A_k - \omega_k}{2\omega_k}} \exp(\mathrm{i}\varphi_k), \quad [4.47]$$

$$\omega_k = \sqrt{A_k^2 - 4|B_k|^2}. \quad [4.48]$$

This second transformation leads to the desired form for the lowest-order bilinear term,

$$E_{\mathrm{d}}^{(2)} = \sum_k \hbar \omega_k b_k^* b_k. \quad [4.49]$$

The phase φ_k in the transformation is related to the azimuthal angle of the wavevector $\mathbf{k}$. The eigenmodes b_k represent elliptical precession of the magnetization, where the ellipticity is determined by the B_k terms. Physically, magnetization precession is elliptical when the transverse demagnetization factors are different, which is the case for in-plane magnetized systems in a thin film geometry. Note also that the ellipticity of a spin-wave mode depends on its propagation direction with respect to the static magnetization orientation, as described by the presence of the phase φ_k.

For nonuniform micromagnetic ground states, the spin-wave eigenmodes are unlikely to be simple plane wave states such as those used in the transformation in Eq. (4.40). In such cases, it is possible to obtain the eigenmode profiles using a Taylor series expansion of the magnetic energy functional (Eq. 4.25). Let $\eta(\mathbf{r})$ and $\xi(\mathbf{r})$ represent fluctuations about the equilibrium magnetic state, defined by the profile $(\Theta_0(\mathbf{r}), \Phi_0(\mathbf{r}))$ in spherical coordinates. Thus, the energy functional $E[\Theta, \Phi]$ can be expanded as

$$E[\Theta_0+\eta,\Phi_0+\xi]=E[\Theta_0,\Phi_0]+\int \mathrm{d}V\left[\frac{\delta E}{\delta\Theta}\right]_{(\Theta_0,\Phi_0)}\eta(\mathbf{r})+\int \mathrm{d}V\left[\frac{\delta E}{\delta\Phi}\right]_{(\Theta_0,\Phi_0)}\xi(\mathbf{r})+\frac{1}{2!}\int \mathrm{d}V\int \mathrm{d}V'\left[\frac{\delta^2 E}{\delta\Theta(\mathbf{r})\delta\Theta(\mathbf{r}')}\right]_{(\Theta_0,\Phi_0)}\eta(\mathbf{r})\eta(\mathbf{r}')+\frac{1}{2!}\int \mathrm{d}V\int \mathrm{d}V'\left[\frac{\delta^2 E}{\delta\Phi(\mathbf{r})\delta\Phi(\mathbf{r}')}\right]_{(\Theta_0,\Phi_0)}\xi(\mathbf{r})\xi(\mathbf{r}')+\ldots, \quad [4.50]$$

where terms such as $\delta E/\delta\Theta(\mathbf{r})$ represent functional derivatives. The first-order functional derivatives vanish as these constitute the differential equations satisfied by the equilibrium state, ($\Theta_0(\mathbf{r})$, $\Phi_0(\mathbf{r})$), by definition. The second-order terms in the expansion typically lead to eigenvalue equations for the fluctuations η and ξ of the form

$$\left[-\nabla^2+f(\eta(\mathbf{r}),\mathbf{r})\right]\eta(\mathbf{r})=\Lambda\eta(\mathbf{r}), \quad [4.51]$$

where the solutions determine the spatial profiles of these fluctuations. By using the appropriate orthogonality relations satisfied by these eigenfunctions, one can use them as the basis for the spin-wave transformation described earlier. An interesting example involves fluctuations about a Bloch domain wall, which represents a special case in which known analytical solutions exist for the ground state and the spin-wave excitations about this state [54,55]. It has been shown that this prescription can be used to obtain bilinear and four-magnon interaction terms to describe how spin waves influence domain wall dynamics under applied fields [56] and spin-polarized currents [57].

By using these transformations to spin-wave coordinates, an approximate spin-wave Lagrangian can be derived,

$$L=\sum_k \mathrm{i}\hbar b_k^* b_k - E, \quad [4.52]$$

where E represents the total spin-wave Hamiltonian. For a harmonic oscillator Hamiltonian $\mathcal{H}=\sum_k \hbar\omega_k b_k^* b_k$, it is straightforward to verify that the Euler–Lagrange equations of motion lead to the expected harmonic time dependence for the spin-wave amplitudes

$$\frac{db_k}{dt} = -i\omega_k b_k. \quad [4.53]$$

In this picture, phenomenological damping can be introduced into the equations of motion directly using the mode-dependent relaxation rate Γ_k,

$$\frac{db_k}{dt} = -i\omega_k b_k - \Gamma_k b_k. \quad [4.54]$$

This represents the dynamics of a damped harmonic oscillator.

3.2. Single-mode theory

The spin-wave formalism developed in the previous section allows for an oscillator model for the spin-torque-driven excitation of a *single* spin-wave mode to be derived. This single-mode theory is largely motivated by experimental observations in which current-driven magnetization oscillations can often be described by the presence of one dominant mode in the power spectrum. As discussed toward the end of this section, the single-mode approximation remains robust even when other competing spin-wave modes are present.

A schematic illustration of how spin-wave excitations are driven by spin torques is shown in Fig. 4.7. There are no excitations at equilibrium at zero

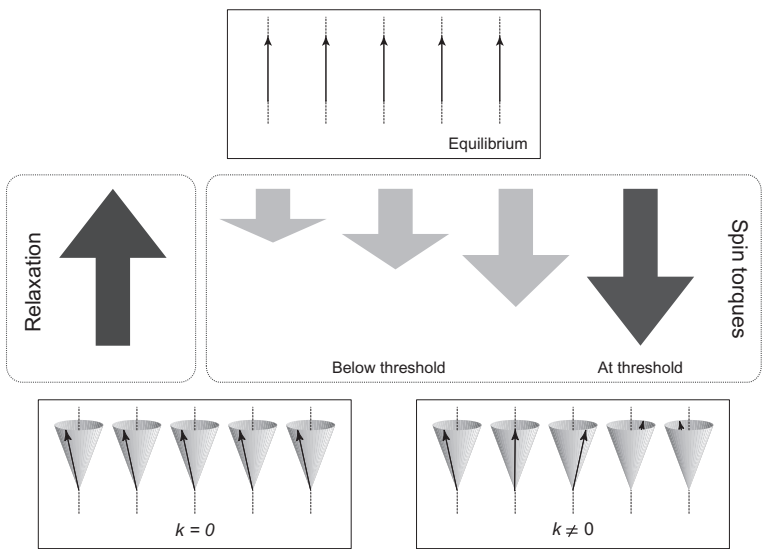

Figure 4.7 Illustration of spin-torque-driven excitations of spin waves. Below threshold, spin torques partially compensate the damping rate of spin waves.

temperature and any excited spin wave decays toward equilibrium through spin-flip processes with a mode-dependent relaxation rate. When a spin-polarized current is present, the transfer of spin angular momentum acts to partially compensate for the spin-wave relaxation. When the rate of spin-transfer matches the relaxation rate of a given mode, a threshold is reached, and self-oscillations of the excited mode appear if the current is further increased. The single-mode theory is based on the premise that the mode with the lowest relaxation rate is excited to self-oscillation.

Let us suppose that a mode of wavevector or index k is driven to self-sustained oscillations by spin-transfer torques. To the fourth order in the spin-wave variables, the Hamiltonian can be written as

$$E_k = \hbar\omega_k b_k^* b_k + T_k b_k^* b_k^* b_k b_k, \tag{4.55}$$

where T_k represents the scattering potential of the four-magnon terms corresponding to the self-interaction of the k mode. As only one mode is assumed to be excited, all three-wave processes that lead to the excitation of modes with either half or double the frequency of the excited mode b_k are neglected in the Hamiltonian. Thus, only self-interacting terms are kept among the possible four-wave processes. By using the random field approximation, averages over pairs of the operators can be made and it is possible to factor out the magnon population $n_k = \langle b_k^* b_k \rangle$ in the four-magnon term. This leads to the simplified form

$$E_k = (\hbar\omega_k + T_k n_k) b_k^* b_k, \tag{4.56}$$

which corresponds to the renormalization of the spin-wave energy due to the finite population n_k of the spin-wave mode.

For a spin polarization $\hat{\mathbf{p}}$ collinear with the quantization axis $\hat{z}$, spin torques result in a change in the damping rate of the spin-wave modes, as the spin angular momentum transferred either enhances or reduces the rate of spin flips associated with the excited magnons. This can be seen by comparing the Slonczewski torque (Eq. 4.20) with the damping term in Eq. (4.15) for an effective field along $\hat{z}$. For parallel orientation of the free- and reference-layer magnetizations, $\hat{p} = \hat{z}$, and a positive $\boldsymbol{J}$ acts to destabilize the free-layer magnetization, while for an antiparallel orientation, $\hat{p} = -\hat{z}$, and a negative $\boldsymbol{J}$ is required for the same effect. In the following discussion, it is assumed that the current flow acts to destabilize the free-layer magnetization.

From Eq. (4.31), the dissipation function is found to be

$$\mathcal{F}_{\mathrm{CPP}} = \eta(\theta)\frac{\hbar J}{\mathrm{e}\, d}\left(m_x \dot{m}_y - m_y \dot{m}_x\right) = \frac{i}{2}\eta(\theta)\frac{\hbar J}{\mathrm{e}\, d}\left(m_+ \dot{m}_- - m_- \dot{m}_+\right). \quad [4.57]$$

After introducing the transformation to spin-wave variables in Eq. (4.40) and ignoring the ellipticity in the precession, the random field approximation can be applied to obtain

$$F_{\mathrm{CPP}} = \int \mathrm{d}V \mathcal{F}_{\mathrm{CPP}} = \mathrm{i}\eta_0 \frac{\hbar}{\mathrm{e}} I \left(\frac{g\mu_{\mathrm{B}}}{M_{\mathrm{s}} V}\right)\left(1 - \frac{g\mu_{\mathrm{B}}}{M_{\mathrm{s}} V} n_k\right)\left(\dot{b}_k^* b_k - b_k^* \dot{b}_k\right), \quad [4.58]$$

where the volume integration is over a film of thickness d and I is the total applied current.

By combining the above results with a phenomenological damping rate Γ_k, the equation of motion for the current-driven mode can be obtained [58]:

$$\frac{\mathrm{d}b_k}{\mathrm{d}t} = -\mathrm{i}\left(\omega_k + \frac{T_k}{\hbar} n_k\right) b_k - \Gamma_k b_k + \eta_0 \frac{\hbar}{\mathrm{e}} I \left(\frac{g\mu_{\mathrm{B}}}{M_{\mathrm{s}} V}\right)\left(1 - \frac{g\mu_{\mathrm{B}}}{M_{\mathrm{s}} V} n_k\right) b_k. \quad [4.59]$$

At this point, it is convenient to rescale the magnon variables,

$$c_k = \left(\frac{g\mu_{\mathrm{B}}}{M_{\mathrm{s}} V}\right)^{1/2} b_k, \quad [4.60]$$

where the new c_k represents a fraction of the spin deviation in scaled units, rather than individual spin flips as given by the b_k variables. Similarly, the magnon population is recast as a dimensionless mode power, $|c_k|^2 = n_k(g\mu_{\mathrm{B}}/M_{\mathrm{s}} V)$, which leads to the simplified form [59,60]

$$\frac{\mathrm{d}c_k}{\mathrm{d}t} = -\mathrm{i}\left(\omega_k + N_k |c_k|^2\right) c_k - \left(\Gamma_k - \sigma I + \sigma I |c_k|^2\right) c_k, \quad [4.61]$$

where

$$N_k = \frac{T_k}{\hbar}\frac{g\mu_{\mathrm{B}}}{M_{\mathrm{s}} V} \quad [4.62]$$

represents a nonlinearity coefficient of the mode frequency and

$$\sigma = \eta_0 \frac{\hbar}{\mathrm{e}}\frac{g\mu_{\mathrm{B}}}{M_{\mathrm{s}} V} \quad [4.63]$$

is a parameter describing the spin-transfer efficiency. The product σI, which has units of angular frequency, represents the rate of spin angular momentum

transferred to the spin-wave mode. For positive currents $I > 0$, the spin transfer opposes Γ_k and can therefore be interpreted as a negative damping.

The nonlinearity in the spin-transfer term gives rise to the self-oscillatory state. The spin-wave mode amplitude c_k can be expressed in terms of its amplitude r and phase ϕ,

$$c_k(t) = r(t)e^{i\phi(t)}, \tag{4.64}$$

which upon substitution into Eq. (4.61) leads to the following coupled equations of motion,

$$\frac{dr}{dt} = -\left(\Gamma_k - \sigma I + \sigma I r^2\right) r, \tag{4.65}$$

$$\frac{d\phi}{dt} = -\left(\omega_k + N_k r^2\right). \tag{4.66}$$

As discussed previously in Section 2, this represents a dynamical system in which a limit cycle appears through a supercritical Hopf bifurcation. It is useful to define the supercriticality parameter ζ as

$$\zeta = \frac{\sigma I}{\Gamma_k} \equiv \frac{I}{I_{th}}, \tag{4.67}$$

where $I_{th} = \Gamma_k/\sigma$ is the threshold current for self-oscillations. Thus, the condition for self-oscillations is defined by the point at which the rate of negative damping, σI, compensates for the rate of positive damping, Γ_k, as illustrated in Fig. 4.7. In the single-mode picture, the underlying assumption is that the excited mode corresponds to the mode with the lowest damping rate Γ_k, which corresponds to the mode with the lowest threshold current. The equation of motion for the mode amplitude becomes

$$\frac{dr}{dt} = -\Gamma_k\left(1 - \zeta + \zeta r^2\right) r. \tag{4.68}$$

In the subcritical regime (or below threshold), $\zeta \leq 1$, the only admissible stationary solution to this equation is the trivial $r_0 = 0$ solution. This corresponds to the case in which the dynamical solution only has a stable fixed point at origin, where all trajectories in phase space spiral toward this fixed point. Above the threshold or in the supercritical regime $\zeta > 1$, we have the appearance of a stable limit cycle with a radius defined by

$$r_0^2 = \frac{\zeta - 1}{\zeta}. \tag{4.69}$$

In this regime, $r_0 = 0$ becomes an unstable fixed point, and all trajectories in phase space spiral toward the limit cycle defined in Eq. (4.69). Note that the nonlinearity in the spin-torque term is required for the existence of the stable limit cycle.

The sign of the frequency nonlinearity depends on the geometry of the free layer and the nature of the spin-wave mode excited. Because this nonlinearity originates from the self-interacting terms in the four-wave scattering processes, its sign depends on the nature of the dominant terms that contribute to these processes. In the systems of experimental interest, the dominant contribution to the nonlinearity arises from the shape anisotropy associated with dipolar interactions.

To see how the nonlinearity coefficient can be obtained in practice, consider the simple example of the uniform precession mode ($k = 0$) in a nanoelement in which the static magnetization is perpendicular to the film plane. Let z represents the axis perpendicular to the film plane and assume that an external field H_0 is also applied along this direction. The magnetic energy in this configuration is

$$E = \mu_0 M_s \int \mathrm{d}V \left(-H_0 m_z(\mathbf{r}) + \frac{1}{2} \mathcal{N}_{zz} M_s m_z(\mathbf{r})^2 \right), \qquad [4.70]$$

where $\mathcal{N}_{zz} \approx 1$ represents the demagnetizing factor for the shape anisotropy in this geometry. By applying the transformation to spin-wave variables as before $b \equiv b_0$, the following Hamiltonian is obtained:

$$\mathcal{H} = \hbar\gamma_0 (H_0 - \mathcal{N}_{zz} M_s) b^* b + \hbar\gamma_0 \mathcal{N}_{zz} \frac{g\mu_B}{2V} b^* b^* b b. \qquad [4.71]$$

As before, a random phase approximation can be applied to factor out the mode population $n_0 = \langle b^* b \rangle$,

$$\mathcal{H} = \hbar\gamma_0 (H_0 - \mathcal{N}_{zz} M_s) b^* b + \hbar\gamma_0 \mathcal{N}_{zz} \frac{g\mu_B}{V} n_0 b^* b. \qquad [4.72]$$

From this, it can be recognized that $T_0 = \hbar\gamma_0 \mathcal{N}_{zz} g\mu_B / V$, from which the nonlinear mode frequency (in oscillator variables) can be deduced to be

$$\omega_0 = \gamma_0 (H_0 - \mathcal{N}_{zz} M_s) + N_0 |c|^2, \qquad [4.73]$$

where

$$N_0 = \gamma_0 M_s \mathcal{N}_{zz} \qquad [4.74]$$

is positive in this case. The mode frequency therefore increases with the mode power (and supercriticality) in this geometry, a phenomenon often referred to as a frequency *blueshift* [61,62].

For in-plane magnetized configurations in thin films, a simple expression for the nonlinear coefficient N_k is more difficult to obtain because magnetization precession is elliptical and Bogoliubov transformations are required to diagonalize the spin-wave Hamiltonian [58]. Nevertheless, for an arbitrary orientation of the equilibrium magnetic state, Slavin and Kabos showed that an approximate form for the nonlinear coefficient N_0 can be obtained from dependence of the ferromagnetic resonance mode as a function of the magnetization angle out of the film plane [59]. It is found that

$$N_0(\theta) \approx \gamma_0 M_s \frac{H_0}{2\sqrt{H_0(H_0 + M_s \cos^2\theta)}} \frac{2 - (1 + M_s/H_0)\cot^2\theta}{1 + (1 + M_s/H_0)\cot^2\theta}, \qquad [4.75]$$

where θ represents the angle between the equilibrium magnetization orientation and the film plane. We note that for the in-plane magnetized case ($\theta = 0$),

$$N_0 \approx -\frac{1}{2}\gamma_0 M_s \sqrt{\frac{H_0}{H_0 + M_s}}. \qquad [4.76]$$

This shows that the nonlinearity leads to a frequency *redshift* in in-plane magnetized systems, which has been confirmed in a number of experiments [13,14,62,63].

3.3. Bullets in nanocontacts

An interesting example of localized spin-wave modes occurs in the nanocontact geometry (see Fig. 4.5). In this geometry, currents are applied to an extended spin valve film through a small metallic contact, with lateral sizes ranging from 20 to 200 nm, which leads to spin torques being applied only locally in the vicinity of the nanocontact. For an in-plane magnetized system, it has been shown earlier that the frequency nonlinearity of quasi-uniform modes leads to a decrease in the mode frequency as the mode amplitude increases. As a result, it is possible for spin torques to drive modes into the spin-wave gap of the film, that is, below the frequency defined by the approximate dispersion relation $\omega(k) = \sqrt{\omega_k(\omega_k + \omega_M)}$, where $\omega_K = \gamma_0 H + Dk^2$, $\omega_M = \gamma_0 M_s$, and H is the applied field in the film plane.

Slavin and Tiberkevich approached this problem by expanding the oscillator equation to account for mode dispersion and the localized nature of the spin torques in nanocontacts [64]. They considered the dynamics of the uniform spin-wave mode for which a spatial variation in the mode amplitude is allowed, $c_0 = c_0(\mathbf{r}, t)$,

$$\frac{dc_0}{dt} = -i\left(\omega_0 - D\nabla^2 + N_0|c_0|^2\right)c_0 - \Gamma_0 c_0 + \sigma I f(r/R_c)\left(1 - |c_0|^2\right)c_0, \quad [4.77]$$

where N_0 is given by Eq. (4.76) and $f(r/R_c)$ is a function that describes the spatial distribution of the applied current, and R_c is the radius of the circular nanocontact. We may recognize that in the absence of damping and current ($\Gamma_0 = 0$, $I = 0$), the ansatz

$$c(r,t) = C_0\psi(r/l)e^{-i\omega t}, \quad [4.78]$$

where $\omega = \omega_0 + N_0 C_0^2$, leads to a nonlinear Schrödinger equation for the dimensionless function $\psi(x)$:

$$\psi'' + \frac{1}{x}\psi' + \psi^3 - \psi = 0. \quad [4.79]$$

As the dispersion $D > 0$ and nonlinearity $N < 0$ have opposite signs, the Lighthill criterion $ND < 0$ indicates that localized solitonic solutions to $\psi(x)$ are possible. This criterion expresses the fact that soliton structures are only stable when the dispersive nature of a wave is compensated by a nonlinearity, for example, in the Bloch domain wall where the exchange interaction prefers to spread out the rotation between neighboring spins (dispersion) but the anisotropy prefers to minimize this spread by aligning spins along the easy axis (nonlinearity). Numerical solutions to this nonlinear differential equation show that the excited mode is a localized nonlinear spin-wave mode, or bullet, which exists primarily in the nanocontact region. It is found that the calculated mode frequency agrees well with measured experimental spectra on nanocontacts [65], as shown in Fig. 4.8a. The stability of the bullet mode has also been confirmed by micromagnetics simulations [66,67], where it is found that the excitation of the mode exhibits a hysteretic behavior as a function of applied current. A comparison of the simulation profiles of the self-localized bullet mode and propagating spin-wave modes in a nanocontact geometry are given in Fig. 4.8b. Clear signatures of the bullet mode have also been brought to light in more recent experiments [68,69], where the existence of the mode as a function of the frequency nonlinearity N_0, varied experimentally by tilting the magnetization out of

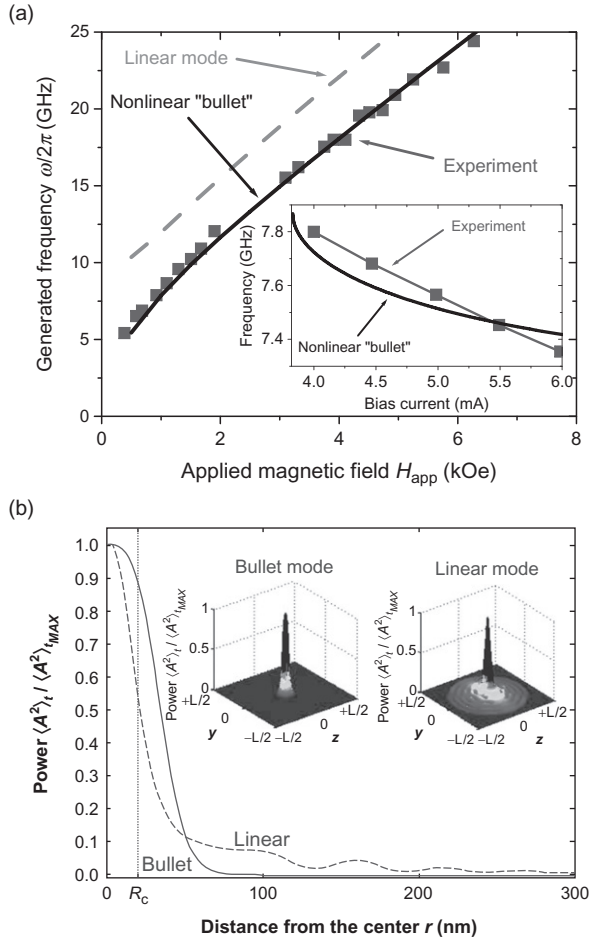

Figure 4.8 Localized spin-wave bullets in magnetic nanocontacts. (a) Comparison between theory and experiment for the field dependence of the bullet frequency, *after Ref. [64]*. (b) Results of micromagnetic simulations showing the difference between the spatial profiles of localized bullet and propagating linear modes. *After Ref. [66]*. © *American Physical Society*.

the film plane, has been studied. Simulations of nanocontacts on a wire geometry have also revealed localized excitations [70].

3.4. Nanocontacts as spin-wave emitters

For systems with magnetization oriented out of the film plane, the frequency blueshift of the excited mode does not lead to self-confinement effects for dynamics in a nanocontact system. In contrast, the driven magnetization

leads to the generation of radiative spin-wave modes that propagate outward from the nanocontact in the magnetic free layer [11,59]. An example of a computed spatial profile of such propagative modes is given in Fig. 4.8b.

Hoefer *et al*. showed that a variety of propagating mode structures appear when the current-induced Oersted–Ampère fields in the nanocontact are taken into account [71]. For current flow perpendicular to the film plane through a circular nanocontact, the associated Oersted–Ampère fields consist of concentric circular field lines centered around the nanocontact, whose magnitude varies as a function of radial distance from the nanocontact center, much like the magnetic fields generated by a cylindrical wire. If an additional uniform magnetic field is applied to the free layer, the circular symmetry of the Oersted–Ampère field is broken. As a result, spin-wave propagation away from the nanocontact becomes anisotropic, leading to the possibility of generating collimated spin-wave beams and vortex spiral waves [71]. The nature of the excited modes is shown to depend strongly on material parameters, such as the film thickness of the free magnetic layer, and the relative magnitude of the external and Oersted–Ampère fields.

Experimental evidence for propagating spin-wave modes was first deduced from measurements of mutual phase-locking between two nanocontact oscillators sharing the same free magnetic layer [72,73]. In this geometry, the nanocontacts are independently current-biased and separated by edge-to-edge distances of 150 nm to 1 μm. When both nanocontacts are driven to self-oscillation, the propagating spin waves emitted at each nanocontact give rise to an effective coupling between the two oscillators [74], which leads to clear signatures of synchronization, such as frequency-pulling and increased power output, over a certain interval of the applied current [72,75]. By using focused-ion beams to physically cut the magnetic film in between the two nanocontacts, it was shown that the mutual phase-locking could be strongly suppressed [73]—a result expected for spin-wave-mediated interactions. Direct measurements of propagating spin waves have been achieved since the development of spatially resolved Brillouin light spectroscopy. Demidov *et al*. produced a two-dimensional map of the spin waves emitted from an elliptical nanocontact and showed that the intensity of the emitted beams depends strongly on the in-plane magnetic field orientation [76,77]. Other Brillouin light scattering experiments by Madami *et al*. showed that the emitted spin waves can be measured up to a few microns from the nanocontact in permalloy films [78]. These results highlight the possibility of employing magnetic nanocontacts as spin-wave emitters for potential applications in magnonics [77,79]. It has

been shown that operation frequencies as high as 65 GHz can be reached in the nanocontact geometry [80].

3.5. Multiple modes

The discussion so far has been centered on a single-mode approximation in which the spin-wave eigenmode with the lowest damping rate dominates the excitation spectrum under spin torques. An interesting question arises when the excitation threshold for two modes is sufficiently close such that the competition between these modes cannot be neglected. To account for this scenario, it is necessary to retain terms in the three- and four-wave interactions that can contribute to the coupling between the two modes.

Consider the following spin-wave Hamiltonian representing two interacting modes:

$$\mathcal{H} = \sum_{k=1,2} \hbar\omega_k b_k^* b_k + \sum_{k,l,m,n=1,2} T_{klmn} b_k^* b_l^* b_m b_n. \qquad [4.80]$$

The four-wave interaction term represents higher-order processes originating from the exchange and dipolar interactions. As before, the interaction term can be simplified by using a mean field approximation in which the magnon population is factored out and ensemble-averaged two-magnon processes, such as $\langle b_k^* b_m \rangle$ for $k \neq m$, are ignored,

$$\sum_{k,l,m,n=1,2} T_{klmn} b_k^* b_l^* b_m b_n \approx \sum_{k,m=1,2} T_{km} \langle b_k^* b_k \rangle b_m^* b_m, \qquad [4.81]$$

where $\langle b_k^* b_k \rangle = n_k$ is recognized as the mode population, as before. By applying similar approximations to the spin-torque term, the modified equation of motion for the mode k in oscillator variables can be written as

$$\frac{\mathrm{d}c_k}{\mathrm{d}t} = -\mathrm{i}\left(\omega_k + N_k|c_k|^2\right)c_k - \left(\Gamma_k - \sigma I + \sigma I|c_k|^2\right)c_k + \left(\mathrm{i}N_{km} + \sigma_{km} I\right)|c_m|^2 c_k. \qquad [4.82]$$

Here, σ_{km} represents the contribution from the spin-torque-induced coupling between the two modes. The equation of motion for the m mode can be obtained by interchanging the k and m indices in Eq. (4.82). This equation shows that the coupling between the two modes depends on the intensity or population of each mode.

De Aguiar *et al.* showed that such an interacting two-mode system leads to a rich nonlinear dynamics, which shares key features of the population

dynamics of predator–prey models [81]. Their calculations are based on material parameters taken from an experimental study of oscillations in a nanopillar device [82]. The modes considered have frequencies of $\omega_1 = 4.275$ GHz and $\omega_2 = 10.09$ GHz, and an identical threshold current is taken for both modes. The population dynamics was obtained using numerical integration of the coupled nonlinear equations of motion, with the thermal magnon population for each mode serving as the initial conditions for the magnon power $|c_k|$. It was found that the coexistence of the two spin-wave modes occurs only within a small interval of the supercriticality, $1 < \zeta < 1.2$, after which only one dominant mode is seen in the steady state. For supercriticalities in the range of $1.2 < \zeta < \zeta_c$, where $\zeta_c \backsimeq 2.662$, only the ω_1 mode exists, while for $\zeta > \zeta_c$, only the ω_2 is seen in the steady state. This mode transition is illustrated in Fig. 4.9a, where the population of the two modes is presented as a function of supercriticality.

The phase portrait of this dynamics is presented in Fig. 4.9b at the supercriticality $\zeta = \zeta_c$ at which the mode transition takes place. One observes the existence of an unstable fixed point at the origin, corresponding to the trivial case of no oscillations, in addition to the presence of two stable fixed points corresponding to finite population levels for either mode 1 or mode 2, and a saddle point at finite population values for both modes. Thus, the nature of the dominant mode excited depends very much on the initial conditions, and fluctuations in experimental systems could potentially lead to different modes being measured depending on how the corresponding

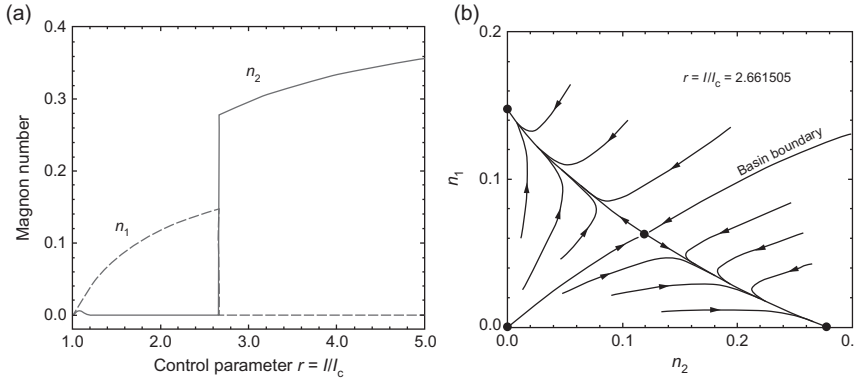

Figure 4.9 Illustration of population dynamics in an interacting two-mode system. (a) Mode population as a function of supercriticality. (b) Phase space of the mode populations, illustrating different scenarios of mode competition at a supercriticality of $\zeta = 2.661505$. *After Figs. 3 and 4 of Ref. [81].* © *American Physical Society.*

experiment would be performed. The phase portrait highlights the analogy with population dynamics in biological systems such as the Lotka–Volterra model [15], which describes the evolution of two competing species with access to the same finite food resources. In such models, the different growth rates of each species and the interaction between the two often lead to one species driving the other to extinction [15]. For the two-mode oscillator, the limit cycle for one oscillation mode is made possible by compensating for damping with the incoming flux of spin angular momentum through spin-transfer torques, at the expense of populating the second mode. Because such dynamics are strongly nonlinear and depend very much on initial conditions and the supercriticality, signatures for such mode transitions in experiment could appear as a hard excitation for one mode (e.g., mode 2 in Fig. 4.9a) or stochastic hopping between the two modes.

4. ROLE OF THERMAL NOISE

4.1. Stochastic oscillator model

Noise is present in any physical system at finite temperatures. In the context of self-sustained oscillations, thermal fluctuations perturb the dynamics such that the oscillator encounters random perturbations to its trajectory along the limit cycle. The influence of noise is important because it determines the line shape of the power spectral density of the oscillations and therefore limits the quality factor and power of such oscillators. While theoretical methods for treating noise in self-sustained oscillators are well established [83–86], spin-torque oscillators present a unique feature in their strong frequency nonlinearity, where frequency shifts can be much larger than spectral linewidths, $N|c_k|^2 \gg \delta\omega$, as observed in Fig. 4.1. As a result, quantitative theories for spin-torque oscillators require this nonlinearity to be accounted for explicitly. In this section, the influence of noise on the self-sustained dynamics of the current-driven spin-wave modes is discussed. In particular, the single-mode theory is extended to include stochastic terms in the equations of motion, which is then solved in certain limits to obtain the spectral properties of the oscillation mode.

Noise can be accounted for in the oscillator model (Eq. 4.61) by including a stochastic term $f_k(t)$ in the equation of motion [87]

$$\frac{\mathrm{d}c_k}{\mathrm{d}t} = -\mathrm{i}\left(\omega_k + N_k|c_k|^2\right)c_k - \left(\Gamma_k - \sigma I + \sigma I|c_k|^2\right)c_k + f_k(t), \qquad [4.83]$$

which results in a stochastic differential equation for the mode amplitude c_k. The stochastic term is a phenomenological representation of the interaction between the excited spin-wave mode and the thermal bath with which it is in contact. A physical choice for describing the spectral properties of the stochastic term is a Gaussian white noise associated with thermal magnons, which has zero mean,

$$\langle f_k(t)\rangle = 0, \tag{4.84}$$

and satisfies the two-time correlation function [88]

$$\left\langle f_k^*(t) f_{k'}(t')\right\rangle = 2\Gamma_k n_{k,0}\left(\frac{g\mu_B}{M_s V}\right)\delta_{k,k'}\delta(t-t'). \tag{4.85}$$

$n_{k,0} = [\exp(\hbar\omega_k/k_B T) - 1]^{-1}$ represents the occupation number of the spin-wave mode k at thermal equilibrium. To convince ourselves that this is indeed a suitable choice, let us consider the linear equation in the absence of spin torques,

$$\frac{dc_k}{dt} = -(i\omega_k + \Gamma_k)c_k + f_k(t), \tag{4.86}$$

which has the formal solution

$$c_k(t) = c_{k,0}e^{-(i\omega_k+\Gamma_k)t} + \int_0^t dt' e^{-(i\omega_k+\Gamma_k)(t-t')} f_k(t'). \tag{4.87}$$

By combining this solution with the stochastic oscillator equation (Eq. 4.83) and the noise properties (Eq. 4.85), a differential equation can be derived for the mode power,

$$\frac{d|c_k|^2}{dt} = c_k\frac{dc_k^*}{dt} + c_k^*\frac{dc_k}{dt} = -2\Gamma_k\left[|c_k|^2 - n_{k,0}\left(\frac{g\mu_B}{M_s V}\right)\right], \tag{4.88}$$

which, when expressed in terms of the spin-wave variables b_k (Eq. 4.60), leads to the simple expression

$$\frac{dn_k}{dt} = -2\Gamma_k\left(n_k - n_{k,0}\right), \tag{4.89}$$

where $n_k = \langle b_k^* b_k\rangle$ represents the mode population, as usual. This equation describes how the mode population n_k relaxes toward its thermal equilibrium value at the characteristic rate given by Γ_k. This justifies the choice of the thermal equilibrium occupation $n_{k,0}$ as the magnitude of the thermal

noise source, as in the absence of any driving terms, the mode occupation n_k must go over to its thermal equilibrium value. In the remainder of this discussion, it is assumed that this noise level remains constant with the nonlinearities and the level of supercriticality considered.

As the spin-wave modes of experimental interest are typically in the gigahertz range, it suffices to use the approximation

$$n_{k,0} \approx \frac{k_B T}{\hbar \omega_k} \tag{4.90}$$

for the thermal mode population. With the definition of the noise amplitude q,

$$q = \frac{\alpha \gamma k_B T}{M_s V}, \tag{4.91}$$

where the approximate relation $\Gamma_k \approx \alpha \omega_k$ has been used for the Gilbert relaxation rate, the autocorrelation function for f_k can be written in a more compact form,

$$\left\langle f_k^*(t) f_{k'}(t') \right\rangle = 2q\delta_{k,k'}\delta(t-t'). \tag{4.92}$$

The key physical quantity of interest is the two-time autocorrelation function of the current-driven mode,

$$\mathcal{K}_k(t) = \left\langle c_k^*(t) c_k(0) \right\rangle, \tag{4.93}$$

which gives a quantitative measure of the coherence of the excitations. The Fourier transform of this correlation function gives the power spectral density $\mathcal{S}(\omega)$ of the oscillations,

$$\mathcal{S}(\omega) = \int_{-\infty}^{\infty} dt\, e^{-i\omega t} \mathcal{K}(t). \tag{4.94}$$

In most experiments, electrical measurements of voltage oscillations in spin valves or magnetic tunnel junctions give access to either Eq. (4.93) in time-domain experiments or Eq. (4.94) in the frequency domain. As the stochastic oscillator equation (Eq. 4.83) represents a nonlinear Langevin equation for which an analytical solution is difficult, if not impossible, to obtain, limiting cases in which the stochastic problem is amenable to analytical approaches is examined in the following section.

4.2. Spectral properties in the subcritical limit

In the subcritical limit well below the threshold for self-oscillation, the nonlinearities in the frequency and spin-torque terms can be neglected,

$$\frac{\mathrm{d}c_k}{\mathrm{d}t} = -(\mathrm{i}\omega_k + \Gamma_k - \sigma I)c_k + f_k(t). \quad [4.95]$$

By using Eq. (4.87), a solution to the autocorrelation function for the excited mode amplitude c_k can be constructed,

$$\mathcal{K}_k(t-t') = c_{k,0}^2 \mathrm{e}^{\mathrm{i}\omega_k(t-t')}\mathrm{e}^{-(\Gamma_k-\sigma I)(t+t')} + 2q\mathrm{e}^{\mathrm{i}\omega_k(t-t')}\mathrm{e}^{-(\Gamma k-\sigma I)|t-t'|}, \quad [4.96]$$

where the spectral properties of f_k have been used to simplify the integrals over terms such as $\langle f_k(t)\rangle$ and $\langle f_k^*(t)f_k(t')\rangle$. The first term on the right-hand side represents the short-time correlations, which can be neglected in the long-time limit of large t and t' after which information about the initial condition $c_{k,0}$ is lost. Thus, the power spectrum of the oscillation mode k is found to be

$$\mathcal{S}(\omega) = \frac{4q(\Gamma_k - \sigma I)}{(\omega-\omega_k)^2 + \left(\Gamma_k^2 - \sigma I\right)^2}. \quad [4.97]$$

The power spectrum of the current-driven spin-wave mode k therefore possesses a Lorentzian line shape with a full width at half maximum of

$$\Delta\omega = 2(\Gamma_k - \sigma I). \quad [4.98]$$

The total integrated spectral power remains constant as a function of supercriticality,

$$\int \mathrm{d}\omega S(\omega) = 4\pi q, \quad [4.99]$$

while the spectral line amplitude increases like

$$S(\omega_k) = \frac{4q}{\Gamma_k - \sigma I}. \quad [4.100]$$

From these expressions, one observes that it is possible to estimate the threshold current in experimental systems by extrapolating the linear dependence of $\Delta\omega$ to zero linewidth, which occurs at $\sigma I = \Gamma_k$, that is, at threshold. This method has been employed in magnetic tunnel junctions in which the breakdown voltage of the insulating tunnel barriers does not permit the threshold to be attained [89]. Alternatively, a linear extrapolation of the inverse power $1/S(\omega_k)$ can be used for the same purposes, which has been shown to be useful for estimating the threshold in spin-valve nanopillars [90,91].

4.3. Spectral properties in the supercritical limit

Far above threshold, self-sustained oscillations are described by dynamics along the limit cycle, which remains well-defined in the presence of noise. In this regime, noise leads to two kinds of fluctuations: phase fluctuations, which lead to random jumps along the limit cycle, and amplitude fluctuations, which lead to deviations perpendicular to the motion along the limit cycle. Schematic illustrations of these two kinds of fluctuations are given in Fig. 4.10. As spin torque oscillators exhibit a strong frequency nonlinearity, fluctuations in the amplitude of oscillations will also lead to fluctuations in the instantaneous frequency, which translates to phase fluctuations. Thus, there is a strong phase–amplitude coupling for the fluctuations in these systems.

For sufficiently large supercriticality, the equations of motion can be linearized around the zero-noise limit cycle r_0. Fluctuations around the excited mode amplitude, $\delta r(t)$, can be introduced as follows:

$$c_k(t) = r(t)\mathrm{e}^{-\mathrm{i}\varphi(t)} = (r_0 + \delta r)\mathrm{e}^{-\mathrm{i}\varphi(t)}, \qquad [4.101]$$

where r_0 satisfies Eq. (4.69) and $\delta r \ll r_0$. By substituting this solution into Eq. (4.83) and retaining linear terms in $\delta r(t)$, the following coupled equations for the amplitude and phase variations are obtained [92,93]:

$$\frac{\mathrm{d}\delta r(t)}{\mathrm{d}t} + 2(\sigma I - \Gamma_k)\delta r(t) = \mathrm{Re}\left[\widetilde{f}_k(t)\right], \qquad [4.102]$$

$$\frac{\mathrm{d}\varphi(t)}{\mathrm{d}t} + \omega\left(r_0^2\right) = -2N_k r_0 \delta r(t) + \frac{1}{r_0}\mathrm{Im}\left[\widetilde{f}_k(t)\right], \qquad [4.103]$$

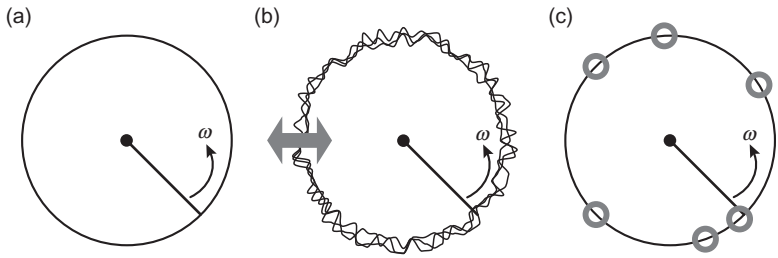

Figure 4.10 Schematic illustration of noise in oscillators. (a) Motion along a circular limit cycle in zero noise at an angular frequency ω. (b) Amplitude noise, which consists of deviations in the amplitude perpendicular to the limit cycle. (c) Phase noise, which consists of jumps along the limit cycle.

where $\omega(r_0^2) = \omega_k + N_k r_0^2$ is the nonlinear mode frequency and $\widetilde{f}_k(t) = f_k(t)e^{i\varphi(t)}$. Terms such as $\delta r(t) f_k(t)$ have been neglected, as it is assumed the noise and amplitude fluctuations are uncorrelated and therefore such terms average to zero. The transformed noise terms $\widetilde{f}_k(t)$ represent noise in the rotating frame of the oscillator. For the oscillator frequencies of interest, it can be assumed that the noise remains white in this rotating frame, such that $\widetilde{f}_k(t)$ possesses the same spectral properties as $f_k(t)$.

The amplitude fluctuations, which are described by an Ornstein–Uhlenbeck process [94], are damped out at a characteristic rate given by

$$\Gamma_a = \sigma I - \Gamma_k = \Gamma_k(\zeta - 1). \qquad [4.104]$$

This rate increases with current, which means that the amplitude of noise-driven excursions from the limit cycle is damped out faster the further the system is driven above threshold. The correlation function for the amplitude fluctuations can be found by integrating the differential equation (Eq. 4.102) and applying spectral properties of the white noise $\widetilde{f}_k$. The fluctuations have zero mean, $\langle \delta r(t) \rangle$, and possess a time correlation of

$$\langle \delta r(t) \delta r(t') \rangle = \frac{q}{2\Gamma_a} e^{-2\Gamma_a |t-t'|}. \qquad [4.105]$$

While $\delta r(t)$ is a Gaussian process by virtue of $\widetilde{f}_k$ being a Gaussian process, the finite relaxation time Γ_a means that these fluctuations have a memory on the order of timescales of Γ_a^{-1}. As such, the amplitude fluctuations have the characteristics of a *colored* noise source. The dissipation rate Γ_a is also an important parameter for determining the oscillator agility, as the rate at which amplitude fluctuations damp out determines the limit at which the oscillator frequency can be modulated. This is a key issue for proposed applications of spin-torque oscillators as field sensors, which are based on the principle of measuring small changes in magnetic fields by detecting concomitant changes in the oscillator frequency [95–97].

The oscillator phase is therefore governed by a stochastic process in which both colored and white noise sources drive the dynamics, as described by the first and second terms on the right-hand side of Eq. (4.103), respectively. By integrating the first-order differential equation (Eq. 4.103), the mean value of the phase is found to be

$$\langle \varphi(t) \rangle = \varphi_0 - \omega(r_0^2)t, \qquad [4.106]$$

where φ_0 is an initial value. By combining this with the spectral properties of $\delta r(t)$ and $\widetilde{f}_k(t)$, and by assuming that these noise sources are uncorrelated, the variance of the phase, $\Delta\varphi^2(t) = \langle\varphi(t)\rangle^2 - \langle\varphi(t)^2\rangle$, can be evaluated to give

$$\Delta\varphi^2(t) = \frac{q}{r_0^2}\left[\left(1+\nu^2\right)|t| - \frac{\nu^2}{2\Gamma_\mathrm{a}}\left(1-\mathrm{e}^{-2\Gamma_\mathrm{a}|t|}\right)\right], \qquad [4.107]$$

where

$$\nu = \frac{N_k}{\Gamma_k\zeta} \qquad [4.108]$$

is a dimensionless nonlinearity parameter. The autocorrelation function for the oscillator can be expressed in terms of the mean and variance of the phase,

$$\mathcal{K}(t) = r_0^2\mathrm{e}^{\mathrm{i}(\langle\varphi(t)\rangle - \langle\varphi(0)\rangle)}\exp\left[-\frac{1}{2}\Delta\varphi^2(t)\right]. \qquad [4.109]$$

The dynamics described in Eq. (4.107) gives rise to features that are not present in oscillatory systems with zero or weak frequency nonlinearities ($\nu \ll 1$). In the linear limit ($\nu = 0$), the phase variance is given by the linear time relation,

$$\Delta\varphi^2(t) = \frac{q}{r_0^2}|t|, \qquad [4.110]$$

where q/r_0^2 can be recognized as a diffusion constant for a Brownian motion-like diffusion in the phase variable. This is a general result for linear frequency oscillators, where the linear time dependence in the phase variance leads to a Lorentzian spectral line shape with a linewidth given by [87]

$$\Delta\omega_0 = \frac{q}{r_0^2}. \qquad [4.111]$$

The linewidth is proportional to the temperature, as $q \propto T$, and is inversely proportional to the mode power, r_0^2. In contrast, spin-torque oscillators can possess a strong frequency nonlinearity, $\nu^2 \gg 1$. It is therefore necessary to consider the nonlinear time dependence of the phase variance (Eq. 4.107) in full.

While no analytical expressions exist for the Fourier transform of the autocorrelation function with the full nonlinear phase variance, it is possible to obtain solutions in two limiting cases. At sufficiently low temperatures where the coherence time of the oscillations, τ_c, is much longer than the

damping rate of the amplitude fluctuations, $\tau_c \gg \Gamma_a^{-1}$, the colored properties of the amplitude fluctuations are unimportant for the phase oscillations and they can be taken to be a white noise source. In this limit, the long-time approximation can be applied to neglect the exponential term in Eq. (4.107), which leads to

$$\Delta\varphi^2(t) \approx \frac{q}{r_0^2}\left(1+\nu^2\right)|t|. \qquad [4.112]$$

A linear time dependence of the phase variance is recovered, but the frequency nonlinearity leads to a renormalization of the linear oscillator linewidth by a factor of $(1+\nu^2)$ [92,93],

$$\Delta\omega_{LT} = \frac{q}{r_0^2}\left(1+\nu^2\right). \qquad [4.113]$$

The spectral line shape is therefore Lorentzian at low temperatures with a linewidth that increases linearly as a function of the temperature. At sufficiently high temperatures at which the coherence time of the oscillations is much shorter than the decay rate of amplitude fluctuations, $\tau_c \ll \Gamma_a^{-1}$, the finite lifetime or "memory" of these fluctuations must be accounted for. A short-time approximation can be used in this limit to expand the exponential in Eq. (4.107) in a power series, giving

$$\Delta\varphi^2(t) \approx \frac{q}{r_0^2}\left(|t| + \nu^2\Gamma_a t^2\right). \qquad [4.114]$$

For sufficiently large frequency nonlinearities, $\nu^2 \gg 1$, the linear term can be neglected and only the quadratic term in t can be retained. In contrast to the linear and low-temperature cases, the spectral function corresponding to a correlation function with a quadratic time dependence is a *Gaussian*,

$$\mathcal{S}_{HT}(\Omega) = \left(\frac{2\pi}{q\Gamma_a}\right)^{1/2}\frac{r_0^{3/2}}{|\nu|}\exp\left[-\frac{r_0^2}{2\nu^2 q\Gamma_a}\left(\Omega-\omega\left(r_0^2\right)\right)^2\right], \qquad [4.115]$$

with a full width at half maximum of

$$\Delta\omega_{HT} = 2\sqrt{2\ln 2}\frac{|\nu|}{r_0}\sqrt{q\Gamma_a}. \qquad [4.116]$$

It is interesting to note that the linewidth in the high-temperature limit varies like $\sqrt{T}$, in contrast to the linear time dependence observed in the linear or low-temperature cases. This behavior is characteristic of *inhomogeneous broadening* [98], where in the present case the amplitude fluctuations lead

to fluctuations in the oscillator frequency as a result of the frequency nonlinearity. This temperature dependence has also been reported in macrospin simulations of spin-torque oscillators [99].

A numerical approach can be used to study the transition between the two regimes. In Fig. 4.11, the temperature dependence of the linewidth is shown for different values of the frequency nonlinearity. The two limiting cases can clearly be identified on the log–log scale, with the linear temperature variation at low temperatures and the $\sqrt{T}$ dependence at high temperatures. The transition between the two regimes occurs over a broad range of temperatures, which shifts toward lower temperatures as the level of frequency nonlinearity increases.

Experimental tests of this theory have been examined by a number of different groups on different systems. Boone *et al.* found good agreement between the analytical theory and the power spectra of spin-torque-driven oscillations in spin-valve systems [100], in particular, on aspects involving the variation of the linewidth, amplitude relaxation rate Γ_a, and line shape as a function of supercriticality. Good agreement has also been found in experiments involving the parametric excitation of spin-torque-driven oscillations

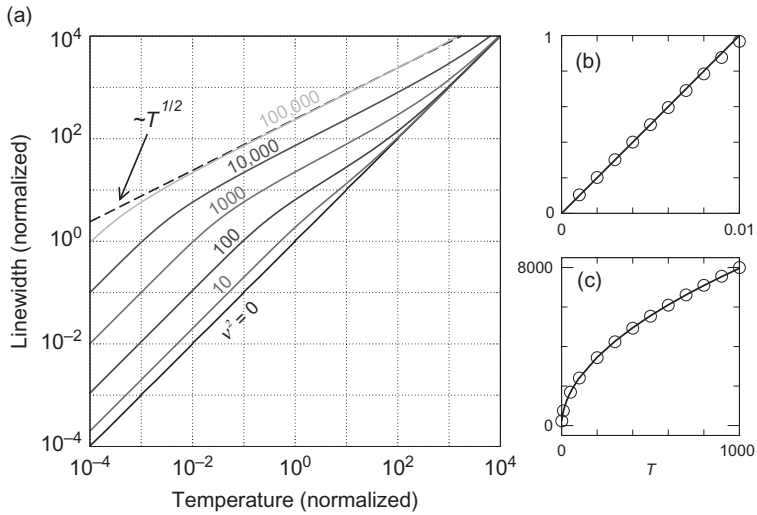

Figure 4.11 Temperature dependence of the oscillator linewidth, with reduced temperature $T' = q/r_0^2$ and time $t' = \Gamma_a t$ variables. (a) Linewidth variations for different values of the frequency nonlinearity parameter ν. (b) Low-temperature behavior for $\nu^2 = 100$, with the solid line being a linear fit. (c) High-temperature behavior for $\nu^2 = 10^4$, with the solid line being a fitted function $\sim T^{0.518}$. Circles in (b) and (c) represent numerical solutions to Eq. (4.107). *After Fig. 1 of Ref. [93].*

in magnetic nanocontacts conducted by Urazhdin *et al.* [101]. Bianchini *et al.* performed time-resolved experiments on current-driven excitations in the synthetic antiferromagnet of a magnetic tunnel junction, in which the phase variance was directly measured as a function of applied current below and above threshold. These measurements allowed for information on the frequency nonlinearity parameter ν and amplitude relaxation rate Γ_a to be extracted [102]. The value of ν has also been determined in magnetic tunnel junctions from studies of the current dependence of the excited power spectra [103]. Quinsat *et al.* studied the amplitude and phase noise in magnetic tunnel junctions using time-resolved measurements, which allowed for the coupling between the phase and amplitude fluctuations to be quantified [104]. A more detailed study on similar structures as a function of temperature has been performed by Sierra *et al.* [105]. However, other time-domain measurements by Keller *et al.* have shown that there are $1/f$ contributions to the low-frequency phase noise [106,107], whose origins remain unknown at present.

Another aspect involves the strong dependence of the spectral linewidth on the nonlinearity parameter, ν. As this parameter is directly related to the nonlinear frequency shift coefficient, N_k, it is possible to vary its magnitude and sign in experiments by changing the nature of the oscillatory mode through applied external magnetic fields. In experiments on magnetic nanocontacts, Rippard *et al.* demonstrated that the spectral linewidth exhibits large variations as a function of the tilt angle of the magnetization with respect to the film plane [108]—a result that was subsequently explained using the oscillator theory presented here [92]. A similar effect has been observed for magnetization dynamics in nanopillars, where a strong linewidth variation has been observed as a function of in-plane orientation of the free-layer magnetization with respect to the easy/hard axes of the nanopillar [109–111]. Similar results have also been observed in magnetic tunnel junctions [112]. It has also been shown theoretically by Gusakova *et al.* that current-induced coupling between the free and reference layers in a magnetoresistive stack can lead to changes in the oscillator linewidth, owing to a modulation of ν [113].

4.4. Line shape distortion near threshold

Simple expressions for the spectral line shape can only be obtained in limiting cases where linearization of the stochastic equations of motion is possible. While such procedures are useful in these limits, a different theoretical approach is required to describe the line shape at arbitrary levels of criticality. In general, the line shape is expected to be non-Lorentzian as a result of the

large coupling between phase and amplitude fluctuations through the strong frequency nonlinearity. A pertinent example of such behavior involves the threshold region, where the amplitude fluctuations are expected to be as large as the oscillation amplitude r_0 itself. In this regime, there is no clear limit cycle about which linearization methods can be applied.

The general problem can be tackled by solving the Fokker–Planck equation associated with the nonlinear Langevin equation in Eq. (4.83). The Fokker–Planck equation describes the time evolution of the probability density function $\mathcal{P}(c_k, t)$, which describes the probability of finding the stochastic oscillator in the state c_k at time t. Because the Fokker–Planck problem involves solving a deterministic linear differential equation, its solution is usually more tractable than the stochastic nonlinear differential equation in Eq. (4.83).

We review the general prescription for constructing the Fokker–Planck problem, which follows the treatment given by Risken [94]. Consider a set of Langevin equations characterizing a set of macroscopic variables $\{x_l\}$,

$$\dot{x}_i = h_i(\{x_l\}) + g_{ij}(\{x_l\})\xi_j, \tag{4.117}$$

where h_i and g_{ij} are functions of the variables $\{x_l\}$, and ξ_j represents a stochastic term with a specified spectral property. If the functions g_{ij} are independent of the variables $\{x_l\}$, then the stochastic processes are termed additive; if they depend on $\{x_i\}$, the processes are termed multiplicative. Now, if the stochastic forces are of the Gaussian white noise type,

$$\langle \xi(t) \rangle = 0; \tag{4.118}$$

$$\langle \xi_i(t)\xi_j(t') \rangle = 2\delta_{ij}\delta(t - t'), \tag{4.119}$$

then the system (Eq. 4.117) describes a Markovian process, which finds an equivalent description in terms of a Fokker–Planck equation for the distribution function $\mathcal{P} \equiv \mathcal{P}(\{x_l\}, t)$,

$$\frac{\partial \mathcal{P}}{\partial t} = \left(-\frac{\partial}{\partial x_i} D_i(\{x_l\}) + \frac{\partial^2}{\partial x_i x_j} D_{ij}(\{x_l\}) \right) \mathcal{P}, \tag{4.120}$$

where D_i is the drift vector,

$$D_i = h_i(\{x_l\}) + g_{kj}(\{x_l\}) \frac{\partial g_{ij}(\{x_l\})}{\partial x_k}, \tag{4.121}$$

and D_{ij} is the diffusion tensor,

$$D_{ij} = g_{ik}(\{x_l\}) g_{jk}(\{x_l\}). \tag{4.122}$$

$\mathcal{P}(\{x_l\},t)$ represents the probability density of finding the system in a state with variables $\{x_l\}$ at an instant t. Unless specified otherwise, summation over repeated indices is assumed.

By applying this approach, the Fokker–Planck equation associated with the amplitude and phase dynamics in Eq. (4.83) can be constructed [114]. Again, the approach relies on the single-mode approximation in which only the mode k is excited. Let $f_k(t)=f_1(t)+\mathrm{i}f_2(t)$. It will also be convenient to scale out the time variable using the relaxation rate as the characteristic time scale, $\tau\equiv\Gamma_k t$. With these definitions, the Langevin equations for the amplitude and phase variables are

$$\frac{\mathrm{d}r}{\mathrm{d}\tau}=-\left(1-\zeta+\zeta r^2\right)r+\frac{1}{\Gamma_k}\left(f_1\cos\varphi+f_2\sin\varphi\right), \qquad [4.123]$$

$$\frac{\mathrm{d}\varphi}{\mathrm{d}\tau}=-\frac{1}{\Gamma_k}\left(\omega_k+N_k r^2\right)+\frac{1}{\Gamma_k r}\left(f_2\cos\varphi-f_1\sin\varphi\right). \qquad [4.124]$$

By using the normalization condition for this coordinate transformation, $\mathcal{P}(r,\varphi,\tau)/r=\mathcal{P}(c_1,c_2,\tau)$, and applying the prescription described earlier, the corresponding Fokker–Planck equation is found to be

$$\frac{\partial\mathcal{P}(r,\varphi,\tau)}{\partial\tau}=\hat{L}_{\mathrm{FP}}\mathcal{P}(r,\varphi,\tau), \qquad [4.125]$$

where the Fokker–Planck operator for the spin-torque oscillator is given by

$$\hat{L}_{\mathrm{FP}}=\frac{\partial}{\partial r}\left[\zeta r^3-(\zeta-1)r-\frac{q}{r}\right]+\left(\widetilde{\omega}_k+\widetilde{N}_k r^2\right)\frac{\partial}{\partial\phi}+q\left(\frac{\partial^2}{\partial r^2}+\frac{1}{r^2}\frac{\partial^2}{\partial\phi^2}\right), \qquad [4.126]$$

with the rescaled parameters

$$\widetilde{N}_k=\frac{N_k}{\Gamma_k},\quad \widetilde{\omega}_k=\frac{\omega_k}{\Gamma_k}. \qquad [4.127]$$

The essence of this technique is to recast the nonlinear Langevin problem in terms of a set of deterministic linear differential equations that can be solved using standard mathematical techniques. Consider the following ansatz for the solution,

$$\mathcal{P}(r,\varphi,\tau)=\mathrm{e}^{-\mathrm{i}\widetilde{\omega}_k\tau}\sum_{m,n}c_{m,n}\xi_m(r)\mathrm{e}^{\mathrm{i}m\varphi}\mathrm{e}^{-\lambda_{m,n}\tau} \qquad [4.128]$$

which leads to an eigenvalue equation for the unknown function $\xi_m(r)$. However, as it stands, the differential equation obeyed by this function is not Hermitian. The Fokker–Planck operator can be brought into Hermitian form with the transformation

$$\hat{L} = \mathrm{e}^{\Phi(r)/2} \hat{L}_{\mathrm{FP}} \mathrm{e}^{-\Phi(r)/2}, \tag{4.129}$$

where

$$\Phi(r) = \frac{1}{2q}\left[\frac{1}{2}\zeta r^4 - (\zeta - 1)r^2\right] - \ln r. \tag{4.130}$$

Thus, if $\xi(r)$ are eigenfunctions of the original Fokker–Planck operator $\hat{L}_{\mathrm{FP}}$, then the functions

$$\psi_{m,n}(r) = \mathrm{e}^{\Phi(r)/2} \xi_{m,n}(r) \tag{4.131}$$

are eigenfuctions of the transformed Hermitian operator $\hat{L}$ with the same eigenvalues $\lambda_{m,n}$. The Hermitian operator leads to a Schrödinger equation for $\psi_{m,n}(r)$,

$$q\frac{\partial^2 \psi_{m,n}}{\partial r^2} - \left[V_n(r) - \lambda_{m,n}\right]\psi_{m,n} = 0, \tag{4.132}$$

where the effective potential has the form

$$V_n(r) = \frac{a_{-2}}{r^2} + a_0 + a_2 r^2 + a_4 r^4 + a_6 r^6, \tag{4.133}$$

which is parameterized by the coefficients

$$\begin{aligned} a_{-2} &= \left(n^2 - \frac{1}{4}\right)q, \\ a_0 &= \zeta - 1, \\ a_2 &= \frac{1}{4q}(\zeta - 1)^2 - 2\zeta - \mathrm{i}\widetilde{N}n, \\ a_4 &= -\frac{(\zeta - 1)\zeta}{2q}, \\ a_6 &= \frac{\zeta^2}{4q}. \end{aligned} \tag{4.134}$$

Thus, the problem of solving the full Fokker–Planck equation is reduced to solving the Schrödinger equation for a fictitious particle in the potential Eq. (4.133).

To compute the spectral line shape of the oscillator, it is necessary to first determine the autocorrelation function $\mathcal{K}(t)$. This function can be expressed in terms of the normalized solutions $\psi_{m,n}(r)$ to the Schrödinger equation,

$$\left\langle c_k^*(t)c_k(t')\right\rangle = \mathrm{e}^{-\mathrm{i}\omega_k t}\sum_m F_{m,1}\mathrm{e}^{-\lambda_{m,1}\Gamma_k|t-t'|}, \qquad [4.135]$$

where only the $n=1$ terms contribute to this sum. (Higher values of the index n are relevant to higher-order correlation functions, such as $n=2$ for correlations of intensity fluctuations $\langle c^*(t)c(t)c^*(t')c(t')\rangle$.) The coefficient $F_{m,n}$ in the series expansion is given by

$$F_{m,n} = \left[\int_0^\infty \mathrm{d}r\, r\psi_{0,0}(r)\psi_{m,n}^*(r)\right] \times \left[\int_0^\infty \mathrm{d}r\, r\psi_{0,0}(r)\psi_{m,n}(r)\right]. \qquad [4.136]$$

As Eq. (4.135) is expressed as a sum of decaying exponential functions in $|t|$, it follows that the Fourier transform of Eq. (4.135) leads to the power spectrum

$$\mathcal{S}(\Omega) = \sum_m \frac{F_{m,1}}{\left[\Omega-\omega_k-\Gamma_k\mathrm{Im}\left(\lambda_{m,1}\right)\right]^2+\left[\Gamma_k\mathrm{Re}\left(\lambda_{m,1}\right)\right]^2}, \qquad [4.137]$$

which consists of a series expansion in terms of partial Lorentzians. Aside from the difference in amplitude $F_{m,1}$, each partial Lorentzian can have a different central frequency and linewidth, depending on the details of the spectrum of complex eigenvalues. The spectral line shape of a spin-torque oscillator is therefore expected to be asymmetric around its central frequency in the general case.

In practice, line shape asymmetry is important only near the threshold, where there are sizable contributions from the first few terms in the expansion (Eq. 4.137). An example of a comparison between theory and experiment is given in Fig. 4.12. The experimental data pertain to a spin-valve nanopillar for which the threshold current is estimated to be $I_{\mathrm{th}} \approx 5.2$ mA. Below this threshold current, the line shape is Lorentzian, where only the lowest-order term in the expansion (Eq. 4.137) contributes to the power spectrum. For applied currents slightly above the threshold, nonnegligible contributions from the higher-order terms are observed, which lead to a measurable distortion in the spectral line profile. This distortion leads to the phenomenon of a linewidth minimum just above threshold [114], which has been observed in experiments on spin-valve nanopillars [63,101,115] and in magnetic tunnel junctions [116].

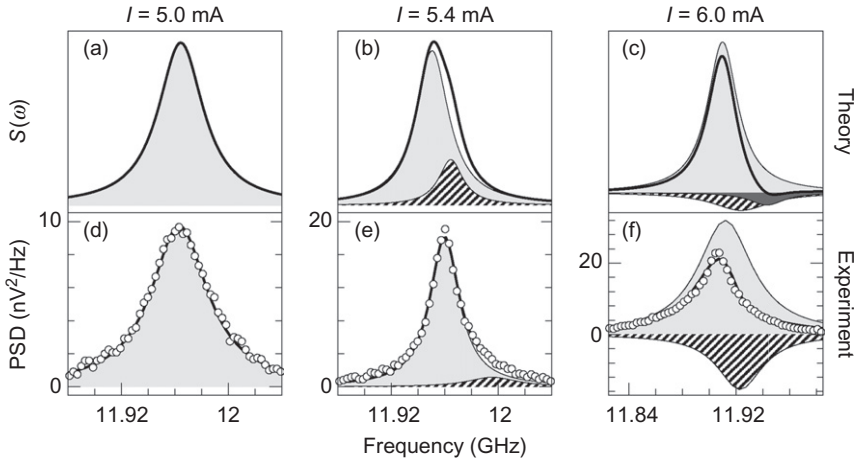

Figure 4.12 Comparison of theoretical and experimental spectral lines near threshold ($I_{th} = 5.2$ mA) for a spin-valve nanopillar oscillator. Thick solid lines in (a)–(c) represent spectral lines as predicted by Eq. (4.137), with the first dominant m modes shown as shaded curves. Circles in (d)–(f) are experimental data at $T = 225$ K taken from Ref. [63] with thick solid lines representing a double Lorentzian fit. Shaded curves are individual Lorentzian profiles used in the fits. *After Fig. 2 of Ref. [114]. © American Physical Society.*

5. VORTEX OSCILLATIONS

5.1. The vortex state and relevant geometries

The discussion in the last two sections has been centered on the self-oscillatory dynamics of linear and nonlinear spin-wave modes. In the linear limit, these modes represent the normal modes of an equilibrium micromagnetic state, which may be spatially nonuniform depending on the oscillator geometry. At large driving currents, nonlinearities arise but can be described as extensions of these linear spin-wave modes. In this section, a different kind of self-sustained dynamics is considered in which the oscillation involves the spatial translation of a well-defined micromagnetic state.

The focus of this section is directed toward the vortex state, which is known to exhibit self-oscillations under spin torques. The vortex state represents a micromagnetic configuration in which the moments curl in the film plane and culminate out of the film plane in a compact region termed the vortex core. The configuration results from a competition between the exchange and dipolar energies of the interacting magnetic moments. This

curling configuration in the film plane, in cylindrical coordinates (r, ϕ, z) for the spatial variable $\mathbf{r}$ (with z being the direction perpendicular to the film plane), can be described by the following ansatz for the azimuthal angle for the magnetization orientation,

$$\Phi_0(\mathbf{r}) = q\phi \pm \frac{\pi}{2}, \qquad [4.138]$$

where $q = \pm 1, \pm 2, \ldots$ is the vorticity and the sign of $\pi/2$ determines whether the moments curl in a clockwise or counterclockwise direction. The $q = 1$ case represents a vortex state where moments rotate by 2π around the vortex core and represents the most common state observed in the experiment, while $q = -1$ corresponds to an antivortex state. By assuming a radially symmetric solution for the polar angle $\Theta(\mathbf{r}) = \Theta(r)$, with the vortex core centered at the origin, the exchange and dipolar terms for the $q = 1$ state gives rise to the total energy

$$E = Ad \int d^2\rho \left[\left(\frac{\partial \Theta(\mathbf{r})}{\partial r} \right)^2 + \frac{\sin^2 \Theta(\mathbf{r})}{r^2} \right] + \frac{\mu_0 M_s^2}{4\pi} \int d^2\rho \int d^2\rho' \cos\Theta(\mathbf{r}) \cos\Theta(\mathbf{r}') G(\rho, \rho'; d), \qquad [4.139]$$

where

$$G(\rho, \rho'; d) = \frac{1}{\|\rho - \rho'\|} - \frac{1}{\sqrt{\|\rho - \rho'\|^2 + d^2}} \qquad [4.140]$$

is a Green's function, with $\mathbf{r} = (\rho, z)$ and d being the film thickness [117]. Note that there are no volume magnetic charges, $\nabla \cdot \hat{\mathbf{m}} = 0$, and the surface magnetic charges are confined to the core region in which there is a magnetization component perpendicular to the film plane. By applying the usual variational scheme, we find that this energy functional is minimized by the equilibrium configuration $\Theta_0(r)$ satisfying the integro-differential equation

$$\frac{\partial^2 \Theta_0(\rho)}{\partial \rho^2} + \frac{1}{\rho} \frac{\partial \Theta_0(\rho)}{\partial \rho} - \frac{\sin 2\Theta_0(\rho)}{2\rho^2} + \frac{\lambda_{ex}}{2\pi d} \sin\Theta_0 \int d^2\rho' G(\rho, \rho'; d) \cos\Theta_0(\rho'), \qquad [4.141]$$

where $\lambda_{ex} = \sqrt{2A/\mu_0 M_s^2}$ is the exchange length. While no analytical solutions exist for the core profile Θ_0, a number of schemes can be used to approximate the solution to differing levels of accuracy [118]. One simple analytical form is the Usov ansatz

$$\cos\Theta_0(\rho) = \begin{cases} p\dfrac{b^2-\rho^2}{b^2+\rho^2} & \rho < b \\ 0 & \rho \geq b \end{cases} \qquad [4.142]$$

where b represents the core radius and p is the vortex core polarization. A comparison of this approximation with a numerically calculated profile is given in Fig. 4.13. As this illustrates, the vortex core represents a compact region in which large changes in the magnetization orientation occur over a characteristic length scale given by λ_{ex}. The lateral extension of the vortex core is typically 10–20 nm and the profiles as shown in Fig. 4.13 have been confirmed in experiments [120].

Vortex states are equilibrium ground states in systems with confined geometries. The simplest example involves the circular magnetic dot in a thin film geometry, where the dot radius L is much larger than the film thickness, $L \gg d$, and $L \gg \lambda_{ex}$. The curling configuration in such systems minimizes the surface magnetic charges at the edges of the dots, as the local moments are parallel to the dot edges everywhere. This configuration therefore minimizes the dipolar energy due to edge surface charges. In spin valves and magnetic tunnel junctions patterned into circular spin valves, it has been shown in a number of experiments that CPP spin torques can drive these vortex states into self-sustained oscillations [121–127].

Vortex states can also be nucleated by localized field sources. An interesting example concerns the magnetic nanocontact, where large electrical currents are applied to a spin-valve multilayer through a small metallic nanocontact, with

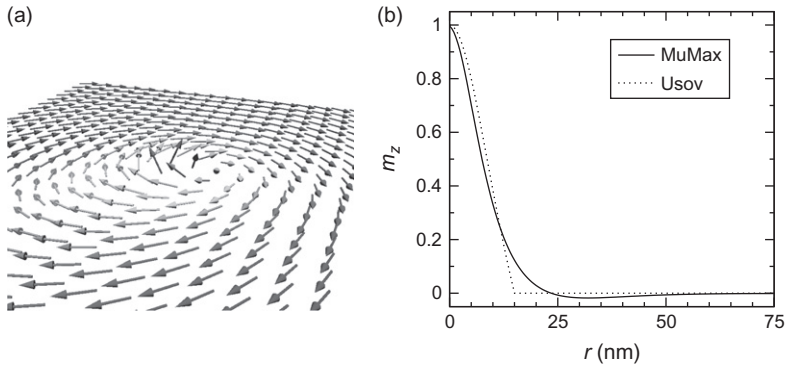

Figure 4.13 Micromagnetic structure of a vortex. (a) Three-dimensional view of the vortex core profile obtained from micromagnetic simulations. (b) Comparison between the simulated core profile, obtained with the MuMax software [119] for a 20-nm-thick permalloy film, and the Usov ansatz (Eq. 4.142).

lateral dimensions of 20–200 nm. As a large component of this current flows perpendicular to the film plane [128,129], the Oersted–Ampère field generated by the current possesses a curling configuration in the film plane, much like the field generated by a perfect cylindrical wire, whose field lines consist of concentric circles around the wire. In such systems, the vortex state appears as a result of minimizing the Zeeman energy associated with this Oersted–Ampère field. In contrast to nanopillars, a combination of CIP and CPP torques is required to drive vortices into self-oscillations in the nanocontact geometry [128,130–133].

5.2. Thiele equation

A magnetic vortex represents a complex micromagnetic structure, so its dynamics requires in principle the time evolution of the magnetization field $\hat{\mathbf{m}}(\mathbf{r},t)$ to be described in all space. However, a reduced set of equations of motion can be obtained by integrating out certain degrees of freedom, much in the same way as the single-mode model for current-driven spin-wave excitations described in the previous sections. One useful approach involves the assumption that the dynamics can be described by a rigid translation of the entire vortex configuration. For dynamics in the film plane (in which magnetization is assumed to be uniform along the film thickness), this approach involves elevating the position of the vortex core, (X_0,Y_0), to a dynamical variable such that the micromagnetic profile becomes $\hat{\mathbf{m}}(\mathbf{r},t)=\hat{\mathbf{m}}[x-X_0(t),y-Y_0(t)]$. Thus, the dynamics of the micromagnetics problem is reduced to a two-dimensional dynamical system defined by $X_0(t)$ and $Y_0(t)$. The resulting equation of motion is referred to as the Thiele equation [134] and forms the basis of the rigid vortex model.

For current-driven vortex dynamics, the Thiele equation can be derived using the Lagrangian formalism detailed in Section 5, where the generalized coordinates are given by $\left(X_0,Y_0,\dot{X}_0,\dot{Y}_0\right)$. Consider first the conservative dynamics given by Eq. (4.25). From the rigid vortex model, the time variation in the azimuthal and polar angles can be expressed as

$$\dot{\Phi}(r,t)=\dot{\mathbf{X}}_0\cdot\nabla_{\mathbf{X}_0}\Phi=-\dot{\mathbf{X}}_0\cdot\nabla_{\mathbf{X}}\Phi \qquad [4.143]$$

and

$$\frac{\mathrm{d}}{\mathrm{d}t}\cos\Theta=-\sin\Theta\left(\dot{\mathbf{X}}_0\cdot\nabla_{\mathbf{X}_0}\Theta\right)=\sin\Theta\left(\dot{\mathbf{X}}_0\cdot\nabla_{\mathbf{X}}\Theta\right), \qquad [4.144]$$

which allows variations of the Berry-phase part of the Lagrangian to be written as

$$\begin{aligned}\frac{\mathrm{d}}{\mathrm{d}t}\frac{\partial L_{\mathrm{B}}}{\partial \dot{X}_0}-\frac{\partial L_{\mathrm{B}}}{\partial X_0}&=-\frac{M_{\mathrm{s}}}{\gamma}\dot{Y}_0\int \mathrm{d}V\sin\Theta\left(\frac{\partial\Theta}{\partial x}\frac{\partial\Phi}{\partial y}-\frac{\partial\Theta}{\partial y}\frac{\partial\Phi}{\partial x}\right),\\ \frac{\mathrm{d}}{\mathrm{d}t}\frac{\partial L_{\mathrm{B}}}{\partial \dot{Y}_0}-\frac{\partial L_{\mathrm{B}}}{\partial Y_0}&=\frac{M_{\mathrm{s}}}{\gamma}\dot{X}_0\int \mathrm{d}V\sin\Theta\left(\frac{\partial\Theta}{\partial x}\frac{\partial\Phi}{\partial y}-\frac{\partial\Theta}{\partial y}\frac{\partial\Phi}{\partial x}\right).\end{aligned} \quad [4.145]$$

These terms can be expressed in a more compact form using the gyrovector,

$$\mathbf{G}=\frac{M_{\mathrm{s}}}{\gamma}\int \mathrm{d}V\sin\Theta(\nabla\Theta\times\nabla\Phi), \quad [4.146]$$

which can be evaluated to be $\mathbf{G}=G\hat{\mathbf{z}}$, where $G=2\pi M_{\mathrm{s}}dpq/\gamma$. By assuming the general form $U=U(X_0,Y_0)$ for the magnetic potential energy experienced by the vortex, the conservative equations of motion associated with the Lagrangian $L=L_{\mathrm{B}}-U$ can be written as

$$\mathbf{G}\times\dot{\mathbf{X}}_0=-\frac{\partial U}{\partial \mathbf{X}_0}, \quad [4.147]$$

where the right-hand side represents the conservative force derived from the potential U. In contrast to more familiar mechanical systems in which a force gives rise to an acceleration, $\mathbf{F}=m\ddot{\mathbf{X}}_0$, the vortex dynamics in the rigid model approximation is manifestly non-Newtonian. The response of the vortex to a force involves motion in a direction perpendicular to this force. For a central potential $U(R_0)$ in which the radial force is directed toward the potential minimum, the vortex dynamics is characterized by a circular gyrotropic motion around the potential minimum. In a general sense, the principle of self-sustained gyration of magnetic vortices involves compensating for damping processes with spin torques such that a dynamical equation like Eq. (4.147) is recovered.

For Gilbert damping, the rigid vortex model leads to terms in the variation of the dissipation function such as

$$\begin{aligned}\frac{\partial W_{\mathrm{G}}}{\partial \dot{X}_0}=&\frac{\alpha M_{\mathrm{s}}}{2\gamma}\int \mathrm{d}V\left[2\dot{X}_0\left(\frac{\partial\Theta}{\partial x}\right)^2+2\dot{Y}_0\left(\frac{\partial\Theta}{\partial x}\right)\left(\frac{\partial\Theta}{\partial y}\right)\right]\\ &+\frac{\alpha M_{\mathrm{s}}}{2\gamma}\int \mathrm{d}V\sin^2\Theta\left[2\dot{X}_0\left(\frac{\partial\Phi}{\partial x}\right)^2+2\dot{Y}_0\left(\frac{\partial\Phi}{\partial x}\right)\left(\frac{\partial\Phi}{\partial y}\right)\right],\end{aligned} \quad [4.148]$$

with a similar expression for $\dot{Y}_0$. These terms can be expressed in a more compact form using the damping dyadic $\overleftrightarrow{\mathbf{D}}$,

$$\overleftrightarrow{\mathbf{D}} = \frac{\mathrm{M_s}}{\gamma}\int \mathrm{d}V\left[\nabla\Theta\otimes\nabla\Theta + \sin^2\Theta(\nabla\Phi\otimes\nabla\Phi)\right], \qquad [4.149]$$

which represents a 2×2 matrix. For the Usov ansatz, the dyadic reduces to $\overleftrightarrow{\mathbf{D}} = \mathrm{D}\overleftrightarrow{\mathbf{I}}$, where $\overleftrightarrow{\mathbf{I}}$ is the identity matrix and $D = (\pi M_s d/\gamma)\ [2+\ln(L/b)]$, where L is the system size and b the vortex core radius. The contribution of the Gilbert term to the equations of motion for the rigid vortex is

$$\frac{\partial W_\mathrm{G}}{\partial \dot{\mathbf{X}}_0} = \alpha D\dot{\mathbf{X}}_0. \qquad [4.150]$$

To obtain the relevant terms describing CPP spin torques, it is useful to decompose the polarization vector $\hat{\mathbf{p}}$ into in-plane and perpendicular-to-plane components, where $\hat{\mathbf{p}} = (p, 0, p_\perp)$ can be defined without loss of generality. For the in-plane component, the relevant term for the dissipation function associated with the CPP torques is

$$\hat{\mathbf{x}}\cdot\left(\hat{\mathbf{m}}\times\frac{\partial\hat{\mathbf{m}}}{\partial t}\right) = \left(\dot{\mathbf{X}}_0\cdot\nabla_{\mathbf{x}}\Theta\right)\sin\Phi + \frac{1}{2}\left(\dot{\mathbf{X}}_0\cdot\nabla_{\mathbf{x}}\Theta\right)\sin 2\Theta\cos\Phi, \qquad [4.151]$$

while for the perpendicular-to-plane component,

$$\hat{\mathbf{z}}\cdot\left(\hat{\mathbf{m}}\times\frac{\partial\hat{\mathbf{m}}}{\partial t}\right) = -\left(\dot{\mathbf{X}}_0\cdot\nabla_{\mathbf{x}}\Theta\right)\sin^2\Theta. \qquad [4.152]$$

This leads to the additional term in the equation of motion,

$$\frac{\partial W_\mathrm{CPP}}{\partial \dot{\mathbf{X}}_0} = \frac{\eta\hbar}{\mathrm{e}d}\int_{\Omega_s}\mathrm{d}V J(\mathbf{r}) \left[p_\parallel(\mathbf{r})\left(\sin\Phi\nabla_{\mathbf{x}}\Theta + \frac{1}{2}\sin 2\Theta\cos\Phi\nabla_{\mathbf{x}}\Phi\right) - p_\perp(\mathbf{r})\sin^2\Theta\nabla_{\mathbf{x}}\Phi\right] \qquad [4.153]$$

where the integration is limited to the volume Ω_s in which the applied currents exist. The integrals above also take into account any spatial variations in the applied current density J and the polarization vector $\hat{\mathbf{p}}$. From the integrals, we can also deduce the role of the $p_{||}$ and $p_\perp$ components of the CPP torques. As $\nabla_{\mathbf{x}}\Theta \neq 0$ and $\sin 2\Theta \neq 0$ only at the vortex core (see profile in Fig. 4.13), the in-plane component of the CPP spin torques acts only on the vortex core region, which results in only a small contribution to the overall

dynamics. On the other hand, $\sin^2\Theta = 1$ everywhere except in the core region, so the perpendicular component of the CPP torques is important.

5.3. Nanocontact oscillations

The rigid vortex model described above gives a suitable approximation to the dynamics in extended systems where boundary conditions are unimportant. A good example of such a system is the magnetic nanocontact where currents are applied locally through a metallic nanocontact, but the spin-valve multilayer is unpatterned and remains a continuous film.

Consider the nanocontact system illustrated in Fig. 4.5, where it is assumed that a vortex state is present in the magnetic free layer and the reference layer is uniformly magnetized but tilted out of the film plane, such that both $p_{||}$ and $p_\perp$ components are nonvanishing. The nanocontact is taken to be circular with radius a. It is assumed that the current flowing through the nanocontact is spatially uniform within the nanocontact, $J(\mathbf{r}) = I/(\pi a^2)$, where I is the applied current, and zero everywhere outside the nanocontact. By using the Usov ansatz, the CPP spin-torque terms can be evaluated to give the force

$$\frac{\partial W_{\mathrm{CPP}}}{\partial \dot{\mathbf{X}}_0} = \frac{\eta \hbar I}{\mathrm{e}} \left(p_{||} \frac{b}{a^2} \begin{bmatrix} p \\ 0 \end{bmatrix} \mathfrak{H}(R_0 - a) + p_\perp \frac{1}{2R_0^2} \begin{bmatrix} -Y_0 \\ X_0 \end{bmatrix} \right), \qquad [4.154]$$

where $\mathfrak{H}(x)$ is the Heaviside function and $R_0 = \sqrt{X_0^2 + Y_0^2}$ is the radial position of the vortex core. The $p_{||}$ contribution is obtained by restricting the integration over the core region, leading to a constant force while the core is located within the nanocontact but vanishes when the core is outside it. As such, this component of the CPP torques is only active for transient dynamics where the core is situated inside the nanocontact region. Otherwise, this term can be neglected for steady-state gyration of the vortex core outside the nanocontact, which is the regime of interest. The $p_\perp$ contribution is obtained by neglecting contributions from the core magnetization, that is, by assuming $\sin^2\Theta_0 \approx 1$ everywhere, and integrating over the whole nanocontact region. This term is active for all positions of the vortex core relative to the nanocontact area. In the following discussion, only the $p_\perp$ will be considered, which allows the CPP torques to be written as

$$\frac{\partial W_{\mathrm{CPP}}}{\partial \dot{\mathbf{X}}_0} = \frac{\eta \hbar I}{2\mathrm{e}} p_\perp \frac{\hat{\mathbf{z}} \times \mathbf{X}_0}{R_0^2}. \qquad [4.155]$$

As discussed in Section 5, the CIP spin torques can be included by generalizing the time derivatives to convective derivatives in the equations of

motion for magnetization. The adiabatic torques can be found by using the substitution $\partial_t \rightarrow \partial_t + \mathbf{u}\cdot\nabla$. Recall that the rigid vortex approximation allows the time derivatives to be expressed in terms of the core velocity, as shown in Eq. (4.143). As the drift term induced by the adiabatic spin torques, $\mathbf{u}\cdot\nabla$, shares the same form as Eq. (4.143), they can be incorporated into the gyrovector term in the equations of motion by inspection using the substitution $\dot{\mathbf{X}}_0 \rightarrow \dot{\mathbf{X}}_0 - \mathbf{u}$ if $\mathbf{u}$ is spatially uniform. To a good approximation, the adiabatic spin torque contribution leads to [135]

$$\frac{\mathrm{d}}{\mathrm{d}t}\frac{\partial L_{\mathrm{ad}}}{\partial \dot{\mathbf{X}}_0} - \frac{\partial L_{\mathrm{ad}}}{\partial \mathbf{X}_0} = -\mathbf{G}\times\mathbf{u}(\mathbf{X}_0). \qquad [4.156]$$

For the nonadiabatic spin-torque terms, the relevant substitution is $\partial_t \rightarrow \partial_t + (\beta/\alpha)\mathbf{u}\cdot\nabla$. By applying the same analogy to the Gilbert damping term, the contribution of the nonadiabatic spin torques can be expressed via the dissipation function [136]

$$\frac{\partial W_{\mathrm{n-ad}}}{\partial \dot{\mathbf{X}}_0} = -\beta D\mathbf{u}(\mathbf{X}_0). \qquad [4.157]$$

By combining these results, the following equation of motion for the current-driven dynamics of a rigid vortex in a nanocontact is obtained:

$$\mathbf{G}\times\left(\dot{\mathbf{X}}_0 - \mathbf{u}(\mathbf{X}_0)\right) + D\left(\alpha\dot{\mathbf{X}}_0 - \beta\mathbf{u}(\mathbf{X}_0)\right) + \frac{\eta\hbar I}{2\mathrm{e}}p_\perp\frac{\hat{\mathbf{z}}\times\mathbf{X}_0}{R_0^2} = -\frac{\partial U}{\partial \mathbf{X}_0}. \qquad [4.158]$$

An illustration of the different forces is given in Fig. 4.14, where a circular motion of the vortex core around a central potential $U(R_0)$ is

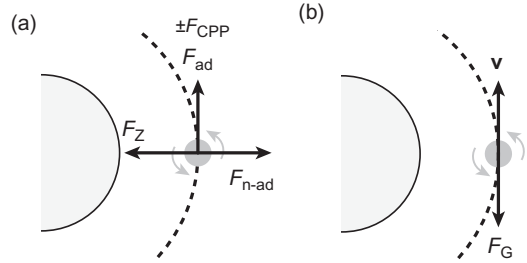

Figure 4.14 Schematic illustration of the forces exerted on the current-driven vortex dynamics in a magnetic nanocontact. (a) The adiabatic F_{ad} and CPP F_{CPP} spin torques lead to tangential forces, where the sign of F_{CPP} depends on the sign of $p_\perp$. (b) The nonadiabatic torques and the Zeeman energy potential give rise to radial forces, $F_{\mathrm{n-ad}}$ and F_z, respectively.

assumed and that the in-plane current $\mathbf{u}$ flows radially away from the nanocontact, $\mathbf{u}(R_0) = u(R_0)\hat{\rho}$. The forces associated with Gilbert damping, $\mathbf{F}_{\mathrm{G}} = -\alpha D\dot{\mathbf{X}}_0$, adiabatic CIP spin torques, $\mathbf{F}_{\mathrm{ad}} = \mathbf{G} \times \mathbf{u}$, and the $p_\perp$ component of CPP spin torques, $\mathbf{F}_{\mathrm{CPP}} = -\hat{\mathbf{z}} \times \mathbf{X}_0$, are all tangential to the orbit, while the forces associated with the Zeeman potential, $\mathbf{F}_z = -\partial U/\partial \mathbf{X}_0$, and nonadiabatic CIP spin torques, $\mathbf{F}_{\mathrm{n-ad}} = \beta D\mathbf{u}$, represent radial forces.

In contrast to centripetal motion in Newtonian mechanics, the gyrotropic nature of the vortex dynamics means that self-sustained gyration at constant radius is governed by the condition that the net tangential force vanishes, rather than the net radial force. In other words, it is required that

$$-\mathbf{G} \times \mathbf{u}(\mathbf{X}_0) + \alpha D\dot{\mathbf{X}}_0 + \frac{\eta\hbar I}{2e} p_\perp \frac{\hat{\mathbf{z}} \times \mathbf{X}_0}{R_0^2} = \mathbf{0}, \qquad [4.159]$$

which leads to the equation of motion,

$$\mathbf{G} \times \dot{\mathbf{X}}_0 = -\frac{\partial U}{\partial \mathbf{X}_0} + \beta D\mathbf{u}(\mathbf{X}_0). \qquad [4.160]$$

An expression for $\dot{\mathbf{X}}_0$ can be found by rearranging Eq. (4.160) and substituting this result into Eq. (4.159), which leads to the following condition for the steady-state radius of self-sustained gyration,

$$-Gu(R_0) + \frac{\alpha D}{G}\frac{\partial U}{\partial R_0} + \frac{\eta\hbar I}{2\mathrm{e}}\frac{p_\perp}{R_0} = 0. \qquad [4.161]$$

To obtain this expression, a term proportional to $\alpha\beta$ has been neglected, as $\alpha\beta \ll 1$ for transition metal ferromagnets of interest.

An explicit expression for the steady-state radius can be found with the following approximations. First, it has been shown that the Zeeman energy potential associated with the Oersted–Ampère fields is well described by the linear function $U(R_0) = \kappa |I| R_0$ for sufficiently large orbital radii [131]. This term is linear in the magnitude of the applied current because the magnitude of the Oersted–Ampère fields depends only on the magnitude of the applied current, and not its sign. Second, it is assumed that the electron current flows from the free layer to the reference layer, such that the electron flow in the film plane is radially outward from the nanocontact. As only a fraction of this current flows in the free layer [129], the spin-drift velocity can be written as $u(R_0) \approx \eta'\hbar I/(2\mathrm{e}R_0)$, where η' represents a reduced effective spin polarization due to this partial current flow. The expression for the steady-state radius becomes

$$R_0 = \mathrm{sgn}(I)\frac{G\kappa}{\alpha D}\frac{2e}{\hbar}(\eta' p - \eta_0 p_\perp)^{-1}. \qquad [4.162]$$

The radius is independent of the applied current, but conditions for its existence depend on the sign of the current, the sign of G through the vortex polarization p, and the overall sign of the quantity $\eta' p - \eta_0 p_\perp$. For example, in the absence of any CPP contributions ($p_\perp = 0$), only positive currents (electron flow from the free to the reference layer) lead to self-sustained gyration, as $Gp \propto p^2 = 1$. This can be understood in terms of the flow of conduction electron spins in the film plane, where the outward flow from the nanocontact gives rise to an outward "pressure" on the magnetic vortex, preventing it from spiraling into the nanocontact center. In the absence of CIP spin torques ($\eta' = 0$), the condition for self-sustained gyration is $\mathrm{sgn}(I)pp_\perp < 0$. This condition can be understood in terms of the perpendicular polarizer concept in nanopillar oscillators [137–139], where the sense of rotation of the magnetization vector in the film plane is determined uniquely by the sign of $p_\perp$ and the current polarity, $\mathrm{sgn}(I)$. As the sense of vortex gyration is given by p, the condition for steady-state gyration is determined by the product of the sign of these three quantities.

In contrast to the oscillatory spin-wave modes presented in previous sections, there is no intrinsic threshold current for self-sustained vortex gyration within the approximations of the rigid vortex model. This feature is a consequence of the Oersted-field-induced Zeeman potential, whose magnitude scales linearly with the current and the radial position of the vortex. From a mathematical perspective, the existence of a limit cycle still appears from a Hopf bifurcation, but it involves material parameters, rather than the applied current itself. Nevertheless, the model is based on the hypothesis that a single vortex state *already* exists in the magnetic free layer; a finite but different threshold current may be required to nucleate this vortex state in the first place. Experiments show that once the nucleation current for vortex oscillations is reached the applied current can be reduced well below this nucleation current without destroying the oscillatory state [140,141]. Therefore, in practical terms, the important threshold current in experimental systems involves the nucleation of the vortex state, rather than the onset of self-sustained oscillations.

With the steady-state radius given in Eq. (4.162), the vortex gyration frequency can be deduced from Eq. (4.160) to be

$$\omega = \frac{1}{GR_0}\left(\frac{\partial U}{\partial R_0} - \beta D u(R_0)\right) \approx \frac{\kappa I}{GR_0}, \qquad [4.163]$$

where the nonadiabatic correction term, proportional to $1/R_0^2$, has been neglected. The gyration frequency varies linearly with the applied current and is inversely proportional to the radius of gyration. This linear variation has been reported in a number of experiments [130–133,142–144]. As the steady-state radius is independent of current, any instantaneous changes to the applied current will result in an immediate change in the gyration frequency. This behavior leads to the prospect of fast frequency modulation using such vortex nanocontact oscillators. Manfrini *et al.* verified this aspect experimentally, where it was shown that square-wave variations in the applied current lead to changes in the frequency over time scales of 20 ns [145]. This figure represents an upper bound for the transition time, which is limited by the temporal resolution of the experiment. It has been suggested that this behavior could allow for frequency-modulation techniques using nanocontact vortex oscillators [146].

5.4. Nanopillar oscillations

In spin-valve or magnetic tunnel junction nanopillars, the equilibrium magnetic state is a vortex due to the confined nature of the nanopillar geometry. As in submicron dots, the vortex state in a nanopillar results from minimizing the stray magnetic fields at the edges, resulting in a curling structure for the magnetization. Due to the importance of these boundary conditions, a slightly different approach is required for describing the vortex dynamics, as the simple translation of a single rigid vortex, an approximation used to good effect for nanocontacts, does not adequately account for the static nature of the edge states.

Consider the circular nanopillar where L denotes the nanopillar radius and d the free-layer thickness. Ivanov and Zaspel showed that the current-driven vortex dynamics in nanopillars can be described using a two-vortex ansatz [147]. The inclusion of the second vortex is analogous to the concept of "mirror charges" in electrostatics. As such, the dynamics of the physical vortex requires the dynamics of the fictive two-vortex magnetization structure to be treated explicitly. This leads to a higher degree of complexity but the problem remains tractable for realistic geometries where simplifying approximations can be made.

For a vortex displacement along the x-axis, the two-vortex ansatz involves the following profile for the azimuthal angle

$$\Phi(x,y) = \tan^{-1}\left(\frac{y}{x - X_0}\right) + \tan^{-1}\left(\frac{y}{x - L^2/X_0}\right) \pm \frac{\pi}{2}, \qquad [4.164]$$

where the $\pi/2$ factor gives the sense of rotation of the moments in the film plane. This configuration ensures that there are no magnetic charges at the edges of the dot. A more general expression exists for arbitrary displacements in the film plane, but this simplified form is sufficient to describe the salient features of the current-driven dynamics.

The magnetic potential $U = U_m + U_z$ experienced by the vortex in this geometry has two contributions. First, the displacement of the vortex core from the dot center leads to the appearance of volume magnetic charges. To the fourth order in the core displacement, it is found that this contribution is given by [147]

$$U_m(R_0) \approx \frac{1}{4}\mu_0 M_s^2 \frac{d^2}{L^2}\left(2.83 d R_0^2 + 60.53 \frac{R_0^4}{L}\right). \qquad [4.165]$$

Second, the Oersted–Ampère field generated by the applied current I gives rise to a current-dependent Zeeman energy. Assuming that the field within the nanopillar is given by that of an infinite cylindrical conductor, $B_{Oe}(r) = \mu_0 Ir/(2\pi L^2)$, the Zeeman energy is found to be [148]

$$Uz(R_0) \approx \frac{2\mu_0 M_s d|I|}{15L} R_0^2. \qquad [4.166]$$

Thus, the total energy $U = U_m + U_z$ can be approximated by the quartic function

$$U(R_0) = \frac{1}{2}(a_2 + a_z|I|)R_0^2 + \frac{1}{4}a_4 R_0^4, \qquad [4.167]$$

where a_2, a_z, and a_4 are positive coefficients related to the two energy terms.

The current flow is almost exclusively perpendicular to the film plane in nanopillars, so only CPP spin torques are important in this geometry. As in the case for nanocontacts, the $p_{||}$ component of the CPP torques only lead to a constant force, which cannot provide the necessary compensatory force required for self-sustained oscillations. The only source of negative damping for vortex dynamics in nanopillars is therefore the $p_\perp$ component.

Consider a configuration in which the reference-layer magnetization is uniform and the current density flowing through the nanopillar, $J(\mathbf{r}) = I/(\pi L^2)$, is also uniform. From Eq. (4.57), the $p_\perp$ component of the dissipation function is found to be

$$F_{CPP} = -\eta_0 \frac{\hbar}{e}\frac{I}{\pi L^2} p_\perp \int d^2x \dot{\Phi} \sin^2\Theta. \qquad [4.168]$$

With the two-vortex ansatz, the resulting force due to the CPP spin tor ques is

$$\frac{\partial F_{\mathrm{CPP}}}{\partial \dot{\mathbf{X}}_0} = \frac{\eta \hbar I}{\mathrm{e}} p_\perp \frac{\hat{\mathbf{z}} \times \mathbf{X}_0}{L^2}. \tag{4.169}$$

This force possesses the appropriate symmetry to compensate Gilbert damping, as illustrated in Fig. 14.

The condition for self-sustained gyration is determined by setting the sum of the two nonconservative forces to zero:

$$\alpha D_2 \dot{\mathbf{X}}_0 + \frac{\eta \hbar I}{\mathrm{e}} p_\perp \frac{\hat{\mathbf{z}} \times \mathbf{X}_0}{L^2} = 0, \tag{4.170}$$

where D_2 denotes the value of the damping tensor evaluated with the two-vortex ansatz. Using the conservative equation (Eq. 4.147), an expression for $\dot{\mathbf{X}}_0$ can be found and substituted into Eq. (4.170), which yields

$$-\frac{\alpha D_2}{G} \frac{\partial U}{\partial \mathbf{X}_0} - \left(\frac{\eta \hbar I}{\mathrm{e}} p_\perp \right) \frac{1}{L_2} \mathbf{X}_0 = 0. \tag{4.171}$$

By substituting the magnetic potential and assuming pure circular gyration, a condition for a steady-state radius is obtained:

$$\alpha D_2 \left[(a_2 + a_z |I|) R_0 + a_4 R_0^3 \right] + G \widetilde{\sigma} I p_\perp R_0 = 0, \tag{4.172}$$

where $\widetilde{\sigma} = \eta \hbar / (\mathrm{e} L^2)$. Therefore, the steady-state radius is either the trivial solution, $R_0 = 0$, or else it satisfies

$$R_0^2 = -\frac{G \widetilde{\sigma} I p_\perp + \alpha D_2 (a_2 + a_z |I|)}{\alpha D_2 a_4}. \tag{4.173}$$

As the coefficients a_i, $\widetilde{\sigma}$, and αD are always positive, physical solutions for R_0 exist only for cases in which the product $p I p_\perp < 0$, where the vortex polarity p enters through the gyrovector, $G \propto p$. The condition for a finite steady-state radius defines the threshold current

$$I = \frac{\alpha D_2 a_2}{|G p_\perp| \sigma - \alpha D_2 a_z}. \tag{4.174}$$

In contrast to the dynamics in nanocontacts, one observes that vortex oscillations in nanopillars are subject to a finite threshold current. Once the steady-state radius is known, the gyration frequency can be obtained from the conservative part of the Thiele equation (Eq. 4.160),

$$\omega = \frac{1}{GR_0}\frac{\partial U}{\partial R_0} = -\frac{\widetilde{\sigma} p_\perp}{\alpha D_2} I. \qquad [4.175]$$

As with dynamics in a nanocontact system, a linear frequency variation with applied current is predicted for vortex oscillations in a nanopillar [149]. An extension to this formalism has been undertaken by Dussaux *et al.*, who included an additional nonlinearity in the damping term [150].

An example of current-driven vortex oscillations calculated by micromagnetics simulations is shown in Fig. 4.15, where the gyration frequency and radius are presented as a function of applied current. The oscillations appear at a threshold current density, below which only damped gyrotropic motion is observed. Above threshold, the orbit radius increases like $\sqrt{I}$, which is consistent with the analytical theory presented earlier. However, the frequency variation appears quite different from the linear current dependence that is expected. Khvalkovskiy *et al.* contend that parameters such as $\widetilde{\sigma}$ and αD_2, obtained using the Thiele approach, may exhibit large differences compared with those extracted from simulation. It is argued that the rigid-vortex approximation, which underpins the Thiele approach, does not correctly account for the dynamics of the edge magnetization states in a nanopillar, which are observed to remain largely unaffected by the gyrotropic motion in simulations.

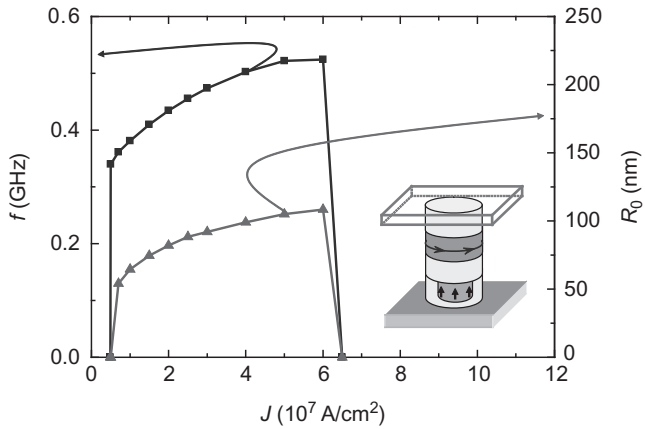

Figure 4.15 Characteristics of current-driven vortex oscillations in nanopillars, computed with micromagnetic simulations. The gyration frequency f and steady-state radius R_0 are shown as a function of applied current density J. The oscillations appear above the threshold current of $J_{th} \approx 4.9 \times 10^6$ A/cm^2. The geometry simulated is shown in the inset. *After Fig. 2 of Ref. [148].* © *American Physical Society.*

Experiments employing scanning transmission X-ray microscopy have provided direct observations of current-induced vortex oscillations in nanopillars [125]. The experiments suggest that the micromagnetic state in the free layer can exhibit large differences from the structure assumed in the rigid vortex model. More importantly, self-sustained gyration is observed for a purely in-plane polarizer ($p_\perp = 0$, $0 < p_\parallel \leq 1$), a scenario that is prohibited by the theoretical treatment described earlier. However, simulations have shown that a nonuniform polarizer can allow for self-sustained oscillations with in-plane CPP torques alone [151], offering a possible explanation for the experimental results. In elliptical nanopillars, experiments and simulations show the possibility of rotating vortex–antivortex pairs [152]. Further studies are therefore required to shed more light on the micromagnetic structure in such confined geometries.

Another issue concerns the spectral linewidth of vortex oscillators. A stochastic theory for vortex oscillations has been developed by supplementing stochastic terms to the Thiele equation, where similar amplitude-phase coupling leading to inhomogeneous broadening has been predicted [153]. While the general features of this stochastic theory does not differ much from the description presented in Section 4, there is a large quantitative discrepancy between experimental observations and theoretical predictions for the spectral linewidths. For gyration frequencies on the order of 100 MHz, theory predicts linewidths in the range of 10 kHz, while experimental values are typically in the range of 1 MHz. Furthermore, studies have shown that the linewidth saturates below temperatures of 100 K [154]. One possible explanation for such behavior involves inhomogeneities in the magnetic film. Experiments on thin film dots have shown that the vortex gyration frequency can be strongly affected by material defects [155,156]. By translating the equilibrium position of a vortex using in-plane fields, it was shown that variations of a few hundred megahertz in the gyration frequency is possible. Significant correlations between the microstructure, as determined from atomic force microscopy, and the spatial variations in the gyration frequency were also reported. These results highlight the importance of spatial fluctuations in the magnetic properties for vortex dynamics, which could lead to additional athermal contributions to the spectral linewidth in such systems.

5.5. Core reversal and relaxation oscillations

In Fig. 4.15, a second critical current is observed, around $J \approx 6.5 \times 10^7$ A/cm^2, above which the self-sustained gyration ceases to exist. This critical current corresponds to the point at which the critical core velocity is

reached, where the core polarity changes sign and consequently the sense of gyration. As a result, the condition for self-sustained oscillations is no longer satisfied for the opposite core polarity, which results in the gyrotropic motion being rapidly damped.

The process of core reversal initially begins with the deformation of the vortex core. The deformation occurs because the static vortex core profiles, satisfying Eqs. (4.138) and (4.141), are only approximate solutions to the dynamical system when the core is in motion. A similar issue arises for domain wall motion, where a mere translation of the static magnetization profile does not satisfy the Landau–Lifshitz equations of motion, but deformations to the static micromagnetic structure are necessary to correctly describe the dynamics [157,158]. As the vortex core moves, a "dip" structure, representing a small component of out-of-plane magnetization oriented antiparallel to the core magnetization, appears in the vicinity of the vortex core [159]. When the amplitude of this dip reaches a threshold level, the dip leads to the nucleation of a vortex–antivortex pair with core polarities opposite to the initial vortex state, and annihilation between the antivortex and initial vortex occurs [160–165]. This process leads to energy dissipation through spin waves [160,161,166] and the resulting state consists of a vortex with a core polarity opposite to that of the initial state. As the dip amplitude depends very much on the core velocity, core reversal occurs when a critical velocity is reached. For permalloy films, this critical velocity is found to be approximately 300 m s^{-1}.

A number of theoretical and experimental studies have shed light on the phenomenon of vortex core reversal. Yamada *et al.* showed that core reversal can be initiated in a micron-sized dot by driving the vortex gyrotropic motion into resonance using in-plane currents [163]. Van Waeyenberge *et al.* used bursts of alternating fields, where the vortex motion was tracked using time-resolved scanning transmission X-ray microscopy [167]. Switching of core polarity using field pulses has been confirmed in simulations [168] and the use of tailored pulse shapes [169,170] or rotating [171] applied fields reported. In magnetic dots, a reversal mode involving edge solitons has been found using micromagnetics simulations [172]. Vansteenkiste *et al.* used such imaging techniques to study the deformation of the vortex core when it is driven to core reversal using an alternating magnetic field [173]. The dip structure has also been shown to be more pronounced in the presence of in-plane spin torques, where deformation to the core can occur even for static vortices [174]. Core switching induced by spin-wave scattering has also been demonstrated experimentally [175] and theoretically for magnetic dots [176].

An interesting phenomenon occurs in nanocontact systems when the vortex gyration is driven to core reversal. As the dominant contribution to spin-torque-driven gyration comes from the CIP terms in this geometry, the only condition for self-sustained gyration involves the current polarity, where an outward flow of spins from the nanocontact is required to prevent the vortex from spiraling toward the nanocontact center. Self-sustained gyration for both core polarities is therefore possible. Consider the scenario in which the critical velocity is first attained in the nanocontact system, for example, following an increase in the gyration frequency brought about by an increase in the applied current. Through the process of vortex–antivortex pair nucleation and annihilation described earlier, the core reversal is accompanied by a slight decrease in the orbital radius just after reversal, followed by the core spiraling outward toward the steady-state radius with the opposite sense of gyration. But the steady-state radius is never attained because the critical velocity is always reached first, leading to another core reversal process. This sequence of events then repeats periodically.

Such dynamics are characteristic of *relaxation oscillations* [15,177]. These are periodic processes involving the slow growth of some quantity (e.g., energy) that is rapidly discharged when a threshold is reached. Relaxation oscillators are characterized by two distinct time scales: a slow time scale representing the gradual accumulation and a fast time scale representing the sudden discharge. For this reason, these oscillators are also referred to as threshold oscillators or integrate-and-fire oscillators. For the dynamics described earlier, the vortex charges in Zeeman energy (associated with the Oersted field) as it spirals out toward the steady-state orbit, and discharges this energy through the spin-wave emission when the core reverses its polarity. Therefore, periodic core reversal in a nanocontact system represents a form of relaxation oscillation.

Petit-Watelot *et al.* showed that such dynamics occur in nanocontacts above a threshold current [178]. Below the threshold, the usual gyrotropic motion is observed, where the vortex gyration around the nanocontact leads to a linear variation in the oscillation frequency as a function of applied current. As the current is increased above the threshold, a number of branches are observed in the power spectrum, which gradually fan out from the central frequency and settle into distinct branches over different current intervals, as shown in Fig. 4.16. These branches are a result of frequency modulation, due to periodic core reversal, on the gyrotropic motion of the vortex around the nanocontact. The presence of clear plateaus, at $f_{\mathrm{mod}}/f = 1/5$, $1/3$, and $1/2$, for example, is indicative of a phase-locking phenomenon between the gyrotropic motion and the relaxation oscillations. It

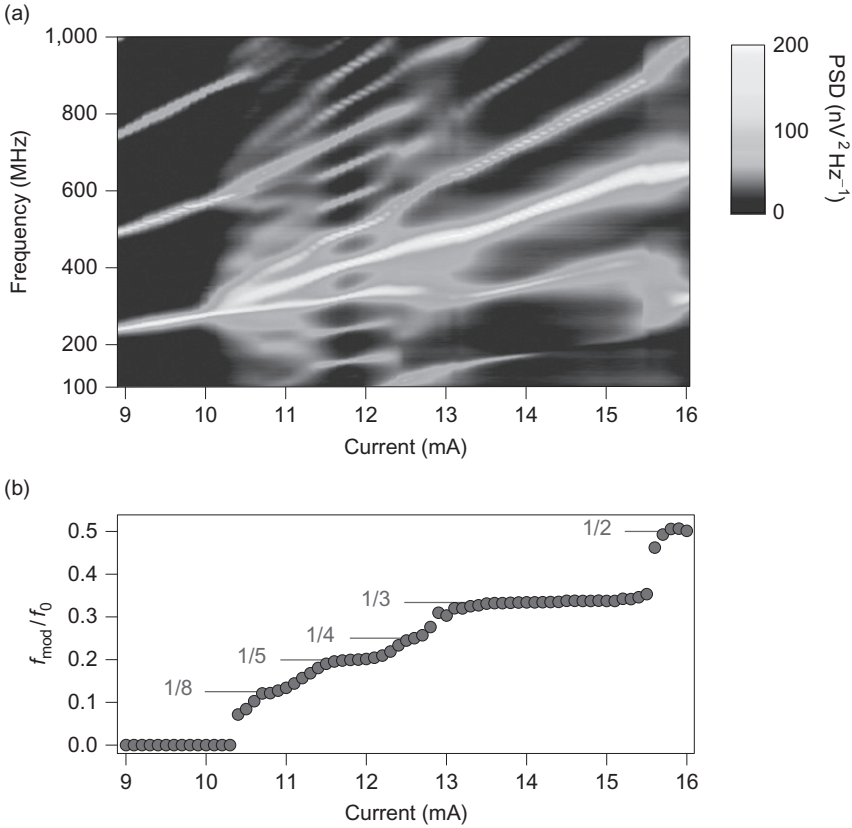

Figure 4.16 Current dependence of the power spectrum in nanocontact vortex oscillations showing modulation due to periodic core reversal. (a) Map of the experimental PSD. (b) Ratio of the modulation and central frequencies as a function of applied current, where well-defined plateaus are seen over different current intervals. *After Fig. 2 of Ref. [178]. © Nature Publishing Group.*

has been shown that the coexistence of gyrotropic and relaxation oscillations gives rise to commensurate and incommensurate states, where the plateau structure in Fig. 4.16 is related to a Devil's staircase [178,179].

6. OTHER NONLINEAR PHENOMENA

6.1. Phase-locking and synchronization

From a technological perspective, spin-torque oscillators are interesting for applications in mobile telecommunications because of their compact size and their potential for frequency tunability. However, most experimental systems studied to date have two important shortcomings. First,

the coherence of spin-torque oscillators is typically poor at room temperature, where the quality factor $Q = f_0/\Delta f$, defined as the ratio between the oscillation frequency and the linewidth, takes values between 100 and 10^4. In contrast, quartz oscillators commonly used in microelectronics possess typical Q values of 10^6 and above. Second, the output power of spin-torque oscillators is comparatively weak for applications. For spin valves, the total integrated power in the current-driven mode is typically in the range of 0.01–1 nW [13,62], while oscillators based on magnetic tunnel junctions can reach the range of 0.1–1 μW [124,180,181]. Attempts to address these shortcomings can involve either improvements in physical properties, for example, engineering larger magnetoresistance values or promoting specific oscillation modes, such as vortex gyration in tailored geometries [124,126], or by applying established methods for oscillators such as phase-locking and synchronization.

Phase-locking refers to the entrainment of the oscillator phase by an external driving force. As the oscillator phase is "free" in the self-sustained regime, it is not subject to a restoring force along the limit cycle and is therefore susceptible to phase noise, as the discussion in Section 4 has shown. If an external driving signal is applied to the oscillator, the oscillator phase can become locked to the phase of the driving signal, with a specific relationship between the two [182]. In this case, the oscillator phase is no longer free, but substantial improvements can be made in reducing the oscillator noise. Electrical circuits like phase-locked loops employ a feedback mechanism in combination with phase-locking to improve the coherence of an oscillator [106]. For potential applications, it is therefore important to identify the useful driving forces for spin-torque oscillators and the conditions under which phase-locking is achievable.

For experimental systems of interest, the main driving mechanisms involve applied fields through the Zeeman interaction or currents through spin-transfer torques [183]. One of the first experimental demonstrations of phase-locking in spin-torque oscillators was conducted on magnetic nanocontacts, where it was shown that locking is possible by superimposing a low ac driving current on top of the dc current above threshold [184]. Detailed experiments on spin-valve nanopillars revealed the efficiency of phase-locking to a microwave current, where it was shown that the Adler model could be extended to account for the locking interval observed [185]. Injection-locking to microwave currents has also been observed for current-driven modes in magnetic tunnel junctions [186] and vortex oscillations in nanopillars [187,188]. In the latter, experiments have also shown

that phase-locking to a microwave current is more efficient at twice the gyration frequency [189]. Micromagnetic simulations show that such locking mechanisms are robust in the presence of thermal fluctuations [190], but dynamical effects leading to phase slips can be important [191]. For nanocontact oscillators driven by external ac fields, hysteresis in the locking interval [192] and fractional synchronization [193,194] have been observed. The transient dynamics associated with phase-locking has also been studied theoretically [195].

In a system where several oscillators interact with one another, a process of mutual phase-locking or *synchronization* can take place without the requirement of an external driving signal. The nature of the synchronized state depends on a number of parameters, such as the strength and range of the interactions, and the distribution of the oscillator frequencies [177,196,197]. Indeed, synchronization is a nonlinear phenomenon that is prevalent in physical, chemical, and biological systems, with prominent examples including the collective flashing of firelies, pacemaker cells in the heart, and electrical power grids.

The first experimental demonstration of synchronization in spin-torque oscillators was achieved for double nanocontact systems [72,75]. In the systems studied, the double nanocontact structure is patterned onto a continuous spin-valve multilayer, with the applied spin torques leading to two well-separated regions of the free layer to be driven to self-oscillation. Synchronization was observed when the two oscillator frequencies were made sufficiently close, which was attained by ramping the applied current through one nanocontact while maintaining a constant current through the other. An example of the experimental results is shown in Fig. 4.17, where the map of the spectral density exhibits a single frequency branch within the locking interval, corresponding to a regime of large power output, with two distinct branches of the nonsynchronized state outside this interval. It has been shown that the exchange of emitted spin waves from the nanocontact is the primary coupling mechanism between the two oscillators [73,74,198–200].

A number of other mechanisms for synchronization are possible. Grollier *et al.* showed through simulations that mutual phase-locking is possible between several nanopillars connected electrically in series, where the coupling occurs through the induced variations in the shared current that flows through the circuit [201]. Calculations also show that such behavior should be possible in magnetic tunnel junctions [202] and more complex synchronized states have been observed in subsequent studies of serially connected

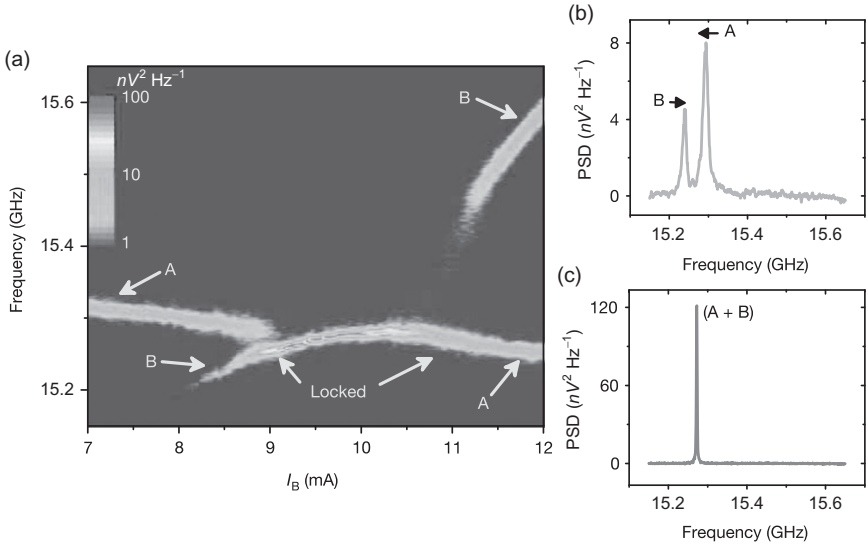

Figure 4.17 Synchronization in double nanocontact oscillators. (a) Map of the power spectral density of nanocontacts A and B with the locking interval indicated. (b) Power spectrum at an applied current of 8.65 mA, below the locking interval. (c) Power spectrum for an applied current of, or within, the locking interval, which exhibits large power increase and dramatic linewidth narrowing. *After Fig. 2 of Ref. [72].* *© Nature Publishing Group.*

oscillators [203]. The roles of the electrical circuit configuration [204] and the stability of the synchronized state [205] have also been examined theoretically. Another scenario involves vortex oscillations in multiple nanocontacts. In experiments on a system with four nanocontacts, organized in a square arrangement on a continuous multilayer, Ruotolo *et al.* showed that the vortex gyration around each nanocontact can be synchronized through mediating antivortex structures separating each vortex [132]. In the experimental spectra, four distinct peaks are observed outside the current locking interval, while only one peak is present within this interval.

6.2. Mode stability and hopping

The theoretical framework for spin waves and vortices given in Sections 3 and 5, respectively, is based on the underlying assumption that the excited mode is stable at all levels of supercriticality. However, a number of studies have shown that mode instabilities can occur under certain experimental conditions.

A possible consequence under large driving currents is a change in the nature of the oscillatory mode. In the macrospin approximation, for example, it is predicted that in-plane precession modes at low currents give way to stable out-of-plane precession modes at high currents [206]. This has been confirmed in experiments and simulations on spin-valve nanopillars, where large-amplitude coherent spin-wave modes have been observed [207]. However, the stability at high currents is not a universal feature [208]. In other experiments on similar nanopillars, large currents lead to loss of coherence and mode power [63]. These results highlight the importance of nonlinearities associated with the spin-wave modes excited [209–211].

In experiments on spin-valve nanopillars [212] and magnetic tunnel junctions [213,214], time-domain measurements reveal regimes in which random transitions between distinct modes occur. The modes observed possess different frequencies, which are separated by intervals that exceed the linewidth of each individual mode. These studies show that the coherence of spin-torque oscillators could in large part be limited by thermally activated (and therefore stochastic) transitions between distinct modes rather than the thermal noise processes discussed in Section 4. Similar transitions have been observed in nanocontact systems. For high-frequency oscillations, simulations have revealed transitions between two kinds of localized bullet modes [215]. In experiments on low-frequency excitations, hopping between two modes has been reported for certain intervals of applied fields [144].

6.3. Droplet excitations

For certain material combinations in the thin film geometry, such as ultrathin CoFeB capped with MgO [216] or Co/Pt [217] and Co/Ni [218] superlattices, a strong uniaxial anisotropy oriented perpendicular to the film plane appears. This anisotropy is an interface effect that originates in induced changes of the electronic band structure. Experiments on magnetic nanocontacts with out-of-plane magnetized Co/Ni free layers have demonstrated the possibility of driving large-angle oscillations using spin torques [219].

For current-driven dynamics in such geometries, a novel kind of soliton excitation—the dissipative droplet soliton—has been predicted to exist [220,221]. The soliton represents a dissipative version of a soliton mode originally studied by Ivanov and Kosevich, who considered the bound state of a large number of magnon modes in a system with uniaxial anisotropy [222]. For a free layer with magnetization oriented in the $+z$ direction, the soliton consists of a profile with partially reversed magnetization along

the z-axis in the nanocontact region and large-angle precession, with cone angles reaching 90°, at the boundary of the soliton [220]. The internal structure of the mode depends strongly on its oscillation frequency, which is well below that for ferromagnetic resonance.

In addition to the balance between nonlinearity and dispersion for conservative solitons, dissipative solitons also depend on the balance between energy gains and losses, as manifested by Gilbert damping and spin torques in magnetic nanocontacts. As such, its existence and dynamics rely on a delicate balance between the conservative and nonconservative torques applied. Hoefler *et al.* have shown theoretically how such droplet solitons can be generated and propagated in magnetic nanocontact systems [221]. By combining soliton perturbation theory with micromagnetics simulations, the authors show how such solitons can be controlled with external magnetic fields, with proposed schemes for propagating the solitons in continuous films. This work highlights some possible schemes for experimental detection of these nonlinear objects.

7. FINAL REMARKS

Intense research efforts over the past decade have established spin-torque oscillators as nanoscale systems in which rich nonlinear physical phenomena can be studied. Spin torques provide a means of driving magnetization dynamics to levels of nonlinearity that are not possible with magnetic fields alone. The central theme of this chapter has involved self-sustained magnetization oscillations in different geometries, with possible modes being linear and nonlinear spin waves, and topological solitons such as vortices. Through the combination of the Zeeman interaction and magnetic nonlinearities, the frequency of spin-torque-driven oscillations can be varied over large frequency ranges through changes in applied fields and currents, leading to many proposals for constructing nanoscale frequency-tunable electrical oscillators based on such systems. The nonlinearities also play an important role in determining the coherence of oscillations at finite temperatures, where strong amplitude-phase coupling can lead to significant broadening of the power spectra. Attempts to improve the noise characteristics of such oscillators include targeting the excitation of specific modes and applying established techniques such as phase-locking to external signals and synchronization between several oscillators, phenomena which draw upon a large body of work from other fields of nonlinear physics. Given the intricate balance between conservative and nonconservative torques that underpin

the dynamics, spin-torque oscillators continue to offer unique opportunities to explore strongly nonlinear dynamics on the nanoscale, as testified by the recent predictions on dissipative droplets. Open questions on both the fundamental and applied levels, such as noise-driven transitions, the role of material imperfections, excitations in strongly coupled systems [223], and the influence of spin-caloric effects [224], for example, should continue to stimulate investigations into the dynamical properties of spin-torque oscillators.

ACKNOWLEDGMENTS

The author is indebted to Robert Camley and Robert Stamps for the encouragement received to undertake writing this chapter. The author would also like to thank the following people, who, through stimulating discussions and fruitful collaborations, have helped to shape this chapter in one way or another over the past decade: Laurence Bianchini, Claude Chappert, Sven Cornelissen, Vincent Cros, Paul Crozat, Thibaut Devolder, Antoine Dussaux, Ursula Ebels, Benoît Georges, Julie Grollier, Annerose Helmer, Gino Hrkac, Mark Keller, Liesbet Lagae, Yann Le Maho, Nicolas Locatelli, Mauricio Manfrini, Peter Metaxas, Quentin Mistral, Rubén Otxoa, Sébastien Petit-Watelot, Matt Pufall, Michaël Quinsat, Antonio Ruotolo, Thomas Schrefl, Tom Silva, Andrei Slavin, Gen Tatara, André Thiaville, Vasil Tiberkevich, Arne Vansteenkiste, Ben Van de Wiele, and Maarten van Kampen. This work was partially supported by the French National Research Agency (ANR), through the VOICE project ANR-09-NANO-006, and the European Commission FP6 Program under contract numbers MRTN-CT-2006-035327 SPINSWITCH and IST-16939-STREP TUNAMOS.

REFERENCES

[1] L. Berger, J. Appl. Phys. 55 (6) (1984) 1954.
[2] P.P. Freitas, L. Berger, J. Appl. Phys. 57 (4) (1985) 1266.
[3] L. Berger, Phys. Rev. B 54 (13) (1996) 9353.
[4] J.C. Slonczewski, J. Magn. Magn. Mater. 159 (1996) L1.
[5] E.B. Myers, D.C. Ralph, J.A. Katine, R.N. Louie, R.A. Buhrman, Science 285 (5429) (1999) 867.
[6] M. Tsoi, R.E. Fontana, S.S.P. Parkin, Appl. Phys. Lett. 83 (1) (2003) 2617.
[7] J. Grollier, P. Boulenc, V. Cros, A. Hamzic, A. Vaurès, A. Fert, G. Faini, Appl. Phys. Lett. 83 (3) (2003) 509.
[8] T. Ishida, T. Kimura, Y. Otani, Phys. Rev. B 74 (1) (2006) 014424.
[9] S. Kasai, Y. Nakatani, K. Kobayashi, H. Kohno, T. Ono, Phys. Rev. Lett. 97 (10) (2006) 107204.
[10] M. Tsoi, A. Jansen, J. Bass, W.-C. Chiang, M. Seek, V. Tsoi, P. Wyder, Phys. Rev. Lett. 80 (19) (1998) 4281.
[11] J.C. Slonczewski, J. Magn. Magn. Mater. 195 (2) (1999) L261.
[12] M. Tsoi, V. Tsoi, J. Bass, A. Jansen, P. Wyder, Phys. Rev. Lett. 89 (24) (2002) 246803.
[13] S.I. Kiselev, J.C. Sankey, I.N. Krivorotov, N.C. Emley, R.J. Schoelkopf, R.A. Buhrman, D.C. Ralph, Nature 425 (6956) (2003) 380.
[14] W. Rippard, M. Pufall, S. Kaka, S. Russek, T. Silva, Phys. Rev. Lett. 92 (2) (2004) 027201.
[15] S.H. Strogatz, Nonlinear Dynamics and Chaos, Perseus Books, Reading, MA, 1994.
[16] A. Hubert, R. Schäfer, Magnetic Domains. The Analysis of Magnetic Microstructures, Springer-Verlag, Berlin, 1998.

[17] T.L. Gilbert, Phys. Rev. 100 (1243) (1956) 1.
[18] T. Gilbert, IEEE Trans. Magn. 40 (6) (2004) 3443.
[19] L. Landau, E. Lifshitz, Phys. Z. Sowjet 8 (1935) 153.
[20] M. Stiles, W. Saslow, M. Donahue, A. Zangwill, Phys. Rev. B 75 (21) (2007) 214423.
[21] V. Tiberkevich, A. Slavin, Phys. Rev. B 75 (1) (2007) 014440.
[22] J. Xiao, A. Zangwill, M. Stiles, Phys. Rev. B 70 (17) (2004) 172405.
[23] X. Waintal, E. Myers, P. Brouwer, D. Ralph, Phys. Rev. B 62 (18) (2000) 12317.
[24] M.D. Stiles, A. Zangwill, J. Appl. Phys. 91 (10) (2002) 6812.
[25] M. Stiles, A. Zangwill, Phys. Rev. B 66 (1) (2002) 014407.
[26] A. Shpiro, P. Levy, S. Zhang, Phys. Rev. B 67 (10) (2003) 104430.
[27] P. Levy, J. Zhang, Phys. Rev. B 70 (13) (2004) 132406.
[28] J. Zhang, P. Levy, Phys. Rev. B 70 (18) (2004) 184442.
[29] J. Zhang, P. Levy, S. Zhang, V. Antropov, Phys. Rev. Lett. 93 (25) (2004) 256602.
[30] J. Zhang, P. Levy, Phys. Rev. B 71 (18) (2005) 184426.
[31] J. Zhang, P. Levy, Phys. Rev. B 71 (18) (2005) 184417.
[32] M. Gmitra, J. Barnaś, Phys. Rev. Lett. 96 (20) (2006) 207205.
[33] J. Xiao, A. Zangwill, M.D. Stiles, Eur. Phys. J. B 59 (4) (2007) 415.
[34] V. Rychkov, S. Borlenghi, H. Jaffres, A. Fert, X. Waintal, Phys. Rev. Lett. 103 (6) (2009) 066602.
[35] O. Boulle, V. Cros, J. Grollier, L.G. Pereira, C. Deranlot, F. Petroff, G. Faini, J. Barnaś, A. Fert, Nat. Phys. 3 (7) (2007) 492.
[36] O. Boulle, V. Cros, J. Grollier, L. Pereira, C. Deranlot, F. Petroff, G. Faini, J. Barnaś, A. Fert, Phys. Rev. B 77 (17) (2008) 174403.
[37] X. Waintal, M. Viret, Europhy. Lett. 65 (3) (2004) 427.
[38] G. Tatara, H. Kohno, Phys. Rev. Lett. 92 (8) (2004) 086601.
[39] S. Zhang, Z. Li, Phys. Rev. Lett. 93 (12) (2004) 127204.
[40] S. Barnes, S. Maekawa, Phys. Rev. Lett. 95 (10) (2005) 107204.
[41] A. Thiaville, Y. Nakatani, J. Miltat, Y. Suzuki, Europhys. Lett. 69 (6) (2007) 990.
[42] M. Hayashi, L. Thomas, Y. Bazaliy, C. Rettner, R. Moriya, X. Jiang, S. Parkin, Phys. Rev. Lett. 96 (19) (2006) 197207.
[43] M. Hayashi, L. Thomas, C. Rettner, R. Moriya, Y. Bazaliy, S. Parkin, Phys. Rev. Lett. 98 (3) (2007) 037204.
[44] O. Boulle, J. Kimling, P. Warnicke, M. Kläui, U. Rüdiger, G. Malinowski, H. Swagten, B. Koopmans, C. Ulysse, G. Faini, Phys. Rev. Lett. 101 (21) (2008) 216601.
[45] C. Burrowes, A.P. Mihai, D. Ravelosona, J.-V. Kim, C. Chappert, L. Vila, A. Marty, Y. Samson, F. Garcia-Sanchez, L.D. Buda-Prejbeanu, et al., Nat. Phys. 6 (1) (2010) 17.
[46] M. Eltschka, M. Wötzel, J. Rhensius, S. Krzyk, U. Nowak, M. Kläui, T. Kasama, R. Dunin-Borkowski, L. Heyderman, H. Van Driel, et al., Phys. Rev. Lett. 105 (5) (2010) 056601.
[47] L. Heyne, J. Rhensius, D. Ilgaz, A. Bisig, U. Rüdiger, M. Kläui, L. Joly, F. Nolting, L. Heyderman, J. Thiele, et al., Phys. Rev. Lett. 105 (18) (2010) 187203.
[48] A. Manchon, W.S. Kim, K.-J. Lee, Role of Spin Diffusion in Current-Induced Domain Wall Motion. (2011), arXiv:110.3487v1.
[49] D. Claudio-Gonzalez, A. Thiaville, J. Miltat, Phys. Rev. Lett. 108 (22) (2012) 227208.
[50] G. Consolo, G. Gubbiotti, L. Giovannini, R. Zivieri, Appl. Math. Comput. 217 (21) (2011) 8204.
[51] T. Holstein, H. Primakoff, Phys. Rev. 58 (12) (1940) 1098.
[52] M. Sparks, Ferromagnetic-Relaxation Theory, McGraw-Hill, New York, 1964.
[53] R.M. White, Quantum Theory of Magnetism, third ed., Springer-Verlag, Berlin, 2007.
[54] J. Winter, Phys. Rev. 124 (2) (1961) 452.

[55] H.-B. Braun, Phys. Rev. B 50 (22) (1994) 16485.
[56] D. Bouzidi, H. Suhl, Phys. Rev. Lett. 65 (20) (1990) 2587.
[57] Y. Le Maho, J.-V. Kim, G. Tatara, Phys. Rev. B 79 (17) (2009) 174404.
[58] S. Rezende, F. De Aguiar, A. Azevedo, Phys. Rev. Lett. 94 (3) (2005) 037202.
[59] A.N. Slavin, P. Kabos, IEEE Trans. Magn. 41 (4) (2005) 1264.
[60] A. Slavin, V. Tiberkevich, IEEE Trans. Magn. 45 (4) (2009) 1875.
[61] S. Kiselev, J. Sankey, I. Krivorotov, N. Emley, M. Rinkoski, C. Perez, R. Buhrman, D. Ralph, Phys. Rev. Lett. 93 (3) (2004) 036601.
[62] W. Rippard, M. Pufall, S. Kaka, T. Silva, S. Russek, Phys. Rev. B 70 (10) (2004) 100406.
[63] Q. Mistral, J.-V. Kim, T. Devolder, P. Crozat, C. Chappert, J.A. Katine, M.J. Carey, K. Ito, Appl. Phys. Lett. 88 (19) (2006) 192507.
[64] A. Slavin, V. Tiberkevich, Phys. Rev. Lett. 95 (23) (2005) 237201.
[65] W.H. Rippard, M.R. Pufall, T.J. Silva, Appl. Phys. Lett. 82 (8) (2003) 1260.
[66] G. Consolo, B. Azzerboni, G. Gerhart, G. Melkov, V. Tiberkevich, A. Slavin, Phys. Rev. B 76 (14) (2007) 144410.
[67] G. Consolo, B. Azzerboni, L. Lopez-Diaz, G. Gerhart, E. Bankowski, V. Tiberkevich, A. Slavin, Phys. Rev. B 78 (1) (2008) 014420.
[68] S. Bonetti, V. Tiberkevich, G. Consolo, G. Finocchio, P. Muduli, F. Mancoff, A. Slavin, J. Åkerman, Phys. Rev. Lett. 105 (21) (2010) 217204.
[69] S. Bonetti, V. Puliafito, G. Consolo, V. Tiberkevich, A. Slavin, J. Åkerman, Phys. Rev. B 85 (17) (2012) 174427.
[70] D. Berkov, C. Boone, I. Krivorotov, Phys. Rev. B 83 (5) (2011) 054420.
[71] M. Hoefer, T. Silva, M. Stiles, Phys. Rev. B 77 (14) (2008) 144401.
[72] S. Kaka, M.R. Pufall, W.H. Rippard, T.J. Silva, S.E. Russek, J.A. Katine, Nature 437 (7057) (2005) 389.
[73] M. Pufall, W. Rippard, S. Russek, S. Kaka, J. Katine, Phys. Rev. Lett. 97 (8) (2006) 087206.
[74] A. Slavin, V. Tiberkevich, Phys. Rev. B 74 (10) (2006) 104401.
[75] F.B. Mancoff, N.D. Rizzo, B.N. Engel, S. Tehrani, Nature 437 (7057) (2005) 393.
[76] V.E. Demidov, S. Urazhdin, S.O. Demokritov, Nat. Mater. 9 (2010) 984.
[77] V. Demidov, S. Urazhdin, V. Tiberkevich, A. Slavin, S. Demokritov, Phys. Rev. B 83 (6) (2011) 060406.
[78] M. Madami, S. Bonetti, G. Consolo, S. Tacchi, G. Carlotti, G. Gubbiotti, F.B. Mancoff, M.A. Yar, J. Åkerman, Nat. Nanotechnol. 6 (2011) 635.
[79] H. Ulrichs, V.E. Demidov, S.O. Demokritov, S. Urazhdin, Appl. Phys. Lett. 100 (16) (2012) 162406.
[80] S. Bonetti, P. Muduli, E. Mancoff, J. Åkerman, Appl. Phys. Lett. 94 (10) (2009) 102507.
[81] F. De Aguiar, A. Azevedo, S. Rezende, Phys. Rev. B 75 (13) (2007) 132404.
[82] I.N. Krivorotov, N.C. Emley, J.C. Sankey, S.I. Kiselev, D.C. Ralph, R.A. Buhrman, Science 307 (5707) (2005) 228.
[83] M. Lax, Rev. Mod. Phys. 32 (1) (1960) 25.
[84] M. Lax, Rev. Mod. Phys. 38 (3) (1966) 541.
[85] M. Lax, Phys. Rev. 160 (2) (1967) 290.
[86] R. Hempstead, M. Lax, Phys. Rev. 161 (2) (1967) 350.
[87] J.-V. Kim, Phys. Rev. B 73 (17) (2006) 174412.
[88] A.S. Mikhailov, J. Exp. Theor. Phys. 42 (1975) 267.
[89] S. Petit, C. Baraduc, C. Thirion, U. Ebels, Y. Liu, M. Li, P. Wang, B. Diény, Phys. Rev. Lett. 98 (7) (2007) 077203.
[90] V. Tiberkevich, A. Slavin, J.-V. Kim, Appl. Phys. Lett. 91 (19) (2007) 192506.
[91] A. Hamadeh, G. De Loubens, V.V. Naletov, J. Grollier, C. Ulysse, V. Cros, O. Klein, Phys. Rev. B 85 (14) (2012) 140408.

[92] J.-V. Kim, V. Tiberkevich, A. Slavin, Phys. Rev. Lett. 100 (1) (2008) 017207.
[93] V. Tiberkevich, A. Slavin, J.-V. Kim, Phys. Rev. B 78 (9) (2008) 092401.
[94] H. Risken, The Fokker-Planck Equation, second ed., Springer-Verlag, Berlin, 1989.
[95] H. Suto, T. Nagasawa, K. Kudo, K. Mizushima, R. Sato, Appl. Phys. Expr. 4 (1) (2010) 013003.
[96] P.M. Braganca, B.A. Gurney, B.A. Wilson, J.A. Katine, S. Maat, J.R. Childress, Nanotechnology 21 (23) (2010) 235202.
[97] T. Nagasawa, H. Suto, K. Kudo, K. Mizushima, R. Sato, J. Appl. Phys. 109 (7) (2011) 07C907.
[98] R. Kubo, in: D. ter Haar (Ed.), Fluctuation, Relaxation and Resonance in Magnetic Systems, Oliver & Boyd, Edinburgh, 1962, pp. 23–68.
[99] J. Sankey, I. Krivorotov, S. Kiselev, P. Braganca, N. Emley, R. Buhrman, D. Ralph, Phys. Rev. B 72 (22) (2005) 224427.
[100] C. Boone, J. Katine, J. Childress, J. Zhu, X. Cheng, I. Krivorotov, Phys. Rev. B 79 (14) (2009) 140404(R).
[101] S. Urazhdin, V. Tiberkevich, A. Slavin, Phys. Rev. Lett. 105 (23) (2010) 237204.
[102] L. Bianchini, S. Cornelissen, J.-V. Kim, T. Devolder, W. Van Roy, L. Lagae, C. Chappert, Appl. Phys. Lett. 97 (3) (2010) 032502.
[103] K. Kudo, T. Nagasawa, R. Sato, K. Mizushima, Appl. Phys. Lett. 95 (2) (2009) 022507.
[104] M. Quinsat, D. Gusakova, J.F. Sierra, J.P. Michel, D. Houssameddine, B. Delaet, M.-C. Cyrille, U. Ebels, B. Dieny, L.D. Buda-Prejbeanu, et al., Appl. Phys. Lett. 97 (18) (2010) 182507.
[105] J.F. Sierra, M. Quinsat, U. Ebels, D. Gusakova, I. Joumard, A.S. Jenkins, L. Buda-Prejbeanu, B. Diény, M.-C. Cyrille, A. Zeltser, et al., Temperature dependence of the emission linewidth in MgO-based spin torque nano-oscillators. (2011), arXiv:1112.2833v1.
[106] M.W. Keller, A.B. Kos, T.J. Silva, W.H. Rippard, M.R. Pufall, Appl. Phys. Lett. 94 (19) (2009) 193105.
[107] M. Keller, M. Pufall, W. Rippard, T. Silva, Phys. Rev. B 82 (5) (2010) 054416.
[108] W. Rippard, M. Pufall, S. Russek, Phys. Rev. B 74 (22) (2006) 224409.
[109] K. Thadani, G. Finocchio, Z.-P. Li, O. Ozatay, J. Sankey, I. Krivorotov, Y.-T. Cui, R. Buhrman, D. Ralph, Phys. Rev. B 78 (2) (2008) 024409.
[110] K. Mizushima, T. Nagasawa, K. Kudo, Y. Saito, R. Sato, Appl. Phys. Lett. 94 (15) (2009) 152501.
[111] V. Tiberkevich, I. Krivorotov, G. Gerhart, A. Slavin, J. Magn. Magn. Mater. 321 (16) (2009) L53.
[112] Z.M. Zeng, P. Upadhyaya, P. Khalili Amiri, K.H. Cheung, J.A. Katine, J. Langer, K.L. Wang, H.W. Jiang, Appl. Phys. Lett. 99 (3) (2011) 032503.
[113] D. Gusakova, M. Quinsat, J.F. Sierra, U. Ebels, B. Dieny, L.D. Buda-Prejbeanu, M.-C. Cyrille, V. Tiberkevich, A.N. Slavin, Appl. Phys. Lett. 99 (5) (2011) 052501.
[114] J.-V. Kim, Q. Mistral, C. Chappert, V. Tiberkevich, A. Slavin, Phys. Rev. Lett. 100 (16) (2008) 167201.
[115] M. Schneider, W. Rippard, M. Pufall, T. Cecil, T. Silva, S. Russek, Phys. Rev. B 80 (14) (2009) 144412.
[116] B. Georges, J. Grollier, V. Cros, A. Fert, A. Fukushima, H. Kubota, K. Yakushijin, S. Yuasa, K. Ando, Phys. Rev. B 80 (6) (2009) 060404.
[117] E. Feldtkeller, H. Thomas, Z. Phys. B Condens. Matter 4 (1965) 8.
[118] Y. Gaididei, V.P. Kravchuk, D.D. Sheka, Int. J. Quant. Chem. 110 (1) (2010) 83.
[119] A. Vansteenkiste, B. Van de Wiele, J. Magn. Magn. Mater. 323 (21) (2011) 2585.
[120] A. Wachowiak, J. Wiebe, M. Bode, O. Pietzsch, M. Morgenstern, R. Wiesendanger, Science 298 (5593) (2002) 577.

[121] V.S. Pribiag, I.N. Krivorotov, G.D. Fuchs, P.M. Braganca, O. Ozatay, J.C. Sankey, D.C. Ralph, R.A. Buhrman, Nat. Phys. 3 (7) (2007) 498.
[122] V. Pribiag, G. Finocchio, B. Williams, D. Ralph, R. Buhrman, Phys. Rev. B 80 (18) (2009) 180411.
[123] R. Lehndorff, D. Bürgler, S. Gliga, R. Hertel, P. Grünberg, C. Schneider, Z. Celinski, Phys. Rev. B 80 (5) (2009) 054412.
[124] A. Dussaux, B. Georges, J. Grollier, V. Cros, A.V. Khvalkovskiy, A. Fukushima, M. Konoto, H. Kubota, K. Yakushiji, S. Yuasa, et al., Nat. Commun. 1 (2010) 8.
[125] X. Yu, V. Pribiag, Y. Acremann, A. Tulapurkar, T. Tyliszczak, K. Chou, B. Bräuer, Z.-P. Li, O. Lee, P. Gowtham, et al., Phys. Rev. Lett. 106 (16) (2011) 167202.
[126] N. Locatelli, V.V. Naletov, J. Grollier, G. De Loubens, V. Cros, C. Deranlot, C. Ulysse, G. Faini, O. Klein, A. Fert, Appl. Phys. Lett. 98 (6) (2011) 062501.
[127] V. Sluka, A. Kákay, A.M. Deac, D.E. Bürgler, R. Hertel, C.M. Schneider, J. Phys. D Appl. Phys. 44 (38) (2011) 384002.
[128] E. Jaromirska, L. Lopez-Diaz, A. Ruotolo, J. Grollier, V. Cros, D. Berkov, Phys. Rev. B 83 (9) (2011) 094419.
[129] S. Petit-Watelot, R.M. Otxoa, M. Manfrini, Appl. Phys. Lett. 100 (8) (2012) 083507.
[130] M. Pufall, W. Rippard, M. Schneider, S. Russek, Phys. Rev. B 75 (14) (2007) 140404.
[131] Q. Mistral, M. Van Kampen, G. Hrkac, J.-V. Kim, T. Devolder, P. Crozat, C. Chappert, L. Lagae, T. Schrefl, Phys. Rev. Lett. 100 (25) (2008) 257201.
[132] A. Ruotolo, V. Cros, B. Georges, A. Dussaux, J. Grollier, C. Deranlot, R. Guillemet, K. Bouzehouane, S. Fusil, A. Fert, Nat. Nanotechnol. 4 (8) (2009) 528.
[133] M. Van Kampen, L. Lagae, G. Hrkac, T. Schrefl, J.-V. Kim, T. Devolder, C. Chappert, J. Phys. D: Appl. Phys. 42 (24) (2009) 245001.
[134] A.A. Thiele, Phys. Rev. Lett. 30 (6) (1973) 230.
[135] J. Shibata, Y. Nakatani, G. Tatara, H. Kohno, Y. Otani, Phys. Rev. B 73 (2) (2006) 020403.
[136] Y. Nakatani, J. Shibata, G. Tatara, H. Kohno, A. Thiaville, J. Miltat, Phys. Rev. B 77 (1) (2008) 014439.
[137] D. Houssameddine, U. Ebels, B. Delaët, B. Rodmacq, I. Firastrau, F. Ponthenier, M. Brunet, C. Thirion, J.-P. Michel, L. Prejbeanu-Buda, et al., Nat. Mater. 6 (6) (2007) 447.
[138] U. Ebels, D. Houssameddine, I. Firastrau, D. Gusakova, C. Thirion, B. Dieny, L. Buda-Prejbeanu, Phys. Rev. B 78 (2) (2008) 024436.
[139] I. Firastrau, D. Gusakova, D. Houssameddine, U. Ebels, M.-C. Cyrille, B. Delaet, B. Dieny, O. Redon, J.-C. Toussaint, L. Buda-Prejbeanu, Phys. Rev. B 78 (2) (2008) 024437.
[140] T. Devolder, J.-V. Kim, M. Manfrini, W. Van Roy, L. Lagae, C. Chappert, Appl. Phys. Lett. 97 (7) (2010) 072512.
[141] T. Devolder, J.-V. Kim, S. Petit-Watelot, R. Otxoa, C. Chappert, M. Manfrini, W. Van Roy, L. Lagae, IEEE Trans. Magn. 47 (6) (2011) 1595.
[142] T. Devolder, J.-V. Kim, P. Crozat, C. Chappert, M. Manfrini, M. Van Kampen, W. Van Roy, L. Lagae, G. Hrkac, T. Schrefl, Appl. Phys. Lett. 95 (1) (2009) 012507.
[143] T. Devolder, J.-V. Kim, M. Manfrini, G. Hrkac, P. Crozat, L. Lagae, T. Schrefl, C. Chappert, Proc. SPIE 7398 (1) (2009) 739808.
[144] M. Kuepferling, C. Serpico, M. Pufall, W. Rippard, T.M. Wallis, A. Imtiaz, P. Krivosik, M. Pasquale, P. Kabos, Appl. Phys. Lett. 96 (25) (2010) 252507.
[145] M. Manfrini, T. Devolder, J.-V. Kim, P. Crozat, N. Zerounian, C. Chappert, W. Van Roy, L. Lagae, G. Hrkac, T. Schrefl, Appl. Phys. Lett. 95 (19) (2009) 192507.
[146] M. Manfrini, T. Devolder, J.-V. Kim, P. Crozat, C. Chappert, W. Van Roy, L. Lagae, J. Appl. Phys. 109 (8) (2011) 083940.
[147] B. Ivanov, C. Zaspel, Phys. Rev. Lett. 99 (24) (2007) 247208.

[148] A. Khvalkovskiy, J. Grollier, A. Dussaux, K. Zvezdin, V. Cros, Phys. Rev. B 80 (14) (2009) 140401.
[149] Y.-S. Choi, K.-S. Lee, S.-K. Kim, Phys. Rev. B 79 (18) (2009) 184424.
[150] A. Dussaux, A. Khvalkovskiy, P. Bortolotti, J. Grollier, V. Cros, A. Fert, Phys. Rev. B 86 (1) (2012) 014402.
[151] A.V. Khvalkovskiy, J. Grollier, N. Locatelli, Y.V. Gorbunov, K.A. Zvezdin, V. Cros, Appl. Phys. Lett. 96 (21) (2010) 212507.
[152] G. Finocchio, O. Ozatay, L. Torres, R. Buhrman, D. Ralph, B. Azzerboni, Phys. Rev. B 78 (17) (2008) 174408.
[153] J.-V. Kim, T. Devolder, Theory of the power spectrum of spin-torque nanocontact vortex oscillators. (2010), arXiv: 1007.3859.
[154] P. Bortolotti, A. Dussaux, J. Grollier, V. Cros, A. Fukushima, H. Kubota, K. Yakushiji, S. Yuasa, K. Ando, A. Fert, Appl. Phys. Lett. 100 (4) (2012) 042408.
[155] R. Compton, P. Crowell, Phys. Rev. Lett. 97 (13) (2006) 137202.
[156] R.L. Compton, T.Y. Chen, P.A. Crowell, Phys. Rev. B 81 (14) (2010) 144412.
[157] J.C. Slonczewski, J. Appl. Phys. 44 (4) (1973) 1759.
[158] N.L. Schryer, L.R. Walker, J. Appl. Phys. 45 (12) (1974) 5406.
[159] M.E. Gouvea, G.M. Wysin, A.R. Bishop, F.G. Mertens, Phys. Rev. B 39 (16) (1989) 11840.
[160] K.-S. Lee, S. Choi, S.-K. Kim, Appl. Phys. Lett. 87 (19) (2005) 192502.
[161] R. Hertel, C. Schneider, Phys. Rev. Lett. 97 (17) (2006) 177202.
[162] K.-S. Lee, K. Guslienko, J.-Y. Lee, S.-K. Kim, Phys. Rev. B 76 (17) (2007) 174410.
[163] K. Yamada, S. Kasai, Y. Nakatani, K. Kobayashi, H. Kohno, A. Thiaville, T. Ono, Nat. Mater. 6 (4) (2007) 270.
[164] D.D. Sheka, Y. Gaididei, F.G. Mertens, Appl. Phys. Lett. 91 (8) (2007) 082509.
[165] K. Guslienko, K.-S. Lee, S.-K. Kim, Phys. Rev. Lett. 100 (2) (2008) 027203.
[166] S. Choi, K.-S. Lee, K. Guslienko, S.-K. Kim, Phys. Rev. Lett. 98 (8) (2007) 087205.
[167] B. Van Waeyenberge, A. Puzic, H. Stoll, K.W. Chou, T. Tyliszczak, R. Hertel, M. Fähnle, H. Brückl, K. Rott, G. Reiss, et al., Nature 444 (7118) (2006) 461.
[168] Y. Gaididei, D.D. Sheka, F.G. Mertens, Appl. Phys. Lett. 92 (1) (2008) 012503.
[169] B. Pigeau, G. de Loubens, O. Klein, A. Riegler, F. Lochner, G. Schmidt, L.W. Molenkamp, Nat. Phys. 7 (1) (2010) 26.
[170] Y.-S. Yu, K.-S. Lee, H. Jung, Y.-S. Choi, M.-W. Yoo, D.-S. Han, M.-Y. Im, P. Fischer, S.-K. Kim, Phys. Rev. B 83 (17) (2011) 174429.
[171] M. Curcic, B. Van Waeyenberge, A. Vansteenkiste, M. Weigand, V. Sackmann, H. Stoll, M. Fähnle, T. Tyliszczak, G. Woltersdorf, C.H. Back, et al., Phys. Rev. Lett. 101 (19) (2008) 197204.
[172] K.-S. Lee, M.-W. Yoo, Y.-S. Choi, S.-K. Kim, Phys. Rev. Lett. 106 (14) (2011) 147201.
[173] A. Vansteenkiste, K.W. Chou, M. Weigand, M. Curcic, V. Sackmann, H. Stoll, T. Tyliszczak, G. Woltersdorf, C.H. Back, G. Schütz, et al., Nat. Phys. 5 (5) (2009) 332.
[174] V.P. Kravchuk, D.D. Sheka, F.G. Mertens, Y. Gaididei, J. Phys. D Appl. Phys. 44 (28) (2011) 285001.
[175] M. Kammerer, M. Weigand, M. Curcic, M. Noske, M. Sproll, A. Vansteenkiste, B. Van Waeyenberge, H. Stoll, G. Woltersdorf, C.H. Back, et al., Nat. Commun. 2 (2011) 279.
[176] M.-W. Yoo, J. Lee, S.-K. Kim, Appl. Phys. Lett. 100 (17) (2012) 172413.
[177] A. Pikovsky, M. Rosenblum, J. Kurths, Synchronization: A Universal Concept in Nonlinear Sciences, Cambridge University Press, Cambridge, 2001.
[178] S. Petit-Watelot, J.-V. Kim, A. Ruotolo, R.M. Otxoa, K. Bouzehouane, J. Grollier, A. Vansteenkiste, B. Van de Wiele, V. Cros, T. Devolder, Nat. Phys. 8 (9) (2012) 682.

[179] P. Bak, Rep. Prog. Phys. 45 (1982) 587.
[180] A.M. Deac, A. Fukushima, H. Kubota, H. Maehara, Y. Suzuki, S. Yuasa, Y. Nagamine, K. Tsunekawa, D.D. Djayaprawira, N. Watanabe, Nat. Phys. 4 (10) (2008) 803.
[181] D. Houssameddine, S.H. Florez, J.A. Katine, J.-P. Michel, U. Ebels, D. Mauri, O. Ozatay, B. Delaet, B. Viala, L. Folks, et al., Appl. Phys. Lett. 93 (2) (2008) 022505.
[182] Y. Zhou, J. Persson, S. Bonetti, J. Åkerman, Appl. Phys. Lett. 92 (9) (2008) 092505.
[183] A. Slavin, V. Tiberkevich, Phys. Rev. B 72 (9) (2005) 092407.
[184] W. Rippard, M. Pufall, S. Kaka, T. Silva, S. Russek, J. Katine, Phys. Rev. Lett. 95 (6) (2005) 067203.
[185] B. Georges, J. Grollier, M. Darques, V. Cros, C. Deranlot, B. Marcilhac, G. Faini, A. Fert, Phys. Rev. Lett. 101 (1) (2008) 017201.
[186] M. Quinsat, J.F. Sierra, I. Firastrau, V. Tiberkevich, A. Slavin, D. Gusakova, L.D. Buda-Prejbeanu, M. Zarudniev, J.-P. Michel, U. Ebels, et al., Appl. Phys. Lett. 98 (18) (2011) 182503.
[187] R. Lehndorff, D.E. Bürgler, C.M. Schneider, Z. Celinski, Appl. Phys. Lett. 97 (14) (2010) 142503.
[188] A. Dussaux, A.V. Khvalkovskiy, J. Grollier, V. Cros, A. Fukushima, M. Konoto, H. Kubota, K. Yakushiji, S. Yuasa, K. Ando, et al., Appl. Phys. Lett. 98 (13) (2011) 132506.
[189] S. Martin, N. De Mestier, C. Thirion, C. Hoarau, Y. Conraux, C. Baraduc, B. Diény, Phys. Rev. B 84 (14) (2011) 144434.
[190] M. d'Aquino, C. Serpico, R. Bonin, G. Bertotti, I. Mayergoyz, Phys. Rev. B 82 (6) (2010) 064415.
[191] G. Finocchio, M. Carpentieri, A. Giordano, B. Azzerboni, Phys. Rev. B 86 (1) (2012) 014438.
[192] P. Tabor, V. Tiberkevich, A. Slavin, S. Urazhdin, Phys. Rev. B 82 (2) (2010) 020407.
[193] S. Urazhdin, P. Tabor, V. Tiberkevich, A. Slavin, Phys. Rev. Lett. 105 (10) (2010) 104101.
[194] D. Li, Y. Zhou, C. Zhou, B. Hu, Phys. Rev. B 83 (17) (2011) 174424.
[195] Y. Zhou, V. Tiberkevich, G. Consolo, E. Iacocca, B. Azzerboni, A. Slavin, J. Åkerman, Phys. Rev. B 82 (1) (2010) 012408.
[196] P. Matthews, S. Strogatz, Phys. Rev. Lett. 65 (14) (1990) 1701.
[197] J. Acebrón, L. Bonilla, C. Pérez Vicente, F. Ritort, R. Spigler, Rev. Mod. Phys. 77 (1) (2005) 137.
[198] S. Rezende, F. De Aguiar, R. Rodríguez-Suárez, A. Azevedo, Phys. Rev. Lett. 98 (8) (2007) 087202.
[199] G. Hrkac, T. Schrefl, S. Bance, D. Allwood, A. Goncharov, J. Dean, D. Suess, J. Magn. Magn. Mater. 320 (17) (2008) L111.
[200] X. Chen, R. Victora, Phys. Rev. B 79 (18) (2009) 180402.
[201] J. Grollier, V. Cros, A. Fert, Phys. Rev. B 73 (6) (2006) 060409.
[202] Y. Zhou, J. Akerman, Appl. Phys. Lett. 94 (11) (2009) 112503.
[203] D. Li, Y. Zhou, B. Hu, J. Åkerman, C. Zhou, Phys. Rev. B 86 (1) (2012) 014418.
[204] B. Georges, J. Grollier, V. Cros, A. Fert, Appl. Phys. Lett. 92 (23) (2008) 232504.
[205] E. Iacocca, J. Åkerman, J. Appl. Phys. 110 (10) (2011) 103910.
[206] J. Xiao, A. Zangwill, M. Stiles, Phys. Rev. B 72 (1) (2005) 014446.
[207] I. Krivorotov, D. Berkov, N. Gorn, N. Emley, J. Sankey, D. Ralph, R. Buhrman, Phys. Rev. B 76 (2) (2007) 024418.
[208] G. Siracusano, G. Finocchio, A. La Corte, G. Consolo, L. Torres, B. Azzerboni, Phys. Rev. B 79 (10) (2009) 104438.
[209] K. Kudo, T. Nagasawa, H. Suto, R. Sato, K. Mizushima, Phys. Rev. B 81 (22) (2010) 224432.
[210] G. Finocchio, G. Siracusano, V. Tiberkevich, I.N. Krivorotov, L. Torres, B. Azzerboni, Phys. Rev. B 81 (18) (2010) 184411.

[211] R. Bonin, M. D'aquino, G. Bertotti, C. Serpico, I.D. Mayergoyz, Eur. Phys. J. B 85 (1) (2012) 47.
[212] I. Krivorotov, N. Emley, R. Buhrman, D. Ralph, Phys. Rev. B 77 (5) (2008) 054440.
[213] D. Houssameddine, U. Ebels, B. Dieny, K. Garello, J.-P. Michel, B. Delaet, B. Viala, M.-C. Cyrille, J. Katine, D. Mauri, Phys. Rev. Lett. 102 (25) (2009) 257202.
[214] P. Muduli, O. Heinonen, J. Åkerman, Phys. Rev. Lett. 108 (20) (2012) 207203.
[215] D. Berkov, N. Gorn, Phys. Rev. B 76 (14) (2007) 144414.
[216] S. Ikeda, K. Miura, H. Yamamoto, K. Mizunuma, H.D. Gan, M. Endo, S. Kanai, J. Hayakawa, F. Matsukura, H. Ohno, Nat. Mater. 9 (9) (2010) 721.
[217] P.F. Carcia, J. Appl. Phys. 63 (10) (1988) 5066.
[218] G.H.O. Daalderop, P.J. Kelly, F.J.A. den Broeder, Phys. Rev. Lett. 68 (5) (1992) 682.
[219] W.H. Rippard, A.M. Deac, M.R. Pufall, J.M. Shaw, M.W. Keller, S.E. Russek, C. Serpico, Phys. Rev. B 81 (1) (2010) 014426.
[220] M. Hoefer, T. Silva, M. Keller, Phys. Rev. B 82 (5) (2010) 054432.
[221] M. Hoefer, M. Sommacal, T. Silva, Phys. Rev. B 85 (21) (2012) 214433.
[222] B.A. Ivanov, A.M. Kosevich, J. Exp. Theor. Phys. 45 (5) (1977) 1050.
[223] D. Gusakova, D. Houssameddine, U. Ebels, B. Dieny, L. Buda-Prejbeanu, M. Cyrille, B. Delaët, Phys. Rev. B 79 (10) (2009) 104406.
[224] G.E.W. Bauer, E. Saitoh, B.J. van Wees, Nat. Mater. 11 (5) (2012) 391.